10-14-2020 2:00 PM

Experimental and Numerical Study of Polymorphism in Crystallization Processes

Mengxing Lin, *The University of Western Ontario*

Supervisor: Rohani，Sohrab, *The University of Western Ontario*
A thesis submitted in partial fulfillment of the requirements for the Doctor of Philosophy degree
in Chemical and Biochemical Engineering
© Mengxing Lin 2020

Abstract

Polymorphism, which is exhibited in more than half of the active pharmaceutical ingredients, has a direct impact on the stability, bioavailability and processability of the product. Despite extensive studies on polymorphism in the field of crystal engineering, the control of polymorphism is still one of the most challenging tasks in pharmaceutical manufacturing.

The aim of this work is to crystallize the desired polymorph with the help of process modeling and process analytical technologies. First, we investigated the crystallization properties of imatinib mesylate, including polymorphism characterization, solubility measurement, polymorphic transformation and kinetic parameter estimation, as they are the fundamental information for the model-based process design and control of crystallization process and were lacking in the literature. Subsequently, the capability of in-situ Raman spectroscopy in measuring solution concentration and solids concentration was proved. The analytical models were developed with several pre-processing methods and multivariable analysis techniques and compared based on the root mean squared errors. Thereafter, the impacts of relative kinetics of the two polymorphs on the polymorphic outcome were studied numerically in batch and MSMPR (mixed suspension and mixed product removal) crystallizers. The optimal operating conditions for harvesting the desired polymorph were analyzed in both modes of operations. Lastly, the effects of the operating conditions in batch and MSMPR crystallization on the product polymorphism, process yield, and crystal size were investigated. The effectiveness of continuous seeding strategy in altering the steady-state condition of MSMPR crystallization and its implementation was also proved and discussed.

In conclusion, this work is concerned with studying the polymorphism phenomenon in crystallization processes experimentally and numerically, providing insights into the design, optimization and control of batch and continuous crystallization processes.

Keywords

Polymorphism, Batch crystallization, Continuous crystallization, Solubility measurement，Characterization, Solution-mediated polymorphic transformation, Parameter estimation, Nucleation and growth rate, FBRM, Raman spectroscopy, MATLAB

Summary for Lay Audience

Crystallization is the process by which the atoms or molecules form solid crystals from a saturated solution or a gas phase. In the pharmaceutical industry, more than 90% of small molecular drugs are delivered in crystalline form and over 80% drug products involve at least one crystallization step. The operation conditions during the crystallization process have significant effects on the product properties, such as crystal size distribution, purity and polymorphism. Polymorphism, which is exhibited in more than half of the active pharmaceutical ingredients, refers to the different arrangements of molecules in solid-state and has a direct impact on the stability, bioavailability and processability of the drug products. Despite extensive studies on polymorphism in the field of crystal engineering, the control of polymorphism is still one of the most challenging tasks in pharmaceutical manufacturing.

This work is concerned with studying the polymorphism phenomenon in crystallization processes experimentally and numerically, providing insights into the process design and optimization. At first, the investigation of the imatinib mesylate properties, was conducted experimentally and thoroughly, in the aspects of characterization, solubility, polymorphic transformation, and nucleation and growth rates. These properties are the fundamental and necessary information for the process design and control. Then, Raman spectroscopy, a process analytic technology, was applied for in-situ monitoring of the solution concentration and slurry density of each polymorph during the crystallization process. Subsequently, the impact of relative kinetics of the two polymorphs on the polymorphic outcome was studied numerically in batch and MSMPR (mixed suspension and mixed product removal) crystallizers. The optimal operating conditions for harvesting the desired polymorph were investigated in both modes of operations. The influence of each manipulated variable on the crystal properties was also studied.

Co-Authorship Statement

Chapter 2: the experimental design, experiments conducting, data analysis and parameter estimation were performed by Mengxing Lin. The manuscript was prepared by Mengxing Lin and reviewed by Dr. Sohrab Rohani. Yuanyi Wu aided in conducting the experiments and data processing.

A version of this chapter has been published in *Journal of Crystal Growth*:

> Lin, M., Wu, Y., & Rohani, S. (2019). A kinetic study of crystallization process of imatinib mesylate with polymorphic transformation phenomenon. *Journal of Crystal Growth*, *507*, 146-153.

Chapter 3: The experiments were designed and conducted by Mengxing Lin. The manuscript was prepared by Mengxing Lin and revised by Dr. Sohrab Rohani. Yuanyi Wu aided in conducting the experiments and data processing.

A version of this chapter has been published in *Crystal Growth & Design*:

> Lin, M., Wu, Y., & Rohani, S. (2020). Simultaneous measurement of solution concentration and slurry density by Raman spectroscopy with artificial neural network. *Crystal Growth & Design*, 20(3), 1752-1759.

Chapter 4: Mengxing Lin implemented the model and wrote the manuscript. Dr. Sohrab Rohani reviewed and revised the manuscript. The modeling results in this chapter were developed in cooperation with Yuanyi Wu.

A version of this chapter has been published in *Crystal Growth & Design*:

> Lin, M., Wu, Y., & Rohani, S. (2020). Identifying the Polymorphic Outcome of Hypothetical Polymorphs in Batch and Continuous Crystallizers by Numerical Simulation. *Crystal Growth & Design*.

Acknowledgments

I would like to take this opportunity to thank those who made this work possible. First of all, I wish to express my deepest appreciation to my supervisor, Dr. Sohrab Rohani, for his invaluable knowledge, warm support and continuous guidance throughout the duration of this work.

I appreciate Dr. Jesse Zhu and Dr. Kibret Mequanint for providing me the chance to study in Western University as an exchange undergraduate, which made it possible to pursue my Ph.D. in Dr. Sohrab Rohani's group.

I also acknowledge China Scholarship Council and Natural Sciences and Engineering Research Council of Canada for the finical support.

Many thanks are directed to my colleagues and friends, Zhenguo Gao, Yuanyi Wu, Soroush Ahmadi Nasrabadi, Pradip Mondal, Weizhong Gong, Yuqing Ye and Huan Jiang for their help on my research and life.

I would like to dedicate this work to my family, especially my parents and bother. Without their unconditional love and endless support, I would not be able to accomplish this project. Special thanks to Xiaoyang Wei for the companion, encouragement and support during my entire study in Western University. I am lucky to have you in my life.

Table of Contents

List of Tables

List of Figures

Nomenclature

Chapter 2

a	solute activity	-
b	nucleation order on supersaturation	-
B	crystal birth rate	#/m³·s
B_s	secondary nucleation rate	#/m³·s
C	solution concentration	kg solute /kg solvent
C^*	equilibrium concentration--solubility	kg solute /kg solvent
C^{cal}	calculated solution concentration	kg solute /kg solvent
C^{exp}	experimental solution concentration	kg solute /kg solvent
D	crystal death rate	#/m³·s
F	objective function	
g	growth order on supersaturation	-
G	crystal growth rate	m/s
ΔG	difference of Gibbs free energy	kJ/mol
j	nucleation order on suspension density	-
k	number of experiments included in the objective function F	-
k_g	growth rate coefficient	m/s
k_{sn}	secondary nucleation rate coefficient	$(\#/m^3 \cdot s)/$(kg/kg solvent)[j]
k_v	crystal volume shape factor	-
L	characteristic size of crystal	m
m	mass of solute	kg
m_s	mass of solvent	kg
M	molecular mass of solute	kg/mol

M_s	molecular mass of solvent	kg/mol
M_t	suspension density	kg solids /kg solvent
n	population density	$\#/m^3 \cdot m$
N	number of samples in each experiment included in the objective function F	-
R	universal gas constant	kJ/mol·K
S	relative supersaturation	-
t	time	s
x	molar fraction of solute	-
ρ_c	crystal density	kg/m^3

Chapter 3

C	solution concentration	kg solute /kg solvent
C_0	initial solution concentration	kg solute /kg solvent
n	number of observations	-
t	time	s
T	temperature	K
$\hat{y}_i$	predicted values of ith observation	
y_i	observed values of ith observation	
τ	residence time	s
ANN	artificial neural network	
ATR-FTIR	attenuated total reflectance Fourier transform infrared spectroscopy	
CPR	characteristic peaks regression	
DOSC	direct orthogonal signal correction	
FBRM	focused beam reflectance measurement	
LGA	L-Glutamic acid	

MLR	multiple linear regression
PAT	process analytical technologies
PCA	principal component analysis
PCA-ANN	principal components as the input of artificial neural network
PCM	paracetamol
PCR	principal component regression
Peak-ANN	characteristic peaks as the input of artificial neural network
PLSR	partial least squares regression
PXRD	powder X-ray diffraction
RMSE	root mean squared error

Chapter 4

b	nucleation rate order	-
B	crystal nucleation rate	#/s/kg solvent
C	solution concentration	kg solute /kg solvent
C^*	solubility	kg solute /kg solvent
C_{feed}	solution concentration in the feed stream	kg solute /kg solvent
d	dissolution rate order	-
D	crystal dissolution rate	m/s
g	growth rate order	-
G	crystal growth rate	m/s
i	polymorph	
k_{b1}	primary nucleation rate constant	#/s/kg solvent
kb_2	secondary nucleation rate constant	#/s/m^3 crystal
k_d	dissolution rate constant	m/s

k_g	growth rate constant	m/s
k_v	crystal volume shape factor	-
L	crystal size	m
m_3	third moment of crystals	m^3 crystal /kg solvent
n	number density	#/m/kg solvent
n_{feed}	number density in the feed stream	#/m/kg solvent
Rdg	ratio of the metastable dissolution rate to the stable form growth rate	
Rkb	ratio between the nucleation rate constants of two polymorphs	
Rkg	ratio between the growth rate constants of two polymorphs	
S	supersaturation	-
t	time	s
ρ_c	crystal density	kg/m^3
τ	residence time	s
MSMPR	mixed suspension and mixed product removal	
SMPT	solution-mediated polymorphic transformation	

Chapter 5

A	adjustable constant to change the seed mass	#
B	crystal nucleation rate	#/s/kg solvent
C	solution concentration	kg solute /kg solvent
C^*	solubility	kg solute /kg solvent
d_c	crystal diameter	μm
D	crystal dissolution rate	m/s
D_i	inner diameter of tube	mm
f	withdrawal frequency	-

F	Durand factor	-
g	gravitational acceleration	m/s^2
k_v	crystal volume shape factor	-
L	crystal size	m
$\bar{L}$	average size of seeds	m
m_{seed}	mass of seeds	kg
n	number density	#/m/kg solvent
n_{seed}	number density of seeds	#/m
P	power number of the cooling policy	-
Q	volumetric flow rate	m^3/s
Q_{feed}	volumetric flow rate from feed tank	m^3/s
Re_p	Reynolds number of particles	-
S	supersaturation	-
t	time	s
t_c	batch time	s
T	temperature	°C
T_f	final temperature	°C
T_i	initial temperature	°C
$U_{horizontal}$	horizontal velocity	m/s
$U_{vetical}$	terminal velocity	m/s
V	solution volume	m^3
ρ_c	crystal density	kg/m^3
ρ_L	fluid density	kg/m^3
ρ_{seed}	crystal density of seeds	kg/m^3
τ	residence time	s

ν	fluid dynamic viscosity	Pa·s
δ	Dirac delta function	
σ	standard deviation of seeds	m
MSMPR	mixed suspension and mixed product removal	
RTD	residence time distribution	
SMPT	solution-mediated polymorphic transformation	

Chapter 1

Introduction

1 Introduction

1.1 Background

1.1.1 Crystallization

Crystallization is one of the oldest separation and purification unit operations in the food, chemical, biochemical, and pharmaceutical industries (A. S. Myerson, 2002). Specifically, in the pharmaceutical industry, the properties of the active pharmaceutical ingredients (APIs) are often controlled by the final crystallization step, since over 90% of the small molecule drugs exist in crystalline form (Alvarez and Myerson, 2010; Variankaval et al., 2008). During the crystallization process, the atoms or molecules are transferred from solution to the solid phase and form solid crystals.

Supersaturation, referring to the ratio of actual concertation and solubility at a given temperature, is the driving force for the crystallization process. Cooling, evaporation, addition of anti-solvent, and chemical reaction can be used to create the supersaturation.

Usually, the crystallization process consists of two major steps: nucleation and growth. The former creates nuclei that are the tiny crystalline phase formed in a supersaturated solution or a supercooled liquid and serve as the core in the crystallization process. The latter indicates the increase in the particle size and leads to larger crystals.

Primary nucleation and secondary nucleation are the two main types of nucleation. The difference between them is whether the crystals/seeds exist in the supersaturated solution when nucleation happens. The control of primary nucleation is hard since it requires high supersaturation for phase transition and causes explosive nucleation, resulting in excessive small crystals. As a result, primary nucleation is not desired in industry. The control of secondary nucleation is widely used since it operates moderately in the metastable zone，the region between the solubility and supersolubility curve.

1.1.2 Polymorphism

Polymorphism refers to the ability of a molecule to crystallize in more than one crystal structure with different packing arrangements and/or conformations. It has been reported

that more than half of the active pharmaceutical ingredients (API) exhibit solid-state polymorphism (Stahly, 2007). Due to the differences in their intra- and intermolecular solid-state structures, polymorphic forms of a drug have different chemical and physical properties, including melting point, solubility, mechanical properties, and bulk density. These properties have a direct impact on the stability and bioavailability of pharmaceutical products (Lee et al., 2011), as well as the processability in the downstream processes, such as filtration, drying, and tableting.

In fact, the emphasis on polymorphism in the pharmaceutical industry originates from several high-profile disasters in the past decades. Take the example of Ritonavir, which is an antiretroviral medication used to treat HIV/AIDS. Only one polymorph was found and introduced to the market in 1996. However, after two years, a more stable and not therapeutically effective polymorph appeared. The new form compromised the oral bioavailability of the drug. Thus, Abbott Company had to withdraw the original capsules from the market and caused a loss of 250 million dollars (Qu et al., 2009)

The occurrence of polymorphism transition in the manufacturing process or transportation and storage can lead to the economic loss, more importantly, the legal and health issues. Hence, all pharmaceutical companies are required to perform thorough polymorphic studies/screening before submitting a New Drug Application by Food and Drug Administration (FDA) and other agencies that monitor the production and distribution of the drug (Raw et al., 2004).

Based on the relative stability of two polymorphs, the relationship between them can be either monotropic or enantiotropic. For monotropic systems, one form has lower solubility, lower Gibbs free energy, and higher thermodynamic stability than the other at all temperatures below the melting point. Whereas, for enantiotropic systems, there exists a transition temperature, and at that point, the Gibbs free energies of two forms are the same. The more stable form depends on what the temperature is, as shown in Figure 1-1. The polymorphism transformation from the metastable to the stable form can occur in either solid state or solutions, called solid state polymorphic transformation (SST) and solution-mediated polymorphic transformation (SMPT) (Mullin, 2001).
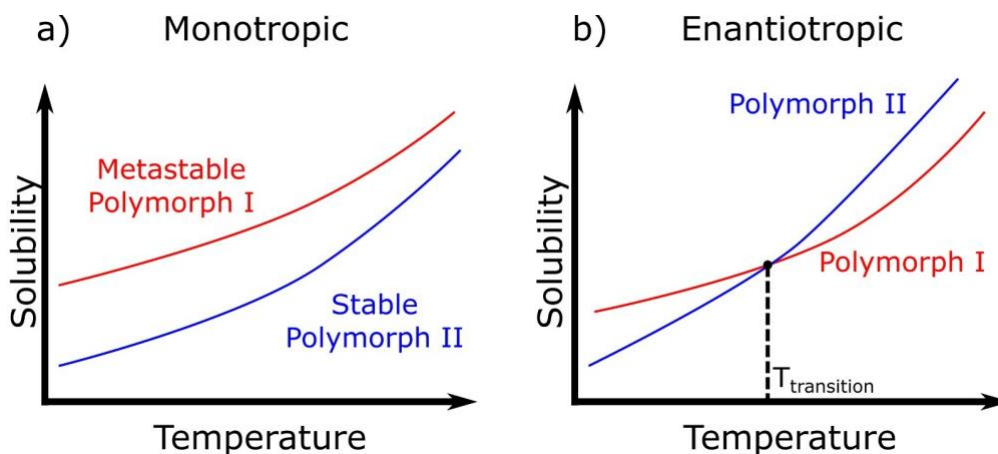
Figure 1-1. Enantiotropic and monotropic polymorphs

1.1.3   Characterization

As mentioned above, polymorphism refers to the different crystalline forms of the same chemical compound, which have different physical and chemical properties, including thermodynamic and spectroscopic properties. These dissimilarities in solid properties can be employed as tools for analyzing the solid forms during or after the crystallization process, granulation, drying and tableting to meet the regulatory and quality criteria.

1.1.3.1   Solubility measurement

Solubility measurement is a strong tool for the study of the stability and transition point of polymorphic systems. The most stable polymorph has the lowest solubility at a given temperature. Additionally, solubility data is the most fundamental information required to design a crystallization process.

Several techniques have been developed for accurate solubility measurement. Among them, the gravimetric method (Zhang et al., 2010) is the most traditional one. In this method, the solution with excess solids should be agitated at a constant temperature for a long time to reach the thermodynamic equilibrium, followed by filtration. Then the filtrate is weighed and placed in an oven to evaporate the solvent. After weighing the residual solid, the solubility at the corresponding temperature, T, can be calculated.

High-performance liquid chromatography (HPLC) (Li et al., 2016) and ultraviolet/visible spectrophotometer (UV/vis) (Mondal et al., 2017), are also widely used to measure the

solubility. Similar to the gravimetric method, the suspension should be agitated and reach equilibrium, before being withdrawn and filtered. Then the concentration of the original or diluted filtrate is detected with HPLC or UV-Vis spectrophotometer.

With the off-line methods mentioned above, the samples have to be taken out from the crystallizer, followed by one or more steps of drying, filtration, dilution, which is time-consuming and subject to human and system errors. The *in-situ* attenuated total reflectance Fourier transform infrared (ATR- FTIR) spectroscopy (Yang et al., 2008) and conductivity meter (Garcia et al., 1999) can measure the solution concentration online, so that they are more convenient and accurate

1.1.3.2   **Differential Scanning Calorimetry (DSC)**

DSC is the most popular thermal method for pharmaceutical analysis. It measures the required heat flow for keeping the temperature of the sample and an empty reference crucible the same. DSC provides thermodynamic data, including glass transition temperature, melting point and heat of fusion.

1.1.3.3   **Thermal Gravimetric Analysis (TGA)**

TGA measures the weight changes of a sample as a function of temperature. It is therefore valuable for cases that are accompanied by weight loss due to heating. Sublimation, desolvation and decomposition processes are accompanied by weight changes, so they can be identified by this method qualitatively and quantitatively. In contrast, solid-solid and solid-liquid transformations are not accompanied by weight loss, so TGA cannot detect them. Combined DSC and TGA present valuable information on thermodynamic data, polymorphic and pseudo-polymorphic states of pharmaceutical solids.

In both DSC and TGA, sample size and heating rate influence the results and may lead to misinterpretation. A lower heating rate results in obtaining thermodynamic equilibrium, while a high heating rate will introduce kinetic factors. A smaller sample size also allows faster and more uniform heat transfer to the solid.

1.1.3.4   X-ray Powder Diffraction (XRPD)

XRPD is a powerful method for distinguishing and identifying polymorphs as it is based on the structural differences of the crystals. When incident X-ray beams to the crystal, it will be reflected only when the angle between the ray and the plane in the crystal matches the Bragg equation:

$$n\lambda = 2d \sin \theta \tag{1-1}$$

where λ is the wavelength of the ray,

   d is the distance between the planes in the crystal,

   θ is the angle between the ray and the plane

   n is the order of the reflection

1.1.3.5   Raman spectroscopy

Raman spectroscopy is widely used to monitor the solid phase in crystallization process, as it can provide the structural fingerprint based on the scattered light from matter. There are two types of scattering: elastic and inelastic (Staveley, 2016). In elastic scattering, also called Rayleigh scattering, the molecule is excited to a new state followed by relaxation to the original state, re-emitting a photon at the same frequency as the incident light. In inelastic scattering, also called Raman scattering, the excited molecules relax to a different vibrational state, emitting photons with a different energy than the incident light.
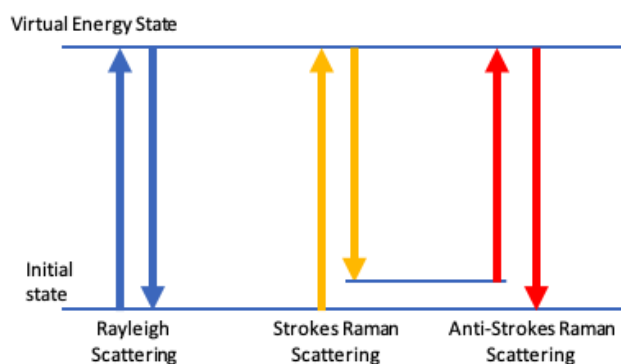
Figure 1-2. Raman scattering

Only a small fraction of molecules undergoes inelastic scattering, so the Raman scattering intensity will be overwhelmed by the reflected incident light. To improve the signal to noise ratio, a high-power laser beam is focused to the focal point to enhance the occurrence of Raman scattering. The spectrometer employs groups of optical elements to filter and amplify the signal with different wavelength than the incident light caused by Raman scattering (Figure 1-3). The cooled image sensor captures each spectrum with a long exposure to accumulate signal. The high-sensitivity setup enables the Raman spectroscopy a perfect tool to monitor the concentrations of both solids and liquid phase as well as detecting the polymorphic transformation of the crystals.
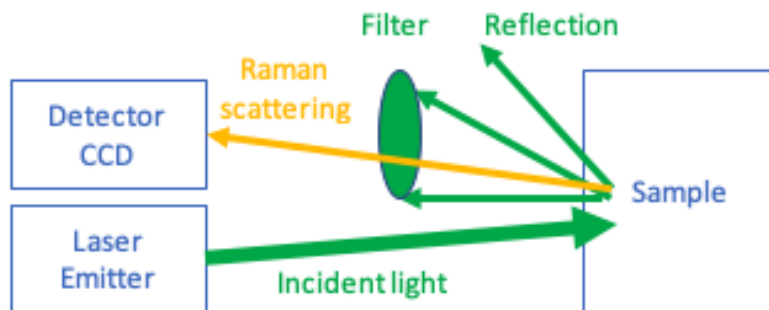
Figure 1-3. Schematics of a Raman spectroscopy meter

1.1.3.6   **Focused Beam Reflection Measurement (FBRM)**

The FBRM uses a confocal laser beam that scans across the surface of the particles passing in front of the probe's sapphire window to measure the chord length distribution (CLD). As shown in Figure 1-4, the rotary optical lens drives the laser beam rotating at a constant speed (2 m/s). When the laser beam hits the crystals near the focal point, the backscattering light is detected, and the durations are converted to the chord length. The confocal mechanism ensures a limited depth of field (DOF), i.e., the crystals far from the laser focal point will not be detected. This helps to resolve the overlapping crystals in different depths when the solids concentration gets high. The chord length depends on the characteristic length, the shape, the surface roughness, the optical properties, and the velocity of the crystals. The chord length tends to underestimate the size of the crystal because of the high probability of scanning shorter chords than the full characteristic length of a crystal.
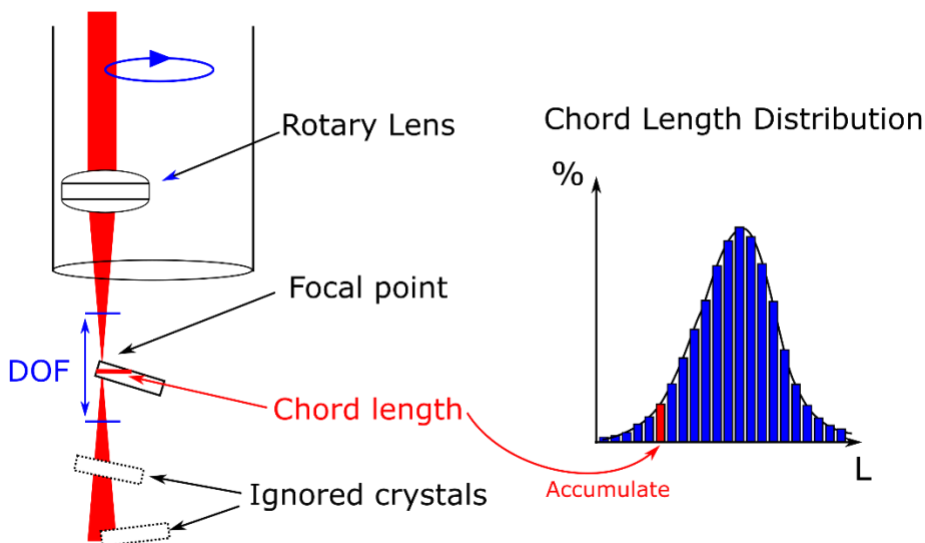
Figure 1-4. FBRM mechanism

FBRM has been extensively used to monitor nucleation event, controlling the crystal number density with direct nucleation control (Saleemi et al., 2012a), and extract aspect ratio and more accurate size distribution with fine-tuned algorithms (Borsos et al., 2017). Its easy-to-use probe design and the ability to work in relatively high solids concentration make it a well-received process analysis technology in both industry and research.

1.1.4 Population balance equation

Besides polymorphism, crystal size distribution (CSD) is another significant property of pharmaceutical products, as CSD influences greatly the downstream processes (e.g. filtration, drying, and tableting) and the product performances (Abu Bakar et al., 2009). Population balance equation (PBE) is widely used to describe the crystal size with respect to time and space in both academic and industrial research (Nagy et al., 2013a). PBE was first proposed by Hulburt and Katz (Hulburt and Katz, 1964) and applied in the crystallization process by Randolph and Larson (Randolph and Larson, 1971). The analytical solutions of PBE were extensively studied by Ramkrishna (Ramkrishna, 2000). Due to the existence of aggregation and breakage, the analytical solutions of PBE do not exist unless some assumptions are applied. So often numerical methods are employed for solving PBE. A comprehensive review of the solution methods of PBE was carried out by Omar and Rohani (Omar and Rohani, 2017).

PBE can be obtained with the Lagrangian or Eulerian approach (Equation (1-2) and (1-3)). The Lagrangian viewpoint tracks a subregion of particle size (L_i—L_{i+1}) in a flow system, while Eulerian viewpoint tracks a volume V of external phase space (Randolph and Larson, 1971).

$$\frac{\partial n}{\partial t} + \nabla.(\boldsymbol{v_e}n) + \nabla.(\boldsymbol{v_i}n) = B - D \tag{1-2}$$

$$\frac{\partial n}{\partial t} + \nabla.(\boldsymbol{v_i}n) + n\frac{d(logV)}{dt} = B - D - \sum_k \frac{Q_k n_k}{V} \tag{1-3}$$

where n is population density, $\boldsymbol{v_e}$ is external velocity vector, $\boldsymbol{v_i}$ is the internal velocity vector, B is crystal birth rate, D is the crystal death rate. V is the crystallizer volume, and $Q_k n_k$ is the volumetric inflow/outflow multiplied by the number density of the inflow/outflow streams. Usually, the particle velocity is assumed to be equal to the liquid velocity. A commonly used one-dimensional PBE

$$\frac{\partial n}{\partial t} + \frac{\partial (Gn)}{\partial L} = B - D \tag{1-4}$$

The birth term represents the new crystals produced from nucleation, aggregation and breakage processes, while the death term presents the particle disappearance due to the dissolution, aggregation and breakage (Bhoi and Sarkar, 2016). The common expression for the birth and death rates are shown in Figure 1-5, where $b(t, x, x')$ is the probability density function for the generation of particles, $a(x)$ and $a(x')$ are the break rates of the particles with size x and x', and $\beta(t, x - x', x')$ is the frequency of collisions between crystals with size $x - x'$ and x' (Qamar et al., 2009).
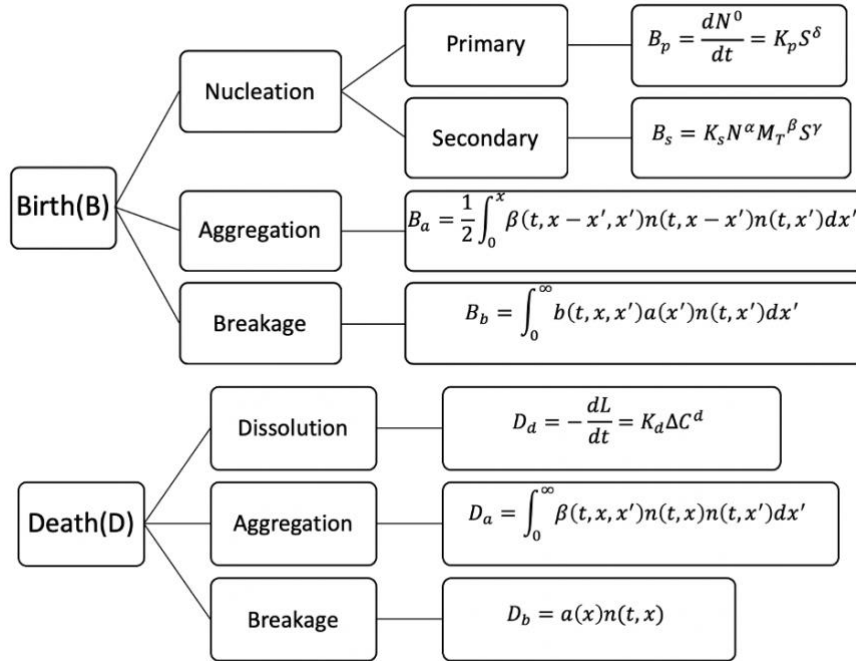
Figure 1-5. Formulation of birth and growth rates

1.1.4.1   **Analytical Solution**

The most common analytical solution of PBE is derived from mixed suspension mixed product removal crystallizers (MSMPR), with the assumption that a crystallizer has a uniform distribution of suspended solids and negligible breakage and agglomeration (A. Myerson, 2002). If the feed of MSMPR is a clear solution without crystals (i.e., $n_i = 0$), and growth rate is size-independent, the PBE for the steady-state MSMPR will be

$$G\frac{\partial n}{\partial L} + \frac{n}{\tau} = 0 \qquad\qquad (1\text{-}5)$$

where G is the growth rate, L is crystal size, and τ is residence time.

The solution of Equation (1-5) is

$$ln\, n = -\frac{1}{G\tau} * L + ln\, n^0 \qquad\qquad (1\text{-}6)$$

where n^0 is the population density of zero-sized crystals. From the definition of nucleation, one can get

$$n^0 = \left(\frac{dN}{dL}\right)_{L\to 0} = \left(\frac{dN}{dt}\Big/\frac{dL}{dt}\right)_{L\to 0} = \frac{B}{G} \tag{1-7}$$

From Equation (1-6) and (1-7), it is known that the slope and intercept of the "ln n vs. L" curve are $-\frac{1}{G\tau}$ and $ln\left(\frac{B}{G}\right)$. Therefore, the analytical solution of MSMPR can be used as one approach for determining the nucleation and growth rates.

1.1.4.2 Numerical methods

As mentioned above, the analytical solutions exist only for some limited simplified cases, so much effort has been invested to numerically solve these equations. There are several numerical methods to solve PBE, such as the method of moments (Hulburt and Katz, 1964; Randolph and Larson, 1971; Ramkrishna, 2000), method of classes (Hounslow et al., 1988; Marchal et al., 1988), finite element method (Tsang and Rao, 1990; Nicmanis and Hounslow, 1998; John et al., 2009), finite volume method (Gunawan et al., 2004a; Szilágyi et al., 2019) and Monte Carlo method (Smith and Matsoukas, 1998; Tandon and Rosner, 1999; Bárkányi et al., 2013).

1.1.4.2.1 Method of moments

The method of moments converts the PBE into ordinary differential equations in terms of moments of the number density. The moments are defined as

$$m_j(t) = \int_0^\infty L^j n(L,t)dL \tag{1-8}$$

where m_j is the jth moment. Substituting Equation (1-8) into Equation (1-2) results in

$$\frac{\partial m_j}{\partial t} - 0^j B(t) - j\int_0^\infty L^{j-1}(t)n(L,t)G(L,t)dL = \int_0^\infty (B-D)dL \tag{1-9}$$

With negligible breakage and size-independent growth rate, Eq. (1-9) can be simplified to

$$\frac{dm_j(t)}{dt} = 0^j B(t) + jG(t)m_{j-1}(t) \tag{1-10}$$

The zeroth to third moments correspond to the total number, total length, total area and total volume of all particles that can be measured by focused beam reflectance measurement (FBRM). The average crystal size can be obtained from $\frac{m_j}{m_{j-1}}$.

The advantage of MOM is that the computational process is relatively simple compared to other methods. The main drawback is that it cannot generate the crystal size distribution (Abbas and Romagnoli, 2007) and it does not work when the kinetic rate is non-linear and size-dependent (Sheikholeslamzadeh, 2013).

1.1.4.2.2 Method of characteristics

The method of characteristics can convert a partial differential equation to a set of ordinary differential equations along the characteristic length. In the case of the population balance equation in crystallization process, the crystal size L is gridded into finite bins, and Eq. (1-4) can be transformed into a finite set of ODEs in terms of particle number density (or particle number) in each size bin, as shown in Eq. (1-11)

$$\frac{\partial n(t,L)}{\partial t} = \frac{G_{j-1}N_{j-1} - G_j N_j}{\Delta L} + \frac{D_{j+1}N_{j-1} - D_j N_j}{\Delta L} \tag{1-11}$$

where ΔL is the spatial step. Compared to the method of moment, the method of characteristics is more advance in the aspect of preserving the crystal size distribution, but it is much more computationally expensive, especially when solving complex systems with small crystal size bins (Lim et al., 2002). The combined method of moments and method of characteristics can solve the PBE accurately with reduced computational cost (Aamir et al., 2009).

1.1.4.2.3 High-resolution finite volume method

High-resolution methods were developed for solving the nonlinear hyperbolic equation, which is common in engineering applications as it describes the dynamics of material, energy, momentum, and population balances (Gunawan et al., 2004b).

$$\frac{\partial n}{\partial t} + G\frac{\partial n}{\partial L} = 0 \tag{1-12}$$

Eq. (1-12) is a simplified population balance equation with a size-independent growth rate ($G > 0$). Numerical difficulties arise when the spatial derivative $\frac{\partial n}{\partial L}$ is very large. For example, the nucleation events can create a significant peak of n at the smallest size grid, leading to a large spatial gradient. Despite the numerical stability, the first-order methods (e.g., upwind scheme) tend to produce numerical diffusion, where the solution is smeared or damped (Figure 1-6 a). The second-order methods (e.g., Lax-Wendroff scheme) introduce numerical dispersion where the local spatial derivative is large, causing nonphysical oscillations in the solutions (Figure 1-6 b) (Morton and Mayers, 1994).
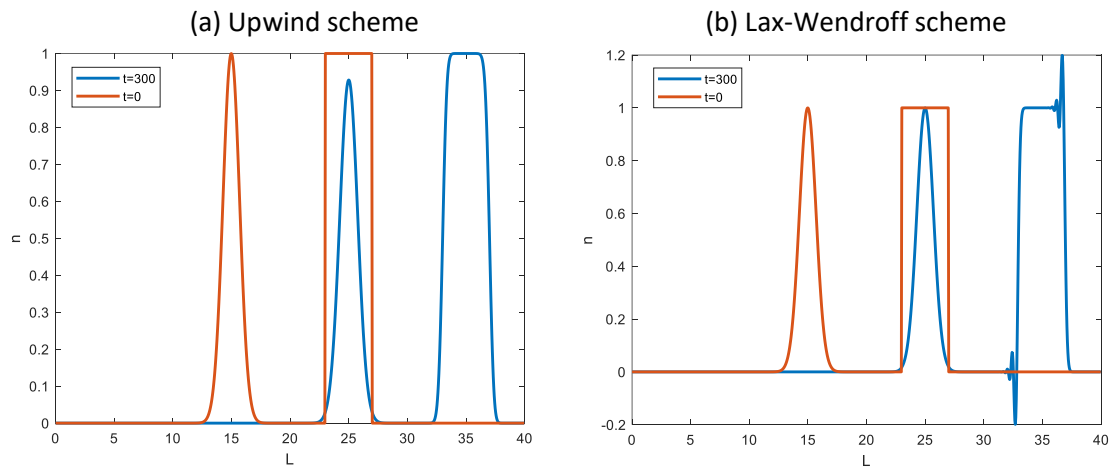
Figure 1-6. Demonstration of numerical diffusion and dispersion in first-order and second-order methods

The high-resolution (HR) methods are designed to leverage both the stability of the first-order methods near the discontinuity and the accuracy and shape-preservation of the second-order methods where the solution is smooth. Modern high-resolution methods are derived from the integral representation for the underlying conservation equations, so they are categorized as finite volume methods (FVMs). This implies the conservation of the interested properties and the accurate simulation of the growth rate kinetics without further specialized processes as required by finite difference methods. Discretizing Eq. (1-12) with discrete FVM method results in Eq. (1-13)

$$n_k^m = n_k^{m-1} + F(\Delta t, \Delta L, n, G) \tag{1-13}$$

where n_k is the k-th element of the discretized size distribution; L_k is the characteristic size of the k-th discretized channel; ΔL and Δt are the spatial and time step size,

respectively; F is the spatial discretization function that can be computed with low-order (upwind scheme) or high-order (Lax-Wendroff scheme) methods (Eq.(1-14)).

$$F = \begin{cases} -\dfrac{G\Delta t}{\Delta L}\left(n_k^{m-1} - n_{k-1}^{m-1}\right), & \text{Upwind } \left(F^{low}\right) \\[4mm] -\dfrac{G\Delta t}{2\Delta L}\left(n_{k+1}^{m-1} - n_{k-1}^{m-1}\right) - \dfrac{(G\Delta t)^2}{2\Delta L^2}\left(2n_k^{m-1} - n_{k-1}^{m-1} - n_{k+1}^{m-1}\right), & \text{Lax-Wendroff } \left(F^{high}\right) \end{cases}$$

$$(1\text{-}14)$$

In high-resolution finite volume methods (HRFVM), the spatial discretization function can switch between the schemes depending on the local derivative of the size distribution with a flux limiter, $\phi(\theta)$. The combined function becomes Eq. (1-15). When $\phi \to 0$, the local derivative is large, it weighs more on the low-order scheme to improve stability ($F^{HR} = F^{low}$). When $\phi \geq 1$, the local derivative is small, so the high-order scheme is emphasized to improve accuracy. Since ϕ is a continuous function, the weights on low-order and high-order schemes are continuously adjusted.

$$F^{HR} = F^{loßw} - \phi(\theta)\left(F^{low} - F^{high}\right) \qquad (1\text{-}15)$$

The flux limiter selectively weighs on low-order and high-order methods depending on the local degree of smoothness (θ) of the size distribution (Eq. (1-17)). In the corner cases when the denominator is zero, θ_k is set to zero; if both numerator and denominator are zero, θ_k is set to 2 (Rajagopalan et al., 2015).

$$\theta_k = \frac{n_k - n_{k-1}}{n_{k+1} - n_k} \qquad (1\text{-}16)$$

Many flux limiters have been proposed, with each one leading to a different high-resolution method. The Van Leer limiter (Eq. (1-17)) provides full second-order accuracy and is proven to work well in the population balance equations.

$$\phi(\theta_k) = \frac{\theta_k + |\theta_k|}{1 + |\theta_k|} \qquad (1\text{-}17)$$

Figure 1-7 demonstrates the Van Leer flux limiter versus local smoothness, θ. When $\theta <$ 0, the local derivative crosses zero, prompting an aggressive local gradient. Therefore, ϕ is capped to zero to switch the low-order method for stability. When $\theta > 0$, the increasing θ indicates the trend of the size distribution is getting flatter, i.e., the absolute derivative is getting smaller. In this case, ϕ increases monotonically with θ so that the high-order scheme starts to play more significantly.
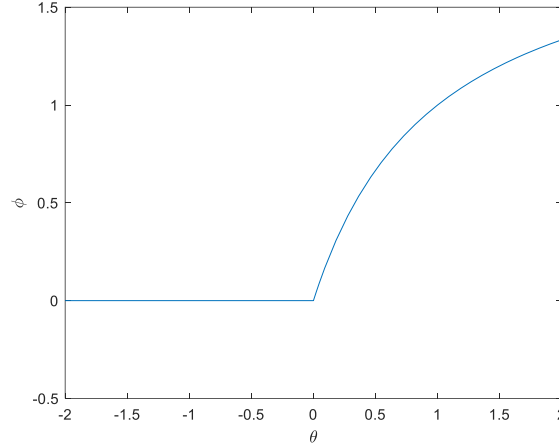
Figure 1-7. Van Leer flux limiter

In this algorithm, the computation of n_k^{m+1} depends on the values of n_{k-2}^m. It is common to assume that these virtual channels to be zero (Gunawan et al., 2004b). When primary and secondary nucleation kinetics are considered, the new-born particles are added to the first channel

$$n_1^m = n_1^m + B \frac{\Delta t}{\Delta L} \tag{1-18}$$

where n_1 is the number density in the first channel; and B is the combined primary and secondary nucleation rate $[s^{-1} \cdot m^{-3}]$ (Rajagopalan et al., 2015).

$$n_k^{m+1} = n_k^m - \frac{G\Delta t}{\Delta L}[n_k^m - n_{k-1}^m] - \frac{G\Delta t}{2\Delta L}\left(1 - \frac{G\Delta t}{\Delta L}\right)[(n_{k+1}^m - n_k^m)\phi_k - (n_k^m - n_{k-1}^m)\phi_{k-1}]$$

$$\tag{1-19}$$

$$n_k^{m+1} = n_k^m + \frac{G\Delta t}{\Delta L}[n_k^m - n_{k+1}^m] + \frac{G\Delta t}{2\Delta L}\left(1 + \frac{G\Delta t}{\Delta L}\right)[(n_{k-1}^m - n_k^m)\phi_k - (n_k^m - n_{k+1}^m)\phi_{k+1}]$$

(1-20)

In summary, the HRFVM discretization of the population balance equation is formulated as Eq. (1-19) for growth ($G > 0$) and Eq. (1-20) for dissolution ($G < 0$). Practically, given the arbitrary spatial step size ΔL, the time step size Δt can be determined with the Courant-Friedrichs-Levy (CFL) condition as in Eq. (1-21) (Gunawan et al., 2004b). By using a smaller α, the time step is divided finer, and the result is more accurate at the cost of computational time, and vice versa.

$$\left| \frac{G\Delta t}{\Delta L} \right| = \alpha \leq 1 \tag{1-21}$$

Figure 1-8 depicts the solution computed with the HRFVM algorithm. Compared to the pure upwind and Lax-Wendroff schemes, the HRFVM is showing minimum numerical dispersion and diffusion, prompting it as an effective approach to numerically solve the population balance equations.
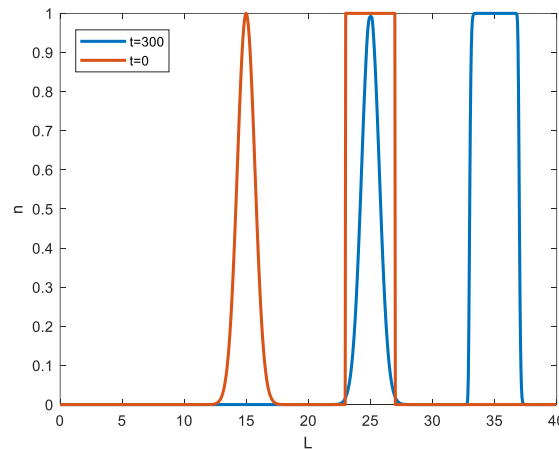
Figure 1-8. Demonstration of HRFVM solution

1.1.5 **Control of crystallization processes**

Crystallization process control is gaining increasing attention and popularity in industry and academic research. Various applications have shown the potentials of crystallization controls including controlling the bioavailability of active pharmaceutical ingredients (APIs), improving the purity of solids products, ensuring the polymorphic stability of

crystals for shelf life, and adjusting the size and shape of the crystals for better downstream processability (Nagy et al., 2013b).

In 2004, The United States Food and Drug Administration (FDA) introduced guidance related to the concept of quality-by-design (QbD) and the use of process analytical technology (PAT) for manufacturing pharmaceutical products (U.S. Food and Drug Administration/Department of Health and Human Services, 2004). The QbD is based on the understanding of the crystallization processes using experiments and modeling techniques to archive the desired product specification and minimize the variability in the product quality. Thirunahari et al. implemented the QbD-based crystallization of tolbutamide with the aid of in-situ PATs to screen the desired polymorph of the products for better downstream processability (Thirunahari et al., 2011). Tulcidas et al. studied the mixing condition in an anti-solvent crystallization process under the framework of QbD to minimize the failure and out-of-specification batches (Tulcidas et al., 2019).

The strategy of quality-by-control (QbC) was developed to complement the QbD, which encourages using feedback control approaches to determine operating trajectories instead of following the predefined optimal operating conditions found in the design stage. The tuned feedback control can reduce the impacts of disturbances and further reduce the product variations and therefore improve the process robustness (Yang et al., 2015). The recent development of online PAT tools enables the effective feedback control and the implementations of QbC concept in crystallization processes (Acevedo et al., 2016; Ma and Wang, 2012; Nagy et al., 2013c). The control of crystal size distribution (CSD) is particularly important since it has a significant impact on the efficiency of downstream operations, where typically large and uniform crystals are desired, whereas fine or broadly distributed particles can cause problems during the filtration and drying processes. However, the control of CSD is still a challenging task because of the stochastic nature of nucleation and the limit and precision of the online PAT tools (Yang et al., 2015).
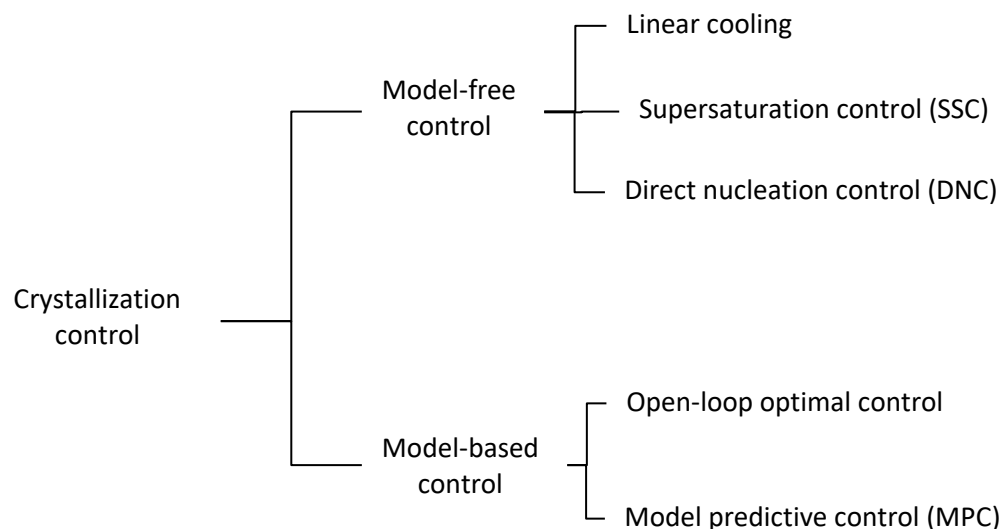
Figure 1-9. Crystallization process control techniques *(Nagy et al., 2013c)*

Various control approaches have been proposed to solve this challenge and control CSD in a crystallization process, which can be categorized into model-based and model-free control strategies (Figure 1-9). Model-based control strategies emerged since the pioneering works by Mullin ((Jones and Mullin, 1974; Mullin and Nývlt, 1971)), which showed the advantages of a programmed optimal cooling profile. Since then, major progress has been made and enabled the model-based control of various important product qualities. The model-based control involves solving the population balance model (PBM) iteratively to optimize the product qualities (e.g., CSD and polymorphism) subject to a set of constraints due to equipment limitations (e.g. temperature range, cooling rates limit, antisolvent addition rate limit, etc.) as well as the productivity constraint that ensures the desired yield at the end of the batch (Corriou and Rohani, 2008). Computational fluid dynamics (CFD) is an auxiliary method for analyzing the flow fields along with the PBM. This is a helpful tool to associate the different geometries and operations of the crystallizers to the temperature and the concentration profiles. The major advantage of the model-based control is the smaller number of experiments required for identifying the system due to the theoretical modeling techniques. Majumder and Nagy (Majumder and Nagy, 2013) predicted the shape distribution of potassium dihydrogen phosphate in the presence of additives by solving the PBE in combination of the crystal impurity model. Furthermore, a crystallization control strategy was designed for the process based on the proposed model. Su et al. (Su et al., 2015) developed a general and robust mathematical model to transform

from a batch operation into a continuous process. A PI (proportional-integral) controller was designed to ensure that the start-up and normal operation fell within the same design-space as the batch operation by maintaining the concentration near the designed optimal profile, which demonstrates its ability of generalization and operating against uncertainties.

Model predictive control (MPC) is a promising model-based control strategy, which controls the system by continuously performing optimization in a prediction horizon that shifts over time with the model and measured outputs. Yang and Nagy (Yang and Nagy, 2015) applied a model predictive control to a two-stage MSMPR crystallizer based to optimize the CSD and yield by adjusting the temperatures and anti-solvent dosing rate in cooling and anti-solvent crystallization. Hermanto et al. (Hermanto et al., 2010) developed an MPC for a polymorphic transformation process (L-glutamic acid) to minimize batch-to-batch variations. The open problems associated with the model-based technique are the deficiency of the kinetic models and the assumptions to approximate the CSD due to the lack of understanding of the process, which can affect the model accuracy and pose a negative impact on the control performance (Nagy and Braatz, 2012).

Model-free control strategies involve the direct use of online measurements and are widely used because of their simplicity, which has been applied in the control of CSD, crystal shape, and polymorph (Powell et al., 2015). Figure 1-9 lists several widely used model-free control approaches. The linear cooling is a simple strategy that is usually used when exploring the crystallization process, so they are often discussed separately from the other novel techniques. Supersaturation control (SSC) is based on the theory to control the crystallization process by adjusting the temperature or antisolvent addition to maintain the supersaturation constant or optimal to maintain minimal unwanted nucleation while keeping high growth rate to ensure high productivity (Hansen et al., 2017). Often this strategy can result in close to optimal crystallization performance after only a few experiments (Nagy et al., 2013c). Direct nucleation control (DNC) is a novel model-free control that directly measures the particle counts with online PATs (e.g., FBRM) and removes fine particles by rapid switching between heating and cooling or solvent or antisolvent addition strategies. The advantages of the DNC have been verified for producing the crystals with a desired mean size (Saleemi et al., 2012b) or polymorphic

form (Bakar et al., 2009). Kacker et al. (Kacker et al., 2016) used microwave heating to eliminate the limitations of heat transfer caused by the traditional approaches, which resulted in a fast fine-removal response during DNC applications and significantly reduced the batch time. Yang et al. (Yang et al., 2015) proposed a DNC to reduce the startup time required for a continuous crystallization process by quickly nucleating the desired number of crystals under the monitoring of FBRM. They further investigate adopting the wet milling in a single-stage MSMPR system to facilitate nucleation and startup process (Yang et al., 2016).

Whether a model-based or a model-free control strategy is used, the crystallization kinetics and particle density in the system are always closely related to the product quality and productivity. For some simple systems that are fully described by a simple nucleation and growth models, the model-based control approach has the ability to exploit the optimal crystallization process and provides a safe process operation. On the other hand, for the systems that are prone to aggregation and breakage or demonstrating special phenomena that is difficult to describe in models (e.g., oiling-out), the model-free control has higher accuracy and flexibility. With the deepening understanding of the crystallization mechanism and rapid development of the online PAT tools, one can foresee the strong potential of the hybrid control strategy combining the model-based and model-free control strategies.

1.2   Research objectives and approach

1.2.1   Research objectives

Due to the hard-to-predict nature of polymorphism (Ainurofiq et al., 2020; Bernstein, 2008; Desiraju, 1997), the control of polymorphism remains challenging in pharmaceutical manufacturing. In this work, the main objective is to produce the desired polymorph of active pharmaceutical ingredients in crystallization processes based on the study of polymorphism phenomenon and process analytic technology.

The detailed objectives are:
- Study the thermodynamic and kinetic properties that are fundamental information for the crystallization process modeling and control.

- Develop a simple analytical method to quantitatively measure the solution concentration and slurry density to implement the real-time monitoring of the crystallization process.

- Study the impact of polymorph relative kinetics of a bi-polymorphic system on the polymorphic outcome, and provide a general approach to determine the optimal crystallization operation to harvest the desired polymorph in batch and continuous operation.

- Study the impacts of operating conditions on the product properties in batch and MSMPR crystallization, and offer general guidance for designing a crystallization process.

1.2.2   **Research approach**

In chapter 2, the polymorphs of imatinib mesylate were identified with powder X-ray diffraction (PXRD). Thermal properties, such as melting point and enthalpy, were measured by differential scanning calorimeter (DSC) and thermal gravimetric analysis (TGA). Optical microscopy and scanning electron microscopy (SEM) provided the morphologic information, and ultraviolet-visible spectroscopy (UV-Vis) was used to measure the solubility. The solution concentration and polymorphic composition of the solid phase during the solution or solution-mediated polymorphic transformation (SMPT) process were monitored by Raman spectroscopy and conductivity meter. The parameter estimation was performed with MATLAB optimization function, $fmincon$, based on the sequential quadratic programming (SQP) method. The population balance equation was solved by the method of characteristics and method of moments.

In chapter 3, the polymorphs of paracetamol and L-Glutamic acid were identified with powder X-ray diffraction (PXRD). The dataset was collected with the Simulink program. Three pre-processing methods (spectra range selection, baseline removal, direct orthogonal signal correction) and four multivariable analysis techniques (characteristic peaks regression (CPR), principal component regression (PCR), partial least squares regression (PLSR) and artificial neural network (ANN)) were applied to analyze the Raman

spectroscopy in MATLAB. Focused Beam Reflectance Method (FBRM) was used to monitor the crystal count.

The simulation of the crystallization process in chapter 4 and chapter 5 was conducted with MATLAB. In chapter 4, the population balance equation was solved by the high-resolution finite volume method. In chapter 5, the population balance equation was solved by the method of characteristics and method of moments.

1.3   Thesis organization

This thesis is in the integrated-article format.

Chapter 1 provides the research background, objectives, approach and thesis structure.

Chapter 2 presents the experimental study of a polymorphic system, including polymorph characterization, solubility measurement, polymorphic transformation, and kinetic parameter estimation.

Chapter 3 discusses the monitoring of the crystallization process of the polymorphic systems. The capability of Raman spectroscopy on in-situ measuring the solution concentration and slurry density was investigated.

Chapter 4 studies the impacts of relative kinetics of the two polymorphs on the polymorphic outcome numerically in batch and MSMPR crystallizers. The investigation of optimal operations for the desired polymorph in both modes of operations is also included.

Chapter 5 reports the effects of the operating conditions in batch and MSMPR crystallization on the crystal properties, including the polymorphism, yield and crystal size distribution. The intermittent seeding and withdrawal strategy has been proven to alter the steady-state conditions and avoid the clogging issue during the suspension transport in MSMPR crystallization.

Chapter 6 consists of the conclusions and recommendations for future works. The Matlab codes developed for the process modeling and data analysis are listed in the Appendix.

1.4 References

Aamir, E., Nagy, Z.K., Rielly, C.D., Kleinert, T., Judat, B., 2009. Combined Quadrature Method of Moments and Method of Characteristics Approach for Efficient Solution of Population Balance Models for Dynamic Modeling and Crystal Size Distribution Control of Crystallization Processes. Ind. Eng. Chem. Res. 48, 8575–8584. https://doi.org/10.1021/ie900430t

Abbas, A., Romagnoli, J.A., 2007. Multiscale modeling, simulation and validation of batch cooling crystallization. Separation and Purification Technology, Biological & Pharmaceutical Products Development Symposium 53, 153–163. https://doi.org/10.1016/j.seppur.2006.06.027

Abu Bakar, M.R., Nagy, Z.K., Saleemi, A.N., Rielly, C.D., 2009. The Impact of Direct Nucleation Control on Crystal Size Distribution in Pharmaceutical Crystallization Processes. Crystal Growth & Design 9, 1378–1384. https://doi.org/10.1021/cg800595v

Acevedo, D.A., Ling, J., Chadwick, K., Nagy, Z.K., 2016. Application of process analytical technology-based feedback control for the crystallization of pharmaceuticals in porous media. Crystal Growth and Design 16, 4263–4271. https://doi.org/10.1021/acs.cgd.6b00303

Ainurofiq, A., Dinda, K.E., Pangestika, M.W., Himawati, U., Wardhani, W.D., Sipahutar, Y.T., 2020. The effect of polymorphism on active pharmaceutical ingredients: A review. International Journal of Research in Pharmaceutical Sciences 11, 1621–1630. https://doi.org/10.26452/ijrps.v11i2.2044

Alvarez, A.J., Myerson, A.S., 2010. Continuous Plug Flow Crystallization of Pharmaceutical Compounds. Crystal Growth & Design 10, 2219–2228. https://doi.org/10.1021/cg901496s

Bakar, M.R.A., Nagy, Z.K., Rielly, C.D., 2009. Seeded batch cooling crystallization with temperature cycling for the control of size uniformity and polymorphic purity of sulfathiazole crystals. Organic Process Research and Development 13, 1343–1356. https://doi.org/10.1021/op900174b

Bárkányi, Á., Németh, S., Lakatos, B.G., 2013. Modeling and simulation of suspension polymerization of vinyl chloride via population balance model. Computers &

Chemical Engineering 59, 211–218. https://doi.org/10.1016/j.compchemeng.2013.06.008

Bernstein, J., 2008. Crystal Polymorphism, in: Novoa, J.J., Braga, D., Addadi, L. (Eds.), Engineering of Crystalline Materials Properties, NATO Science for Peace and Security Series B: Physics and Biophysics. Springer Netherlands, Dordrecht, pp. 87–109. https://doi.org/10.1007/978-1-4020-6823-2_5

Bhoi, S., Sarkar, D., 2016. Modeling and experimental validation of ultrasound assisted unseeded batch cooling crystallization of L -asparagine monohydrate. CrystEngComm 18, 4863–4874. https://doi.org/10.1039/C6CE00937A

Borsos, Á., Szilágyi, B., Agachi, P.Ş., Nagy, Z.K., 2017. Real-Time Image Processing Based Online Feedback Control System for Cooling Batch Crystallization. Org. Process Res. Dev. 21, 511–519. https://doi.org/10.1021/acs.oprd.6b00242

Corriou, J.-P., Rohani, S., 2008. A new look at optimal control of a batch crystallizer. AIChE Journal 54, 3188–3206. https://doi.org/10.1002/aic.11614

Desiraju, G.R., 1997. Crystal Gazing: Structure Prediction and Polymorphism. Science 278, 404–405.

Garcia, E., Veesler, S., Boistelle, R., Hoff, C., 1999. Crystallization and dissolution of pharmaceutical compounds: An experimental approach. Journal of Crystal Growth 198–199, 1360–1364. https://doi.org/10.1016/S0022-0248(98)01023-9

Gunawan, R., Fusman, I., Braatz, R.D., 2004a. High resolution algorithms for multidimensional population balance equations. AIChE Journal 50, 2738–2749. https://doi.org/10.1002/aic.10228

Gunawan, R., Fusman, I., Braatz, R.D., 2004b. High resolution algorithms for multidimensional population balance equations. AIChE Journal 50, 2738–2749. https://doi.org/10.1002/aic.10228

Hansen, T.B., Simone, E., Nagy, Z., Qu, H., 2017. Process Analytical Tools to Control Polymorphism and Particle Size in Batch Crystallization Processes. Organic Process Research and Development 21, 855–865. https://doi.org/10.1021/acs.oprd.7b00087

Hermanto, M.W., Braatz, R.D., Chiu, M.-S., 2010. Integrated Batch-to-Batch and Nonlinear Model Predictive Control for Polymorphic Transformation in Pharmaceutical Crystallization. AIChE Journal. https://doi.org/10.1002/aic.12331

Hounslow, M.J., Ryall, R.L., Marshall, V.R., 1988. A discretized population balance for nucleation, growth, and aggregation. AIChE Journal 34, 1821–1832. https://doi.org/10.1002/aic.690341108

Hulburt, H.M., Katz, S., 1964. Some problems in particle technology. Chemical Engineering Science 19, 555–574. https://doi.org/10.1016/0009-2509(64)85047-8

John, V., Mitkova, T., Roland, M., Sundmacher, K., Tobiska, L., Voigt, A., 2009. Simulations of population balance systems with one internal coordinate using finite element methods. Chemical Engineering Science, 3rd International Conference on Population Balance Modeling 64, 733–741. https://doi.org/10.1016/j.ces.2008.05.004

Jones, A.G., Mullin, J.W., 1974. Programmed cooling crystallization of potassium sulphate solutions. Chemical Engineering Science 29, 105–118. https://doi.org/10.1016/0009-2509(74)85036-0

Kacker, R., Salvador, P.M., Sturm, G.S.J., Stefanidis, G.D., Lakerveld, R., Nagy, Z.K., Kramer, H.J.M., 2016. Microwave Assisted Direct Nucleation Control for Batch Crystallization: Crystal Size Control with Reduced Batch Time. Crystal Growth and Design 16, 440–446. https://doi.org/10.1021/acs.cgd.5b01444

Lee, A.Y., Erdemir, D., Myerson, A.S., 2011. Crystal Polymorphism in Chemical Process Development. Annual Review of Chemical and Biomolecular Engineering 2, 259–280. https://doi.org/10.1146/annurev-chembioeng-061010-114224

Li, J., Trout, B.L., Myerson, A.S., 2016. Multistage Continuous Mixed-Suspension, Mixed-Product Removal (MSMPR) Crystallization with Solids Recycle. Org. Process Res. Dev. 20, 510–516. https://doi.org/10.1021/acs.oprd.5b00306

Lim, Y.I., Le Lann, J.-M., Meyer, X.M., Joulia, X., Lee, G., Yoon, E.S., 2002. On the solution of population balance equations (PBE) with accurate front tracking methods in practical crystallization processes. Chemical Engineering Science 57, 3715–3732. https://doi.org/10.1016/S0009-2509(02)00236-1

Ma, C.Y., Wang, X.Z., 2012. Closed-loop control of crystal shape in cooling crystallization of l-glutamic acid. Journal of Process Control 22, 72–81. https://doi.org/10.1016/j.jprocont.2011.10.007

Majumder, A., Nagy, Z.K., 2013. Prediction and control of crystal shape distribution in the presence of crystal growth modifiers. Chemical Engineering Science 101, 593–602. https://doi.org/10.1016/j.ces.2013.07.017

Marchal, P., David, R., Klein, J.P., Villermaux, J., 1988. Crystallization and precipitation engineering—I. An efficient method for solving population balance in crystallization with agglomeration. Chemical Engineering Science 43, 59–67. https://doi.org/10.1016/0009-2509(88)87126-4

Mondal, P.K., Rao, V., Mittapalli, S., Chopra, D., 2017. Exploring Solid State Diversity and Solution Characteristics in a Fluorine-Containing Drug Riluzole. Crystal Growth & Design 17, 1938–1946. https://doi.org/10.1021/acs.cgd.6b01894

Morton, K.W., Mayers, D.F., 1994. Numerical Solution of Partial Differential Equations. An Introduction. Cambridge University Press.

Mullin, J.W., 2001. Crystallization. Elsevier.

Mullin, J.W., Nývlt, J., 1971. Programmed cooling of batch crystallizers. Chemical Engineering Science 26, 369–377. https://doi.org/10.1016/0009-2509(71)83012-9

Myerson, A., 2002. Handbook of Industrial Crystallization. Butterworth-Heinemann.

Myerson, A.S. (Ed.), 2002. Handbook of industrial crystallization, 2nd ed. ed. Butterworth-Heinemann, Boston.

Nagy, Z.K., Braatz, R.D., 2012. Advances and new directions in crystallization control. Annual Review of Chemical and Biomolecular Engineering 3, 55–75. https://doi.org/10.1146/annurev-chembioeng-062011-081043

Nagy, Z.K., Fevotte, G., Kramer, H., Simon, L.L., 2013a. Recent advances in the monitoring, modeling and control of crystallization systems. Chemical Engineering Research and Design, The 60th Anniversary of the European Federation of Chemical Engineering (EFCE) 91, 1903–1922. https://doi.org/10.1016/j.cherd.2013.07.018

Nagy, Z.K., Fevotte, G., Kramer, H., Simon, L.L., 2013b. Recent advances in the monitoring, modeling and control of crystallization systems. Chemical Engineering Research and Design 91, 1903–1922. https://doi.org/10.1016/j.cherd.2013.07.018

Nagy, Z.K., Fevotte, G., Kramer, H., Simon, L.L., 2013c. Recent advances in the monitoring, modeling and control of crystallization systems. Chemical Engineering Research and Design. https://doi.org/10.1016/j.cherd.2013.07.018

Nicmanis, M., Hounslow, M.J., 1998. Finite-element methods for steady-state population balance equations. AIChE Journal 44, 2258–2272. https://doi.org/10.1002/aic.690441015

Omar, H.M., Rohani, S., 2017. Crystal Population Balance Formulation and Solution Methods: A Review. Crystal Growth & Design 17, 4028–4041. https://doi.org/10.1021/acs.cgd.7b00645

Powell, K.A., Bartolini, G., Wittering, K.E., Saleemi, A.N., Wilson, C.C., Rielly, C.D., Nagy, Z.K., 2015. Toward Continuous Crystallization of Urea-Barbituric Acid: A Polymorphic Co-Crystal System. Crystal Growth and Design 15, 4821–4836. https://doi.org/10.1021/acs.cgd.5b00599

Qamar, S., Warnecke, G., Elsner, M.P., 2009. On the solution of population balances for nucleation, growth, aggregation and breakage processes. Chemical Engineering Science 64, 2088–2095. https://doi.org/10.1016/j.ces.2009.01.040

Qu, H., Alatalo, H., Hatakka, H., Kohonen, J., Louhi-Kultanen, M., Reinikainen, S.-P., Kallas, J., 2009. Raman and ATR FTIR spectroscopy in reactive crystallization: Simultaneous monitoring of solute concentration and polymorphic state of the crystals. Journal of Crystal Growth 311, 3466–3475. https://doi.org/10.1016/j.jcrysgro.2009.04.018

Rajagopalan, A.K., Ochsenbein, D., Iggland, M., 2015. Crystallization Analysis Toolbox.

Ramkrishna, D., 2000. Population Balances: Theory and Applications to Particulate Systems in Engineering. Elsevier.

Randolph, A., Larson, M., 1971. Theory of Particulate Processes: Analysis and Techniques of Continuous Crystallization. Elsevier.

Raw, A.S., Furness, M.S., Gill, D.S., Adams, R.C., Holcombe, F.O., Yu, L.X., 2004. Regulatory considerations of pharmaceutical solid polymorphism in Abbreviated New Drug Applications (ANDAs). Advanced Drug Delivery Reviews, Pharmaceutical solid polymorphism in drug development and regulation 56, 397–414. https://doi.org/10.1016/j.addr.2003.10.011

Saleemi, A., Rielly, C., Nagy, Z.K., 2012a. Automated direct nucleation control for in situ dynamic fines removal in batch cooling crystallization. CrystEngComm 14, 2196–2203. https://doi.org/10.1039/C2CE06288G

Saleemi, A., Rielly, C., Nagy, Z.K., 2012b. Automated direct nucleation control for in situ dynamic fines removal in batch cooling crystallization. CrystEngComm 14, 2196. https://doi.org/10.1039/c2ce06288g

Sheikholeslamzadeh, E., 2013. Pharmaceutical Process Modeling, Optimization, and Control.

Smith, M., Matsoukas, T., 1998. Constant-number Monte Carlo simulation of population balances. Chemical Engineering Science 53, 1777–1786. https://doi.org/10.1016/S0009-2509(98)00045-1

Stahly, G.P., 2007. Diversity in Single- and Multiple-Component Crystals. The Search for and Prevalence of Polymorphs and Cocrystals. Crystal Growth & Design 7, 1007–1026. https://doi.org/10.1021/cg060838j

Su, Q., Nagy, Z.K., Rielly, C.D., 2015. Pharmaceutical crystallisation processes from batch to continuous operation using MSMPR stages: Modeling, design, and control. Chemical Engineering and Processing: Process Intensification 89, 41–53. https://doi.org/10.1016/j.cep.2015.01.001

Szilágyi, B., Borsos, Á., Pal, K., Nagy, Z.K., 2019. Experimental implementation of a Quality-by-Control (QbC) framework using a mechanistic PBM-based nonlinear model predictive control involving chord length distribution measurement for the batch cooling crystallization of l-ascorbic acid. Chemical Engineering Science 195, 335–346. https://doi.org/10.1016/j.ces.2018.09.032

Tandon, P., Rosner, D.E., 1999. Monte Carlo Simulation of Particle Aggregation and Simultaneous Restructuring. Journal of Colloid and Interface Science 213, 273–286. https://doi.org/10.1006/jcis.1998.6036

Thirunahari, S., Chow, P.S., Tan, R.B.H., 2011. Quality by design (QbD)-based crystallization process development for the polymorphic drug tolbutamide. Crystal Growth and Design 11, 3027–3038. https://doi.org/10.1021/cg2003029

Tsang, T.H., Rao, A., 1990. A moving finite element method for the population balance equation. International Journal for Numerical Methods in Fluids 10, 753–769. https://doi.org/10.1002/fld.1650100704

Tulcidas, A., Santos, B., Pawlowski, S., Rocha, F., 2019. Quality by Statistical Control in Crystallization - Assessment of Mixing Conditions and Probability of Obtaining the

Desired Particle Size. Industrial and Engineering Chemistry Research 58, 20162–20172. https://doi.org/10.1021/acs.iecr.9b04023

U.S. Food and Drug Administration/Department of Health and Human Services, 2004. Guidance for Industry Guidance for Industry PAT — A Framework for Innovative Pharmaceutical.

Variankaval, N., Cote, A.S., Doherty, M.F., 2008. From form to function: Crystallization of active pharmaceutical ingredients. AIChE Journal 54, 1682–1688. https://doi.org/10.1002/aic.11555

Yang, X., Lu, J., Wang, X., Ching, C.B., 2008. *In situ* monitoring of the solution-mediated polymorphic transformation of glycine: characterization of the polymorphs and observation of the transformation rate using Raman spectroscopy and microscopy. J. Raman Spectrosc. 39, 1433–1439. https://doi.org/10.1002/jrs.2016

Yang, Y., Nagy, Z.K., 2015. Application of nonlinear model predictive control in continuous crystallization systems. Proceedings of the American Control Conference 2015-July, 4282–4287. https://doi.org/10.1109/ACC.2015.7172002

Yang, Y., Song, L., Nagy, Z.K., 2015. Automated Direct Nucleation Control in Continuous Mixed Suspension Mixed Product Removal Cooling Crystallization. Crystal Growth and Design. https://doi.org/10.1021/acs.cgd.5b01219

Yang, Y., Song, L., Zhang, Y., Nagy, Z.K., 2016. Application of wet milling-based automated direct nucleation control in continuous cooling crystallization processes. Industrial and Engineering Chemistry Research 55, 4987–4996. https://doi.org/10.1021/acs.iecr.5b04956

Zhang, X., Yin, Q., Gong, J., Liu, Z., 2010. Solubility of 5-Amino-N,N′-bis(2,3-dihydroxypropyl)-2,4,6-triiodobenzene-1,3-dicarboxamide in Ethanol + Water Mixtures. J. Chem. Eng. Data 55, 2355–2357. https://doi.org/10.1021/je9008156

Chapter 2

A Kinetic Study of Crystallization Process of Imatinib Mesylate with Polymorphic Transformation Phenomenon

2 A Kinetic Study of Crystallization Process of Imatinib Mesylate with Polymorphic Transformation Phenomenon

Abstract

For pharmaceutical crystallization design and control, the kinetics of nucleation and growth of crystals are significant parameters, especially for the system exhibiting polymorphic transformation. In this study, imatinib mesylate, whose solubility, nucleation and growth kinetics are lacking in the literature, was thoroughly explored in the aspects of characterization, solubility and polymorphic transformation, and evaluation of nucleation and growth rate. Two forms of imatinib mesylate, α and β, were characterized by X-ray powder diffraction, scanning electron microscopy and differential scanning calorimetry. The solubility measurement of the two forms was performed with ultraviolet–visible spectroscopy in three solvents from 278.15 to 333.15 K at atmospheric pressure. The results indicated the β-form is more stable in methanol,1-propanol, and 2-propanol under the experimental condition. The solubility order is methanol >1-propanol >2-propanol. The solution-mediated polymorphic transformation (SMPT) of imatinib mesylate from α-form to β-form was studied with the in-situ Raman spectroscopy and conductivity meter. It is found that the SMPT process of imatinib mesylate from α-form to β-form in methanol is controlled by nucleation and growth of β-form. Finally, the nucleation and grow rate of β-form of imatinib mesylate were estimated by minimizing the difference between the calculated and experimental solution concentration with MATLAB optimization function.

2.1   Introduction

Depending on the arrangement of molecules, a solid can be a crystal, a quasicrystal or an amorphous. A phenomenon called polymorphism, exists widely in the crystalline solids, especially in organic compounds(Stahly, 2007). Even though polymorphs have the same molecular formula, they are different in molecular conformations and/or packing arrangements in the solid state, resulting in the distinct physical and chemical properties, such as morphology, melting point, flow properties, mechanical properties, solubility, and Gibbs free energy(Myerson, 2002). In terms of active pharmaceutical ingredients (API), polymorphism would affect the processability, bioavailability and stability of the API(Lee

et al., 2011). Therefore, the identification and control of polymorphs of a given API are essential for the pharmaceutical industry.

Comparing with the stable polymorph, the metastable polymorph has higher solubility and Gibbs free energy. The divergence in Gibbs energy drives polymorphism to transit from the metastable form to the stable state. Generally, there are two ways to realize the transition: solid-state polymorphic transformation (SST) and solution-mediated polymorphic transformation (SMPT)(Mullin, 2001). The SMPT process consists of three steps: dissolution of the metastable form, nucleation of stable form, and growth of stable form. The slowest step of the SMPT process limits the whole transition rate. Based on the relative rate of dissolution, nucleation, and growth, O'Mahony et al. rationalized the SMPT process into four possible scenarios: dissolution-controlled, nucleation-dissolution-controlled, growth-controlled, nucleation-growth-controlled (O'Mahony et al., 2012).

In order to model and control a crystallization process, the kinetic parameters, namely nucleation rate, growth rate, dissolution rate, agglomeration, and breakage have to be determined first through experiments. For the nucleation and growth rate, there are three experimental methods commonly used to determine the nucleation and growth rate. The first one relies on the crystal size distribution of the final product obtained from a Mixed-Suspension, Mixed-Product Removal (MSMPR) crystallizer. The slope and intercept of the "particle number density vs. crystal size" curve provide the information necessary to extract the nucleation and growth rates (Myerson, 2002). The second method which is somewhat approximate, is based on the count and chord length distribution measured by the Focused Beam Reflectance Measurement (FBRM) device (Trifkovic et al., 2012). The change in the count of fine crystals presents the nucleation rate, while the change in average chord length refers to the growth rate. The last method uses a rigorous parameter estimation algorithm and works by finding a set of proper constants in the kinetic equations to minimize the difference between the experimental data (measured solute concentration and/or crystal size distribution) and modeling results (Morris et al., 2015).

The compound studied in this work is imatinib mesylate. Imatinib mesylate (Figure 2-1), chemically   4-[(4-methylpiperazin-1-yl)   methyl]-N-[4-methyl-3-[(4-pyridin-3-

ylpyrimidin-2-yl) amino]-phenyl] benzamide methanesulfonate, was developed by Novartis under the trade name "Gleevec/Glivec®" in the late1990s. It was designed as a protein tyrosine kinase inhibitor and shows a remarkable therapeutic effect in Philadelphia chromosome positive chronic myelogenous leukemia (CML) and metastatic malignant gastro intestinal stromal tumors (GISTs) (Al-Hadiya et al., 2014). Many polymorphs of crystalline imatinib mesylate have been observed by precipitating from a solution that consists of an organic solvent, imatinib base and methanesulfonic acid. The different solvents lead to different polymorphs of the final product (Amala et al., 2005; Kompella et al., 2006; M. Mutz, 2007; Mutz M., 2007; Parthasaradhi et al., 2003; Patel et al., 2006; Pathi et al., 2005; Zimmermann et al., 1999).

Table 2-1. Some patents about polymorphs of imatinib mesylate

Patent	Solvent	Polymorph	Ref.
WO 1999/03854	α: non-alcoholic solvents β: a suitable polar solvent, especially alcohol, most or also a ketone or mixtures thereof	Needle α and cubic β form	(Zimmermann et al., 1999)
WO 2004/106326	Chlorinated solvents	H1	(Parthasaradhi et al., 2003)
WO 2005/077933	isopropanol	$\alpha 2$	(Amala et al., 2005)
WO 2006/024863	Alcoholic solvents (C2 to C4 alcohols) or ketonic solvents.	Nonhygroscopic α crystalline form	(Pathi et al., 2005)
WO 2006/048890	A polar protic or aprotic solvent, a non-polar solvent, water or mixture thereof.	Non-Needle α form	(Kompella et al., 2006)
WO 2006/054314	Chloroform and water	I, II	(Patel et al., 2006)
WO 2007/023182	δ: acetone and methanol ε :ethyl acetate and ethanol	δ, ε	(Mutz M., 2007)
WO 2007/059963	F—benzyl Alcohol G—a mixture of 3-Pentanone and cyclohexane H—a mixture of 3-Pentanone and N.N-Dimethylformamide I—a mixture of Ethyl Acetate and Diethyl Ether K—a mixture of Ethyl Acetate and N,N-Dimethylformamide	F, G, H, I, K	(M. Mutz, 2007)

Among the dozens of polymorphs of imatinib mesylate, the α-form and the β-form proposed in WO99/03854 (Zimmermann et al., 1999) are the most frequent and commercialized. The cubic-shaped β-form has the lower hygroscopic ability, higher flow properties, and higher stability at temperatures below 140° C than the needle-shaped α-form, as summary in Table 2-2. Therefore, the β-form shows better performance than α-form in terms of processability, manufacturing, pharmaceutical preparation, and storage (Zimmermann et al., 2005).
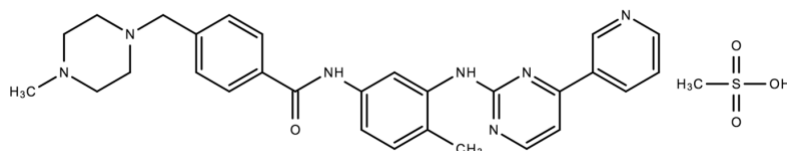
Figure 2-1. Schematic of imatinib mesylate

Table 2-2. Physical properties of α and β form imatinib mesylate

Imatinib mesylate	α-form	β-form
Crystal shape	needle-shaped	block-shaped
Hydroscopicity	hygroscopic	less hygroscopic
Stability	metastable	more stable at T<140° C
flow properties	unfavorable	more favorable

Grillo et al. revealed the crystal structure of α-form and β-form imatinib mesylate and found these two polymorphs have significantly different molecular conformations. By grinding them, the amorphous imatinib mesylate was produced that converted to a crystalline phase by either thermal treatment or aging (Grillo et al., 2012). Veverka et al. modified the morphology of α-form imatinib mesylate with various organic solvent mixtures by precipitation (Veverka et al., 2012). Srivastava et al. presented a comprehensive study of the vibrational spectroscopies of β-form with the FT-Raman and FT-IR spectra (Srivastava et al., 2013). The polymorphic composition of two polymorphs

mixture was determined quantitatively with PXRD, ATR-FTIR, and DSC in the literature (Bellur Atici and Karlığa, 2015). The results show that PXRD technique is more accurate than ATR-FTIR and DSC.

Despite the mentioned studies, the investigation of the imatinib mesylate properties, particularly those related to the crystallization process, was still lacking. The solubility data has not been published up to date. In this study, we measured the solubility of two forms of imatinib mesylate in three solvents (methanol, 1-propanol, and 2-propanol) from 278.15 to 333.15 K at atmospheric pressure to study their relative stability. Subsequently, the solution-mediated polymorphic transformation (SMPT) from metastable α-form to stable β-form was studied in-situ with Raman spectroscopy and conductivity meter. Finally, the nucleation and grow rate of β-form imatinib mesylate were estimated by minimizing the difference between the calculated and experimental solute concentration with MATLAB optimization function.

2.2   Material and experiments

2.2.1   Material

The α-form imatinib mesylate was supplied by Apotex Pharmachem Inc. (Brantford, ON, Canada) and used without any further processing. The β-form was obtained by the solution-mediated polymorphic transformation from α-form in methanol. The solvents (methanol, ethanol, isopropanol, n-propanol, 1-butanol, acetone, acetonitrile, and tetrahydrofuran) with HPLC grade were purchased from Sigma-Aldrich (Milwaukee, WI,) and no further purification was performed.

2.2.2   Characterization

2.2.2.1   Powder X-Ray Diffraction (PXRD)

The polymorphs of solid-state α-form and β-form imatinib mesylate were identified with powder X-ray diffraction (Rigaku, Miniflex, Tokyo, Japan) with the Cu-Kα source ((λ for Kα = 1.54059 Å) at room temperature. The conditions of voltage (30kV), current (15mA), scan angle (2° to 50°) and scan speed (2°/min) were kept the same for all samples.

2.2.2.2   Differential Scanning Calorimetry (DSC)

Thermal properties of crystals, such as melting point and enthalpy, were measured by differential scanning colorimeter ((DSC, Mettler Toledo, Chicago, United States). The samples (5-10 mg) were placed in a 40-μl aluminum crucible with a pierced lid for gas escaping and then heated from 25°C to 250°C with 10°C/min heating rate under nitrogen purge at a flow rate of 40 ml/min.

2.2.2.3   Optical microscopy and Scanning Electron Microscopy (SEM)

The optical microscopy (Axioskop 40, Carl Zeiss Light Microscopy, Germany) with a magnification of 500 times was used as an off-line method to give a rough judgement of the polymorphic composition of solid-state imatinib mesylate in suspension. Scanning electron microscope (LEO 1450XB，Zeiss, Oberkochen, Germany) was employed for detailed morphologic information. The samples have been coated with coated with 5 nm of osmium metal in Osmium Plasma Coater (OPC80T, Filgen Inc. Japan) before SEM testing.

2.2.2.4   Raman spectroscopy

A Raman RXN Analyzer spectroscopy (Kaiser Optical Systems, Inc., Ann Arbor, MI, USA) equipped with a diode laser (784.8-nm) and a fiber optic probe was applied to monitor the polymorphic composition of solid-phase during the SMPT process from α-form to β-form. The characteristic peaks of α-form and β-form of imatinib mesylate are at 1664 cm^{-1} and 1656 cm^{-1}, and the single point baseline is at 1640 cm^{-1}.

2.2.3   Solubility measurement

To study the stability of two forms, we used Ultraviolet-visible spectroscopy (UV-Vis, Cary Bio 100 spectrophotometer, Varian, Mississauga, ON) to measure the solubility of imatinib mesylate in methanol, 1-propanol, and 2-propanol. The calibration curve of "Absorbance-Concentration" should be determined with a series of known concentration solutions at room temperature at first. The characteristic UV-Vis absorption band at 271-nm and 275-nm was applied for quantification in methanol and propanol, respectively. Then, an excessive sample was added to the selected solvent in a 5-ml glass vial. The vials

were immersed in a constant temperature bath with an accuracy of 0.1 °C and agitated for several hours at a specific temperature to reach equilibrium. After 30 mins standing, the supernatant was taken by a syringe and filtered with a 0.45-µm membrane syringe filter (VWR, Mississauga, ON), followed by proper dilution and concentration measurement with UV-Vis. The excess solids in the vials were filtered, dried, and checked with PXRD.

As the α-form imatinib mesylate transformed to β-form in methanol during the solubility measurement，the solubility of α-form imatinib mesylate was determined during the transition process (see Section 2.2.4 for more details).
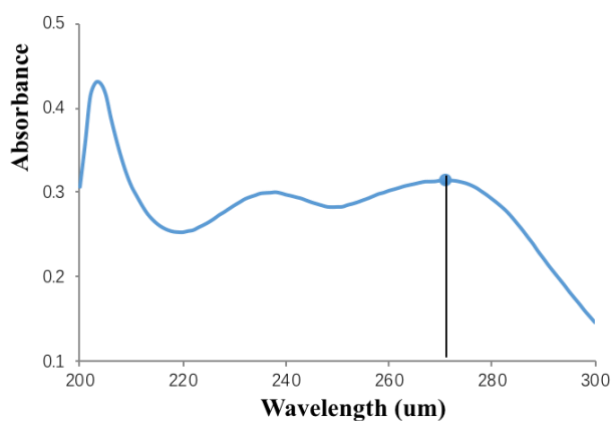
Figure 2-2. UV-Vis absorption spectra of imatinib mesylate in methanol with a characteristic peak at 271-nm

2.2.4   SMPT experiments

Eight solvents (methanol, ethanol, isopropanol, n-propanol, 1-butanol, acetone, acetonitrile, and tetrahydrofuran) were screened for mediating the polymorphism transformation. An excessive amount of α-form imatinib mesylate was added to the solvents and agitated in a thermostatic shaker for 2 weeks. The start time of transition was determined by the morphology of the crystals remaining in the solution with the microscope. After filtration and drying, the crystal polymorph was determined by PXRD.

Subsequently, the SMPT process from α-form to β-form imatinib mesylate was investigated in methanol at different temperatures. A carefully excess weighed amount of α-form was added to 35-ml methanol in a 50-mL double-jacketed crystallizer. The crystallizer temperature was kept constant by a water bath circulator (FP-50, Julabo

LABORTECHNIK GMBH, Germany). The solute concentration and solid-phase polymorphic composition were monitored by a conductivity meter (Pinnacle Series: M541P) and Raman spectroscopy. The start and end time of the transition process was determined through the morphology of the undissolved crystals with the optical microscope. The solubility of α-form was detected during the SMPT process when the transition did not happen.

2.3   Theory

2.3.1   Solubility models

In this work, the solubility of two forms of imatinib mesylate in the selected solvents was fitted with the modified Apelblat equation, as shown in Eq. (1-4)

$$lnx = A + \frac{B}{T} + ClnT \qquad (2\text{-}1)$$

where x is the molar fraction of solute in the solution, T is the absolute temperature in Kelvin, and A, B, and C are dimensionless parameters. The value of three parameters were estimated with MATLAB curve fitting toolbox.

The solubility, in molar fraction, can be calculated using Eq.(2-2):

$$x = \frac{m/M}{m/M + m_s/M_S} \qquad (2\text{-}2)$$

where m and m_s are the mass of solute and solvent, M and M_S are the molecular mass of solute and solvent, respectively.

Solubility reflects the Gibbs energy and stability. The more stable a polymorph is, the lower the solubility it is at a given temperature. The difference of Gibbs free energy between two polymorphs relates to the solubility by Eq. (2-3)

$$\Delta G = RTln\left(\frac{a_1}{a_2}\right) \approx RTln\left(\frac{x_1}{x_2}\right) \qquad (2\text{-}3)$$

where ΔG is the difference of Gibbs free energy (J/mol), and a is the solute activity in the solution(Grunenberg et al., 1996).

2.3.2   Transition process

The SMPT process consists of three steps: the dissolution of metastable form, nucleation of stable form and growth of stable form. The empirical equations for secondary nucleation and growth rate are expressed as Eq. (2-4) and (2-5) (Ranodolph, 2012):

$$B_{sn} = \frac{dn_0}{dt} = k_{sn}M_T{}^j S^b \tag{2-4}$$

$$G = \frac{dL}{dt} = k_g S^g \tag{2-5}$$

where B_{sn} is secondary nucleation rate [#/(m³· s)], G is growth rate (m/s), S is relative supersaturation, M_T is suspension density (kg solute /kg solvent). k_{sn}, k_g, j, b and g are parameters, representing the nucleation rate coefficient, growth rate coefficient, nucleation order on suspension density, nucleation order on supersaturation, and growth order on supersaturation.

$$S = \frac{C - C^*}{C^*} \tag{2-6}$$

where C is the solution concentration, and C^* is the equilibrium concentration both in kg solute /kg solvent.

2.3.3   Parameter estimation

The population balance equation (PBE) coupled with solute mass balance provides a mathematical framework of the crystallization processes. The PBE with the Lagrangian approach (Ranodolph, 2012) describes the change in crystal population density with respect to time and space, as shown in Eq. (2-7).

$$\frac{\partial n}{\partial t} + \nabla.(v_e n) + \nabla.(v_i n) = B - D \tag{2-7}$$

where n is population density, v_e is external velocity vector, v_i is internal velocity vector, B is crystal birth rate, and D is crystal death rate. Assuming that a crystallizer has a uniform distribution of suspended solids, a size-independent growth rate, and negligible breakage and agglomeration, Eq. (2-7) can be simplified to a 1-D PBE as following when $L \neq 0$:

$$\frac{\partial n(t,L)}{\partial t} + G(t)\frac{\partial n(t,L)}{\partial L} = 0 \tag{2-8}$$

The boundary condition at $L = 0$ is

$$n(t,0) = \frac{B(t)}{G(t)}|_{L=0} \tag{2-9}$$

Hu et al.(Hu et al., 2005) proposed a methodology by converting Eq. (2-8) from a partial differential equation (PDE) to a set of ordinary differential equations (ODE). The method was applied in this study to solve Eq. (2-8) in MATLAB software. The single objective to minimize the sum of squares of the difference between the calculated and experimental solute concentration of all independent experiments is defined,

$$min \quad F = \sum_{k=1}^{k}\sum_{i=1}^{N}\left(C_{i,k}^{exp} - C_{i,k}^{cal}\right)^2 \tag{2-10}$$

where N is the sample number and k is the experiment number. $C_{i,k}^{exp}$ and $C_{i,k}^{cal}$ experimental and calculated solution concentration, respectively. In this work, the last step of SMPT process at different temperature was used to estimate the parameters of nucleation and growth rate of β-form imatinib mesylate. The single objective function was solved with the MATLAB optimization function, $fmincon$, based on the sequential quadratic programming (SQP) method.

The solute mass balance is

$$\frac{dC(t)}{dt} = -3k_v\rho_c\int_0^\infty G(t,L)\,n(t,L)L^2dL \tag{2-11}$$

where k_v is the crystal volume shape factor (k_v=1 for a cube), and ρ_c is crystal density.

The average relative deviation (ARD) was introduced to evaluate the accuracy of estimation,

$$ARD = \frac{1}{N}\sum_{i=1}^{N}\left|\frac{C_{i,k}^{cal} - C_{i,k}^{exp}}{C_{i,k}^{exp}}\right| \qquad (2\text{-}12)$$

2.4   Results and discussion

2.4.1   SEM, PXRD and DSC

α-form imatinib mesylate supplied by Apotex Pharmachem Inc, and β-form transformed from α-form in methanol at 293K were used for SEM,   powder XRD, and DSC test.

Figure 2-3 shows the SEM images of the α-form and β-form imatinib mesylate. Obviously, the α-form is needle-shaped while β-form is cubic-shaped. According to the morphology, we can distinguish the crystal polymorph easily.
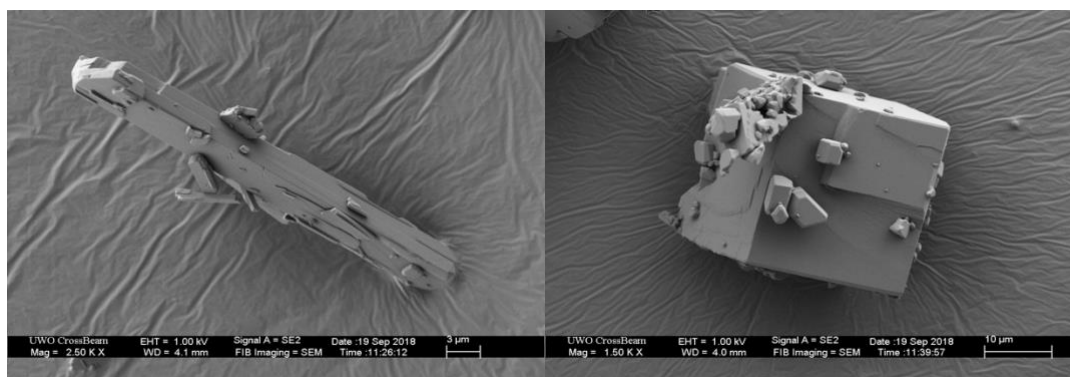
Figure 2-3. SEM images of imatinib mesylate. Left: α-form (3-μm), Right: β-form (10-μm)

Figure 2-4 displays the powder XRD patterns of α-form and β-form imatinib mesylate. The results are consistent with the α-form and β-form single-crystal XRD patterns, which were collected at 293K by Grillo et al.(Grillo et al., 2012) and deposited in the Cambridge Crystallographic Data Center with publication numbers CCDC 821869 and 821871. α-form shows strong peaks at scattering angle (2θ) of 4.8°, 10.4°, 14.8°, 19.0°, 24.8° and 28.5°, whereas β-form has characteristic peaks at 9.7°, 13.9°, 18.2°, 20.0° 21.1° and 30.8°.

The distinct differences on the XRPD spectrum can be used for polymorph identification of imatinib mesylate.
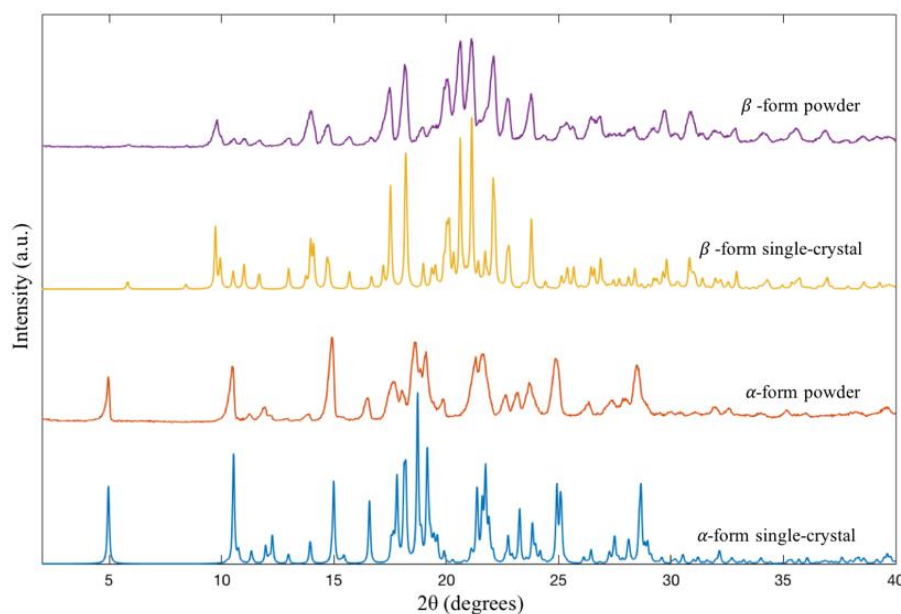
Figure 2-4. The XRD patterns of α-form and β-form imatinib mesylate

For both of α-form and β-form imatinib mesylate, there is only one endothermic peak observed in the DSC curves (Figure 2-5). The peaks are related to the melting event, which was confirmed with hot-stage microscopy and thermogravimetric analysis. The onset (start point) of the peak corresponds to the melting point, and the heat of fusion is equal to the integral of heat flow over time divided by sample mass. According to the heat of fusion rule (Burger and Ramberger, 1979), α-form and β-form imatinib mesylate are enantiotropic, as the α-form imatinib mesylate has higher melting point and lower heat of fusion than β-form.
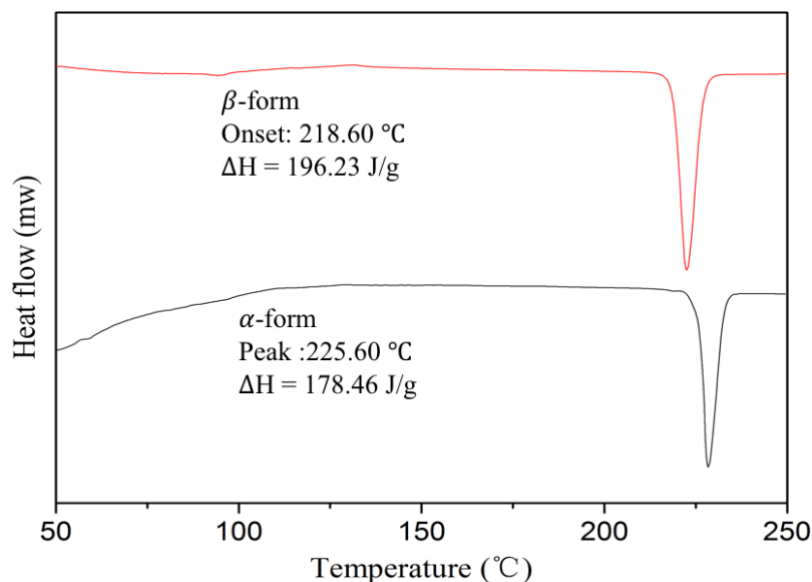
Figure 2-5. The DSC curves at a heating rate of 10 K/min of α-form and β-form imatinib mesylate

2.4.2 Solubility

The PXRD results of the residual solids demonstrated that no transformation or conversion occurred during the solubility experiments, except for the α-form in methanol. Figure 2-6 shows the solubility of α-form and β-form imatinib mesylate in methanol, 1-proponal and 2-proponal. As shown in Figure 2-6, the α-form has higher solubility than β-form in methanol,1-proponal and 2-proponal. The solubility order for both forms is methanol>1-propanol >2-propanol. The fitting parameters are listed in Table 2-3 and the results indicate that the modified Apelblat equation matches the solubility well with all R^2 greater than 0.99.
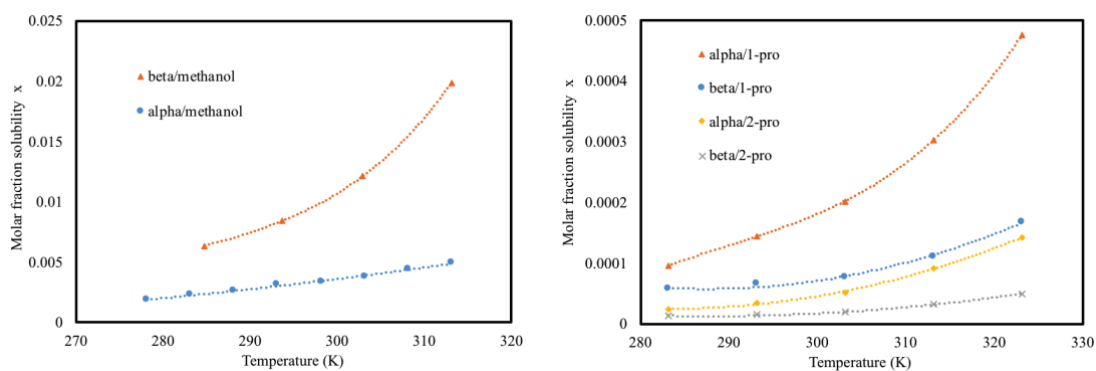
Figure 2-6. The molar fraction solubility of α-form and β-form imatinib mesylate in methanol, 1-proponal and 2-proponal. Dashed line: calculated curve with modified Apelblat equation

Table 2-3. Parameters of the modified Apelblat equation for imatinib mesylate in three solvents

		A	B	C	R^2
Methanol	α-form	-685.8	2.73E+04	103.5	1
	β-form	144.2	-8.61E+03	-21.24	0.9938
1-proponal	α-form	-279.2	9116	42.11	0.9983
	β-form	-762.2	3.18E+04	113.4	0.9972
2-proponal	α-form	-455.2	1.66E+04	68.38	0.9982
	β-form	-933.4	3.89E+04	139	0.9949

As concluded above, α-form and β-form imatinib mesylate are enantiotropic. Figure 2-7 presents that the difference of Gibbs free energy between α-form and β-form imatinib mesylate increases with temperature. So, the transition temperature should be lower than 283.15K, which means that the β-form is always more stable than α-form above 283.15K.
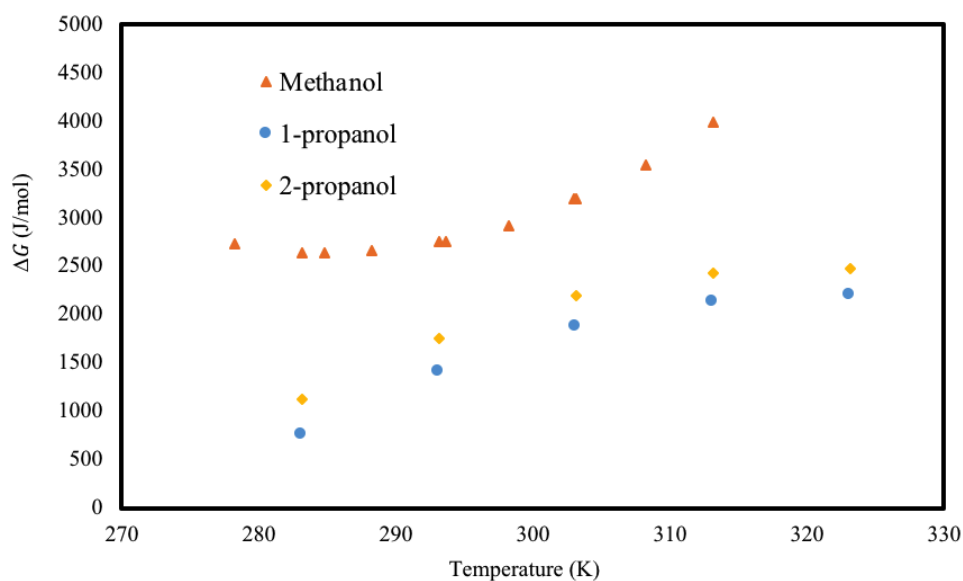
Figure 2-7. The difference of Gibbs free energy between α-form and β-form imatinib mesylate in methanol, 1-proponal and 2-proponal

2.4.3   Solution-Mediated Polymorphic Transformation (SMPT)

Through the solvent screening, we found that the SMPT from α-form to β-form imatinib mesylate could occur in methanol, ethanol, isopropanol, n-propanol, and 1-butanol. The transition time increased with the solvent in the order of methanol, ethanol, 1-propanol, 2-propanol and 1-butanol. Thus, methanol was chosen as the solvent to investigate the SMPT process at different temperatures by in-situ Raman spectroscopy and conductivity meter.

Due to the apparent fluctuations in the baseline, the relative heights of the Raman spectrum were used for quantitative analysis to reduce the effect produced by disturbance variables (Caillet et al., 2006). Here, the peaks at 1664 cm^{-1} and 1656 cm^{-1} were selected as the characteristic peaks of α-form and β-form imatinib mesylate, and the single point baseline was at 1640 cm^{-1}. Generally, the conductivity of a binary conducting solution is a function of temperature and solute concentration. For an isothermal process, conductivity increase in direct proportion to concentration, so the conductivity meter can be used for real-time measurement of the concentration.
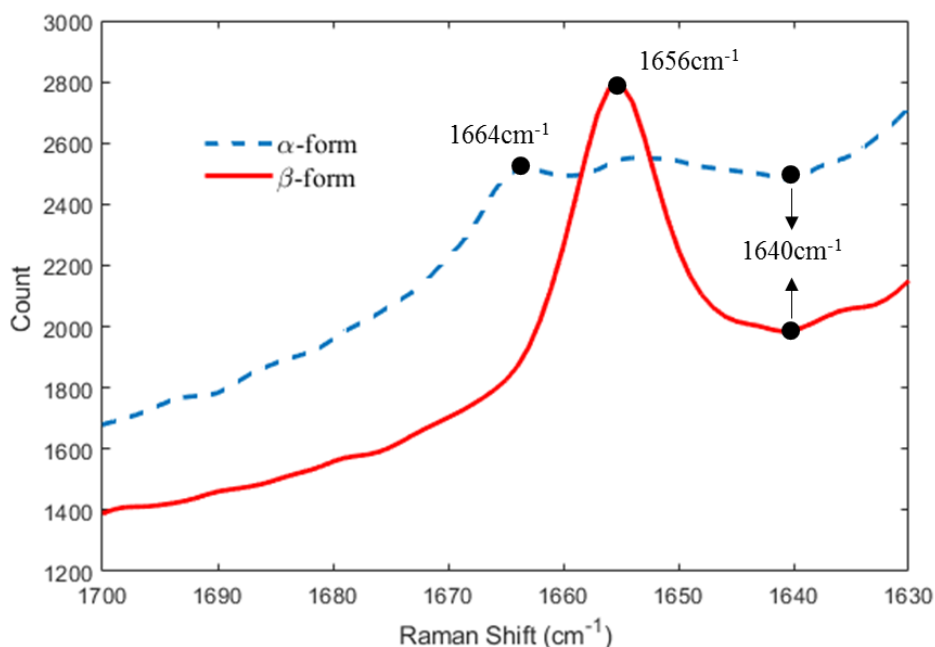
Figure 2-8. Raman spectra of α-form and β-form imatinib mesylate

Figure 2-9 displays how the concentration and solid composition change during the SMPT process in methanol at 293.15K. The process can be divided into four steps. At the

beginning, the concentration increased rapidly as α-form dissolved, and the undissolved solid was pure α-form. The second step involves the nucleation of β-form. Meanwhile, the conductivity and the Raman intensity for both forms kept constant. The dissolution of α-form and growth of β-form happened during the third step, resulting in a decreased Raman intensity of α-form and an increased intensity of β-form. In the last step, the Raman intensity of α-form did not change, illustrating that all α-form crystals had been dissolved and the solid-phase were pure β-form. The nucleation and growth of β-form led to the drop of conductivity and a gradual increase of Raman intensity of β-form.

During the SMPT process, namely the third step, the concentration was close to the solubility of α-form, which indicated the dissolution rate of α-form is much faster than growth rate of β-form. Therefore, it can be concluded that the SMPT from α-form to β-form imatinib mesylate is nucleation-growth controlled of β-form.
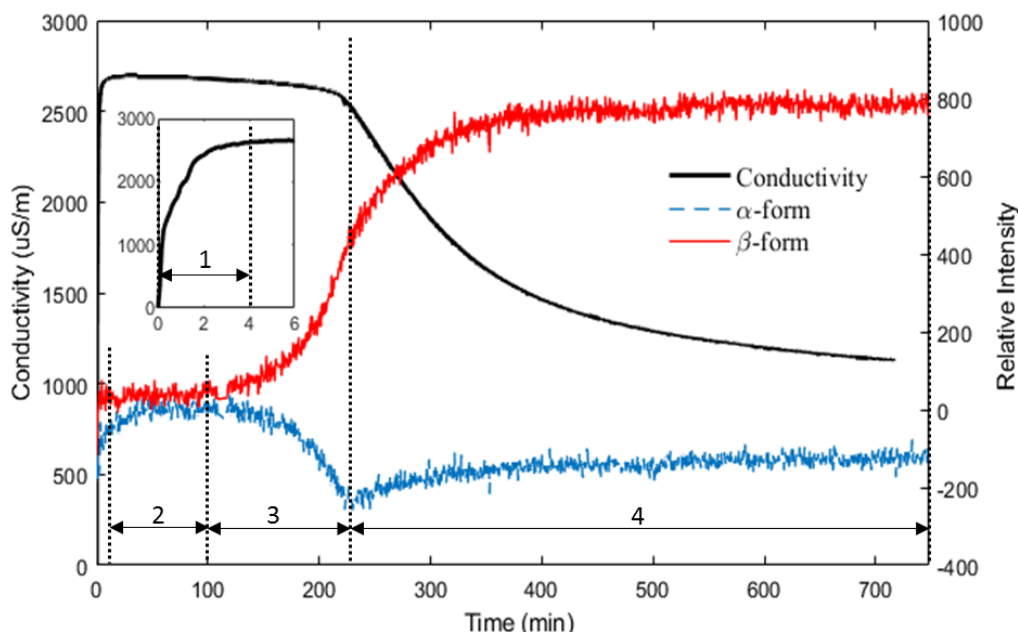
Figure 2-9. Solution-mediated polymorphic transformation from α-form to β-form imatinib mesylate at 293k

2.4.4   Kinetic parameter estimation

As mentioned in Section 2.4.3, all α-form crystals had dissolved and only β-form crystals existed in the solid-phase in the last step (step 4) of the solution mediated polymorphic transformation. Therefore, the last step of the SMPT process can be regarded as a seeded

isothermal batch crystallization. During the process, the solute concentration was measured by the conductivity meter and the suspension density was calculated by solute mass balance. Hence, the nucleation and growth can be estimated through minimizing the difference between the calculated and experimental solute concentration measured in all independent experiments. The estimated parameters are listed in Table 2-4.

The nucleation order with respect to supersaturation (b) is much higher than the nucleation order with respect to suspension density (j), indicating that supersaturation affects the secondary nucleation rate more significantly than slurry density does. In addition, $b > g$ shows that the nucleation rate has a stronger relationship with supersaturation than the growth rate, hence the mean crystal size will decrease at high supersaturation. The estimated kinetic parameters are useful for optimizing and controlling the cooling crystallization process of β-form imatinib mesylate.

Table 2-4. Kinetic parameter estimated from optimization

Kinetic parameter	Estimated value	Units
k_b	9.22×10^{11}	$[(\#/m^3 \cdot s)/(kg/kgsolvent)^j]$
j	0.754	$[-]$
b	3.12	$[-]$
k_g	9.12×10^{-11}	$[m/s]$
g	1.23	$[-]$
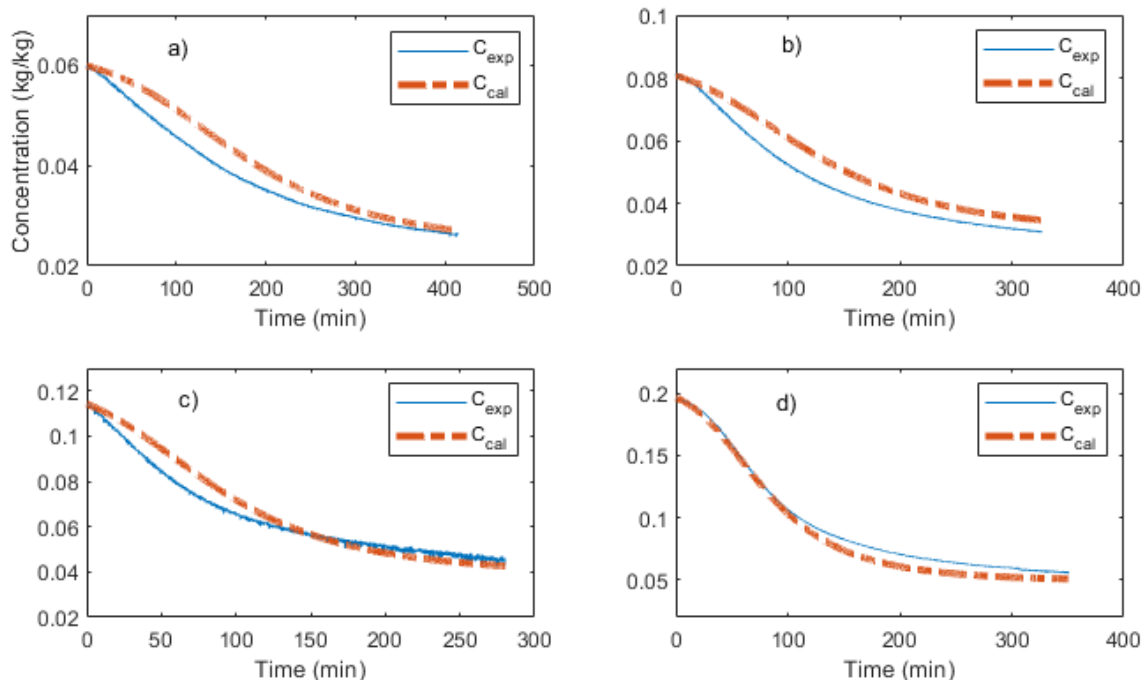
**Figure 2-10. Calculated and experimental solution concentration
a)284.75 K, b)293.65 K, c)302.95 K and d) 313.15K**

The calculated and experimental solute concentration at different temperatures are plotted in Figure 2-10. The ARD of the four experiments are 7.6%, 12.19%, 6.44 %, and 8.62%, respectively, which indicates the empirical equations (Eq. 4, 5, 7) used in this work are suitable for β-form imatinib mesylate. The PBE combined with agglomeration and breakage would give better estimation performance with considerable increase in computation time.

2.5　Conclusions

In this work, the α-form and β-form imatinib mesylate, were characterized by powder X-ray diffraction, scanning electron microscopy and differential scanning calorimetry firstly.

Then, we measured their solubility in methanol,1-propanol, and 2-propanol with UV-Vis. The modified Apelblat equation was used to fit the solubility data. According to the DSC and solubility results, we found that α-form and β-form imatinib mesylate are enantiotropically related and the transition temperature is lower than 283.15K. Above 283.15K, α-form always has a higher solubility and lower stability than β-form in methanol, 1-proponal and 2-proponal. The solubility order in selected solvents is methanol>1-

propanol>2-propanol. After solvent screening, the solution-mediated polymorphic transformation (SMPT) from α-form to β-form imatinib mesylate was investigated in methanol. The solute concentration was monitored by a conductivity meter, while the solid phase was monitored by Raman spectroscopy. As the concentration was close to the solubility of metastable form during the SMPT process, it can be concluded that SMPT process of imatinib mesylate from α-form to β-form in methanol is controlled by nucleation and growth of β-form. Finally, the nucleation and grow rate of β-form of imatinib mesylate were estimated by minimizing the difference between the calculated and experimental solution concentration with MATLAB optimization function.

2.6 **References**

Al-Hadiya, B.M.H., Bakheit, A.H.H., Abd-Elgalil, A.A., 2014. Chapter Six - Imatinib Mesylate, in: Brittain, H.G. (Ed.), Profiles of Drug Substances, Excipients and Related Methodology. Academic Press, pp. 265–297. https://doi.org/10.1016/B978-0-12-800173-8.00006-4

Amala, K., Srinivasa, R.T., Adibhatla, K.S.B.R., Rachakonda, S., Venkaiah, C.N., Podili, K., 2005. Novel polymorphic form of imatinib mesylate and a process for its preparation. WO2005077933A1.

Bellur Atici, E., Karlığa, B., 2015. Quantitative determination of two polymorphic forms of imatinib mesylate in a drug substance and tablet formulation by X-ray powder diffraction, differential scanning calorimetry and attenuated total reflectance Fourier transform infrared spectroscopy. Journal of Pharmaceutical and Biomedical Analysis 114, 330–340. https://doi.org/10.1016/j.jpba.2015.06.011

Burger, A., Ramberger, R., 1979. On the polymorphism of pharmaceuticals and other molecular crystals. I. Mikrochim Acta 72, 259–271. https://doi.org/10.1007/BF01197379

Caillet, A., Puel, F., Fevotte, G., 2006. In-line monitoring of partial and overall solid concentration during solution-mediated phase transition using Raman spectroscopy. International Journal of Pharmaceutics 307, 201–208. https://doi.org/10.1016/j.ijpharm.2005.10.009

Grillo, D., Polla, G., Vega, D., 2012. Conformational Polymorphism on Imatinib Mesylate: Grinding Effects. Journal of Pharmaceutical Sciences 101, 541–551. https://doi.org/10.1002/jps.22772

Grunenberg, A., Henck, J.-O., Siesler, H.W., 1996. Theoretical derivation and practical application of energy/temperature diagrams as an instrument in preformulation studies of polymorphic drug substances. International Journal of Pharmaceutics 129, 147–158. https://doi.org/10.1016/0378-5173(95)04283-0

Hu, Q., Rohani, S., Jutan, A., 2005. New numerical method for solving the dynamic population balance equations. AIChE Journal 51, 3000–3006. https://doi.org/10.1002/aic.10585

Kompella, A.K., Adibhatla, K.S.B.R., Podili, K., Venkaiah, C.N., 2006. Polymorphic forms of imatinib mesylate. WO2006054314A1.

Lee, A.Y., Erdemir, D., Myerson, A.S., 2011. Crystal Polymorphism in Chemical Process Development. Annu. Rev. Chem. Biomol. Eng. 2, 259–280. https://doi.org/10.1146/annurev-chembioeng-061010-114224

Lin, M., Wu, Y., Rohani, S., 2019. A kinetic study of crystallization process of imatinib mesylate with polymorphic transformation phenomenon. Journal of Crystal Growth 507, 146–153. https://doi.org/10.1016/j.jcrysgro.2018.10.061

Morris, G., Power, G., Ferguson, S., Barrett, M., Hou, G., Glennon, B., 2015. Estimation of Nucleation and Growth Kinetics of Benzoic Acid by Population Balance Modeling of a Continuous Cooling Mixed Suspension, Mixed Product Removal Crystallizer. Org. Process Res. Dev. 19, 1891–1902. https://doi.org/10.1021/acs.oprd.5b00139

Mullin, J.W., 2001. Crystallization. Elsevier.

Mutz M., 2007. Delta and Epsilon Crystal Forms of Imatinib Mesylate. WO/2007/023182.

Mutz, M., 2007. F,g,h,i and K Crystal Forms of Imatinib Mesylate. WO/2007/059963.

Myerson, A., 2002. Handbook of Industrial Crystallization. Butterworth-Heinemann.

O'Mahony, M.A., Maher, A., Croker, D.M., Rasmuson, Å.C., Hodnett, B.K., 2012. Examining Solution and Solid State Composition for the Solution-Mediated Polymorphic Transformation of Carbamazepine and Piracetam. Crystal Growth & Design 12, 1925–1932. https://doi.org/10.1021/cg201665z

Parthasaradhi, R.B., Rathnakar, R.K., Raji, R.R., Muralidhara, R.D., Subash, C.R.K., Limited, H.D., 2003. Novel polymorphs of imatinib mesylate.

Patel, H., Jani, R., Thennati, R., 2006. Imatinib Mesylate Crystal Form and Process for Preparation Thereof. WO/2006/048890.

Pathi, S.L., Puppala, R., Kankan, R.N., Rao, D.R., Limited, C., Wain, C., 2005. Stable crystal form of imatinib mesylate and process for the preparation thereof.

Ranodolph, A., 2012. Theory of Particulate Processes: Analysis and Techniques of Continuous Crystallization. Elsevier.

Srivastava, A., Joshi, B.D., Tandon, P., Ayala, A.P., Bansal, A.K., Grillo, D., 2013. Study of polymorphism in imatinib mesylate: A quantum chemical approach using

electronic and vibrational spectra. Spectrochimica Acta Part A: Molecular and Biomolecular Spectroscopy 103, 325–332. https://doi.org/10.1016/j.saa.2012.10.066

Stahly, G.P., 2007. Diversity in Single- and Multiple-Component Crystals. The Search for and Prevalence of Polymorphs and Cocrystals. Crystal Growth & Design 7, 1007–1026. https://doi.org/10.1021/cg060838j

Trifkovic, M., Rohani, S., Sheikhzadeh, M., 2012. Kinetics Estimation and Polymorphic Transformation Modeling of Buspirone Hydrochloride. Journal of Crystallization Process and Technology 02, 31–43. https://doi.org/10.4236/jcpt.2012.22006

Veverka, M., Šimon, P., Lokaj, J., Veverková, E., 2012. Crystal habit modifications of imatinib mesylate under various precipitation conditions. Monatshefte für Chemie - Chemical Monthly 143, 65–71. https://doi.org/10.1007/s00706-011-0562-y

Zimmermann, J., Sutter, B., Bürger, H.M., 2005. Crystal modification of a N-phenyl-2-pyrimidineamine derivative, processes for its manufacture and its use. US6894051B1.

Zimmermann, J., Sutter, B., BÜRGER, H.M., 1999. Crystal modification of a n-phenyl-2-pyrimidineamine derivative, processes for its manufacture and its use. WO1999003854A1.

Chapter 3

Simultaneous Measurement of Solution Concentration and Slurry Density by Raman Spectroscopy with Artificial Neural Network

3 Simultaneous Measurement of Solution Concentration and Slurry Density by Raman Spectroscopy with Artificial Neural Network

Abstract

In this work, the capability of Raman spectroscopy to measure the solution concentration and slurry density simultaneously and quantitatively was studied. Paracetamol-ethanol and L-glutamic acid-water systems were chosen as model systems. Different pre-processing methods (spectra range selection, baseline removal, direct orthogonal signal correction-DOSC or no processing) and multivariable analysis techniques (characteristic peaks regression (CPR), principal component regression (PCR), partial least squares regression (PLSR) and artificial neural network (ANN)) were applied and compared based on the root mean squared error (RMSE). It was demonstrated that the solution and solids concentration can be extracted separately from Raman spectroscopy. It is found that DOSC pre-processing can improve the fitting performance of the linear regression models (CPR, PCR, and PLSR), but not for ANN model. On the other hand, ANN method, owing to its non-linear prediction ability, had better predicted results than the linear models when the signal was weak.

3.1 Introduction

Crystallization is one of the oldest unit operations and widely used for separation and purification in chemical industry. The driving force for crystallization process is supersaturation, which is the difference/ratio between the actual temporal concentration and the solubility. The desupersaturation profile has a significant effect on the product quality. Therefore, the concentration measurement is essential for design and optimization of the crystallization process.

Several techniques have been employed to determine the solution concentration, such as gravimetric method (Zhang et al., 2010), high-performance liquid chromatography (HPLC) (Li et al., 2016), ultraviolet/visible spectrophotometer (Mondal et al., 2017), conductivity meter (Cheng et al., 2006), attenuated total reflectance Fourier transform infrared (ATR-FTIR) spectroscopy (Yang et al., 2008) and Raman spectroscopy (Hu et al., 2005). With

the gravimetric method, HPLC, or off-line UV/vis, the samples have to be removed from the crystallizer, followed by drying, filtration, and/or dilution steps, which is time-consuming and induce inaccuracy in the measurement. On the contrary, the *in-situ* process analytical technologies (PAT) are more convenient and accurate to monitor crystallization process and implement feedback control.

ATR-FTIR is the most common PAT tool for solution concentration measurement. Due to the low penetration depth (about 2-3μm) of ATR-FTIR beam, the ATR-FTIR probe can monitor liquid-phase in spite of the existence of the solid-phase (Nicoud et al., 2019) (Cornel et al., 2008). However, it is difficult to characterize the systems that have low solubility or low infrared activity with ATR-FTIR (Bötschi et al., 2018).

Raman spectroscopy is another *in-situ* PAT tool that has been used widely for monitoring the polymorphic composition of the solid phase (Nicoud et al., 2019). The solid concentration for each polymorph is usually calculated by mass balance, assuming the total solute mass in the crystallizer is constant during the crystallization process. Nevertheless, this assumption only holds for the batch crystallization process or the continuous crystallization in steady-state condition. In case of unsteady continuous crystallization, the solute may accumulate/dissipate during the process, defying the assumption.

On the other hand, few studies have been performed in the literature to utilize Raman for the solution concentration measurement. For the first time, Hu et al.(Hu et al., 2005) demonstrated that Raman can measure the solute concentration in liquid-phase and polymorphic form in solid-phase simultaneously in flufenamic acid systems. Later, Cornel et al. successfully estimated the solution concentration and slurry density of L-glutamic acid, in spite of the complete overlap in the signals of liquid phase and solid phase (Cornel et al., 2008). Raman spectroscopy method to measure the solute concentration of paracetamol and carbamazepine were developed by Powell et al.(Powell et al., 2016) and Acevedo et al (Acevedo et al., 2018).

It is worth noting that all the aforementioned references employed the multiple linear regression (MLR) models to relate the measured variables (e.g. Raman or FTIR spectroscopies) to the independent variables (e.g. solution concentration or polymorphic

composition). Three MLR models were widely applied. The first one, characteristic peak regression (CPR), relies on the absolute height/area of the characteristic peaks or the difference/ratio of the intensities of two characteristic peaks (Nicoud et al., 2019). Compared to the other two models, namely, principal component regression (PCR)(Cornel et al., 2008) and partial least squares regression (PLSR) (Powell et al., 2016), the characteristic peak method is more straightforward, but it is time-consuming to select the peaks manually and subject to human error. Since PCR and PLSR utilize the full spectrum instead of some specific peaks, their results are more accurate than peak selection method (Cornel et al., 2008)(Pratiwi et al., 2002). In addition, PCR and PLSR can overcome the multicollinearity problem that is common in spectroscopy.

Artificial neural networks (ANN), which is a non-linear modeling technique, has successfully predicted the polymorphic composition in multi-component powder mixtures from diffuse reflectance FTIR spectroscopy (Kachrimanis et al., 2007) and the co-crystal formulations from Raman and ATR-FTIR spectroscopy (Barmpalexis et al., 2018). It was demonstrated that the ANN model has better fitting performance than PLS regression in these two cases (Kachrimanis et al., 2007).

The objective of this paper is to develop a simple analytical method to quantitatively measure the solution concentration and slurry density from Raman spectrum directly, with the aid of the MLR models (CPR, PCR, and PLSR) and non-linear ANN models, without imposing any assumption. In this work, paracetamol-ethanol and L-glutamic acid-water were chosen as model systems. Two polymorphs of L-glutamic acid and one stable form of paracetamol were investigated. This article is organized as follows. First, the experiments for collecting training data for establishing the models are described. Different preprocessing and multivariable analysis were applied to estimate the solution and solids concentration from Raman spectra, and their performance were compared based on the mean squared error (RMSE). Then, the validation experiments were designed to verify the reliability of the developed models. Finally, the conclusions of this work are presented.

3.2   **Experimental section**

3.2.1   **Material**

Paracetamol (stable form I PCM, 98%, Sigma-Aldrich Chemical Inc., MO, USA), ethanol (100%, Commercial Alcohols Inc., ON, Canada), L-Glutamic acid (stable β-form LGA, 99+ %, Alfa Aesar, MA, USA), and deionized water supplied in our lab were used in this study without any further processing. The metastable α-form LGA was produced by fast cooling crystallization from aqueous solution, followed by filtration and drying. All polymorphs were identified with powder X-ray diffraction (PXRD, Rigaku, Miniflex, Tokyo, Japan). The comparison between the theoretical and experimental PXRD patterns of PCM and LGA is shown in Figure 3-1and Figure 3-2, respectively. The theoretical patterns were generated from the files downloaded from Cambridge Crystallographic Data Center (CCDC deposition number: Form I PCM-735853, α-form LGA- 1206530, β-form LGA- 1206531) with software Mercury (version 3.10.3, CCDC, Cambridge, UK). α-form LGA shows strong scattering at the angle of 18.3°, 23.7°, 26.7°, and 37.0°, whereas the characteristic peaks of β-form LGA are at 10.3°, 13.7°, 20.0°, 20.5°, 25.6°, 26.1° and 35.6°.
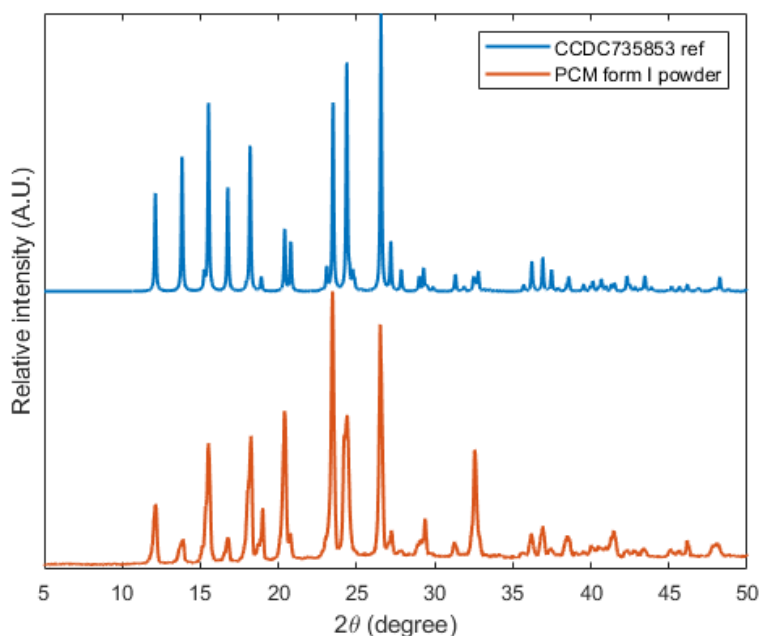
Figure 3-1. PXRD patterns of Form I paracetamol
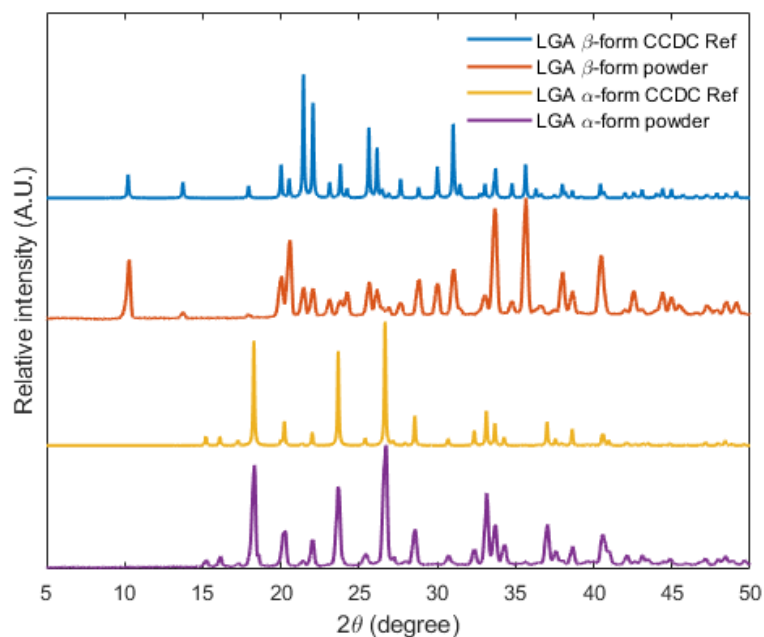
Figure 3-2. PXRD patterns of α-form and β-form L-glutamic acid

3.2.2 Raman spectroscopy

The Raman spectrum was collected by a Raman RXN Analyzer spectroscopy (Kaiser Optical Systems, Inc., Ann Arbor, MI, USA) coupled with a diode laser (784.8-nm) and a fiber optic probe. The data was acquired by the iCRaman software (Mettler Toledo, Columbus, OH) in the Raman shift range of 3425-100 cm^{-1} with a resolution of 1 cm^{-1}. Due to the weakness of the solution concentration signal and the readout noise of the charge coupled device (CCD) detector, one accumulation with 15s exposure time was used to increase the signal/noise ratio.

The ambient fluorescent light may attribute to some prominent peaks in the Raman spectroscopy. These peaks vary with the slurry concentration due to the obstruction of the ambient light. Therefore, the experiment should be carried out with a shaded container to prevent the undesired spikes in the results. In this study, all the experiments were done in the crystallizers, whose surface are covered by black tape, to eliminate the effect of the ambient light. It was demonstrated by experiments that the Raman spectrums kept same regardless of the presence and absence of outer lights.

3.2.3   Training data collection

The training datasets were obtained with some prepared solutions/suspensions, whose solution concertation and slurry density of each polymorph were known. The inputs of the model were temperature and Raman spectrum, and solution concentration and slurry density were considered as the output of the model. The temperature was measured by a digital temperature sensor DS1820 (Maxim Integrated, Inc., CA, USA). Figure 3-3.a shows the schematic design of the experimental setup used in this study. The Simulink program built for merging the input and output data simultaneously is shown in Figure 3-3.b.
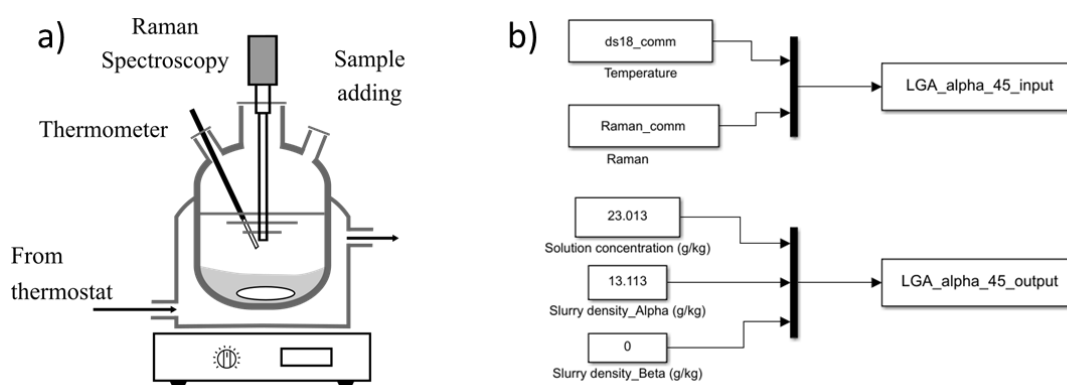
Figure 3-3. a) Schematic of the experimental setup (Note: the surface of crystallizer was covered by black tap); b) Simulink block diagram for data acquisition

The dataset included three parts: pure solvent at different temperature, clear solution with different concentrations at different temperature, and suspension with different slurry density at different temperature. At first, the Raman spectrum of pure solvents at different temperature was measured. Secondly, the dataset of clear solution with different concentrations at different temperature was collected. The procedure is illustrated in Figure 3-4.a. A solution with known low concentration was prepared at room temperature and then heated to a high temperature to ensure all crystals were dissolved. Next, the system was cooled to enter the metastable zone. The solution temperature and Raman spectrum were recorded during the cooling process. Focused beam reflectance measurement (FBRM) (S400, Mettler Toledo, WA, USA) was used to confirm no nucleation happened. After that, a known amount of crystals was added to the solution to increase the solution concentration. By repeating the heating, cooling, and crystal addition steps, the Raman spectrum of clear

solutions for a range of concentrations and temperatures, both in the unsaturated zone and metastable zone, were collected. The solution concentration was calculated by the mass of the added crystals. Lastly, the dataset of suspension with different slurry density was obtained by adding various amount of crystals to the saturated solutions at different temperature, as shown in Figure 3-4.b. The solution concentration was assumed to be saturated, and the slurry density was calculated through the solute mass balance.
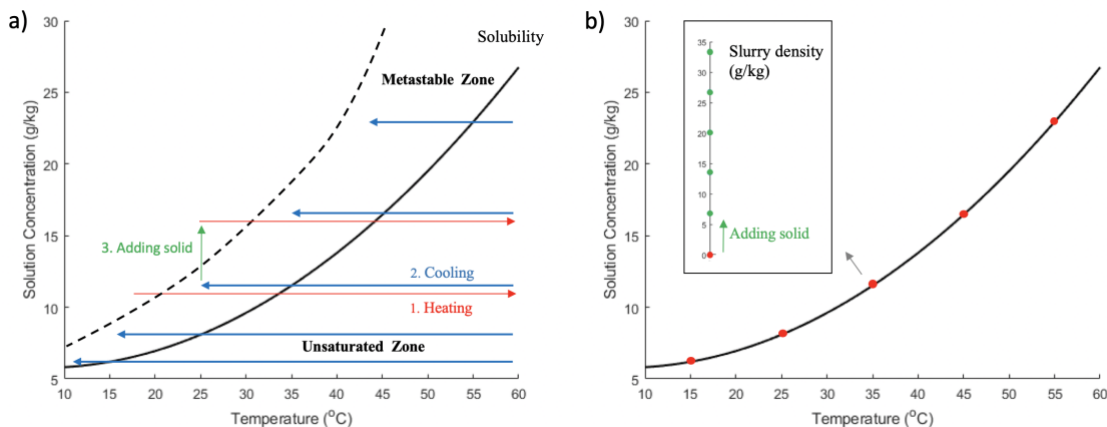
Figure 3-4. Illustration of data collection procedure for β-form LGA: a) clear solution and b) suspension

3.2.4   Data preprocessing

To improve the model performance and reduce the effect of irrelevant variables, three preprocessing methods were investigated: 1) baseline removal to eliminate the baseline shifting problem, 2) spectral range selection to reduce the dimensionality of the input data, and 3) direct orthogonal signal correction (DOSC)(Westerhuis et al., 2001) to remove the variables in the input data that are orthogonal to the outputs and to reduce the variation that is caused by system random fluctuations. The baseline removal of the full spectrum was implemented with Matlab function 'msbackadj' with default setting (200 for window size and step size). The wavenumber range, from 1825 cm^{-1} to 100 cm^{-1}, were selected as the optimal spectral range, since the prominence peaks for both systems are located in this spectra region.

3.2.5   **Multiple Linear Regression (MLR)**

As the temperature and Raman intensities have different orders of magnitudes, the standardization algorithm was adopted to normalize the input data by subtracting its mean and then dividing each data point by its own standard deviation to avoid numerical instability problem. After the standardization procedure, CPR, PCR, and PLSR were applied as the MLR models for comparison with the ANN model, and was completed with Matlab software. To implement CPR, the 'findpeaks' function was used to find the intensities of most characteristic peaks, and the 'fitlm' function was employed to establish the linear correlation between peak intensities and the known variable (solution concentration or slurry density). PCR and PLSR, on the other hand, used the principal components to reduce the dimension of the input signal, which can be achieved in Matlab with 'pca' and 'plsregress' functions. The numbers of principal components of PCR and PLSR were chosen with cross-validation.

3.2.6   **Artificial Neural Networks (ANN)**

ANN was developed with Matlab Neural Network Fitting Tool ('nftool'). A two-layer Back Propagation Neural Network with four hidden neurons were adopted. The collected samples were randomly divided into two sets: 90% for training and 10% for validation. The error of the validation set was monitored during the training process to evaluate the neural network performance and prevent overfitting by applying "early-stopping" strategy. When the training did not improve validation performance for six times, the training was stopped to prevent overfitting the neural network. The Levenberg–Marquardt algorithm was used for training the ANN, as it is the fastest network training algorithm. Due to the high dimensionality of the input data (3327 points), principal component analysis and characteristic peak method were used to reduce the dimension of the inputs of the neural network and decrease the model complexity. The first 50 components of PCA or the characteristic peaks selected by peak method were employed. They are denoted as PCA-ANN and Peak-ANN, respectively.

The root mean squared error (RMSE) was used to assess the prediction performance:

$$RMSE = \sqrt{\frac{\sum_{i=1}^{n}(\hat{y}_i - y_i)^2}{n}} \tag{3-1}$$

where n is the number of observations, $\hat{y}_i$ and y_i are predicted and observed values, respectively.

3.2.7   Validation experiment

3.2.7.1   Dilution experiment of PCM-ethanol system

A dilution experiment was performed to validate the solution concentration models. Pure ethanol was continuously pumped into a clear PCM-ethanol solution, and the diluted solution was continuously withdrawn. The inlet and outlet flow rates were kept the same and constant. The solution concentration during the dilution process can be calculated by Eq.(3-2):

$$C = C_0 \times \exp\left(-\frac{t}{\tau}\right) \tag{3-2}$$

where C_0 is initial solution concentration, and τ is residence time. They are 0.2877 kg/kg and 28.5 min, respectively, in this study.

3.2.7.2   Dissolution and nucleation process of PCM-ethanol system

An amount of 10.59 g PCM was added to 40 mL ethanol in a 50 mL double-jackets crystallizer at 25 ℃ to make a suspension with 0.3355 kg/kg total solute concentration, which corresponds to the solubility at 50 ℃. Then the suspension was heated to 60 ℃ with a slow heating rate (1 ℃/min), followed by cooling the solution back to 25 ℃ at 1 ℃/min rate. FBRM was employed to monitor the crystal count.

The predicted concentrations from Raman were then compared to the solubility equation for form I PCM in ethanol, as shown in Eq.(3-3).(Li et al., 2014)

$$C_{form\ I\ PCM} = 7.915 \times 10^{-7}T^3 - 6.439 \times 10^{-4}T^2 + 1.765 \times 10^{-1}T - 16.17 \tag{3-3}$$

where C is the solubility in [kg solute/ kg solvent], and T is temperature in K.

3.2.7.3 Dissolution process of β-form LGA-water system

The solubility[kg solute/kg solvent] of β-form LGA in water at temperature $T(°C)$ were obtained by fitting the experimental data(Hermanto et al., 2008) with a second-order polynomial:

$$C_{\beta-form} = 8.664 \times 10^{-3}T^2 - 1.925 \times 10^{-1}T + 7.958 \tag{3-4}$$

Similar to the heating process of PCM-ethanol system, 0.7803 g of β-form LGA was added to 40 g water at 25°C to make a suspension with 19.5 g/kg total solute concentration, which corresponds to the solubility at 50 °C. The suspension was heated to 70 °C at a slow heating rate (1 °C/min) and then cooled back to 25°C. FBRM was used to monitor the crystal count.

3.3 Results and discussion

3.3.1 Raman spectroscopy
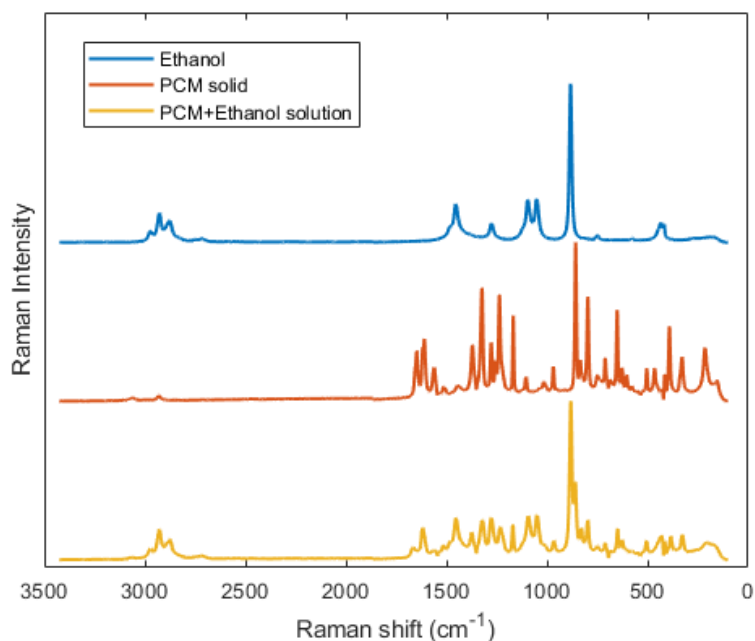
Figure 3-5. Raman spectra of ethanol, paracetamol and paracetamol-ethanol solution
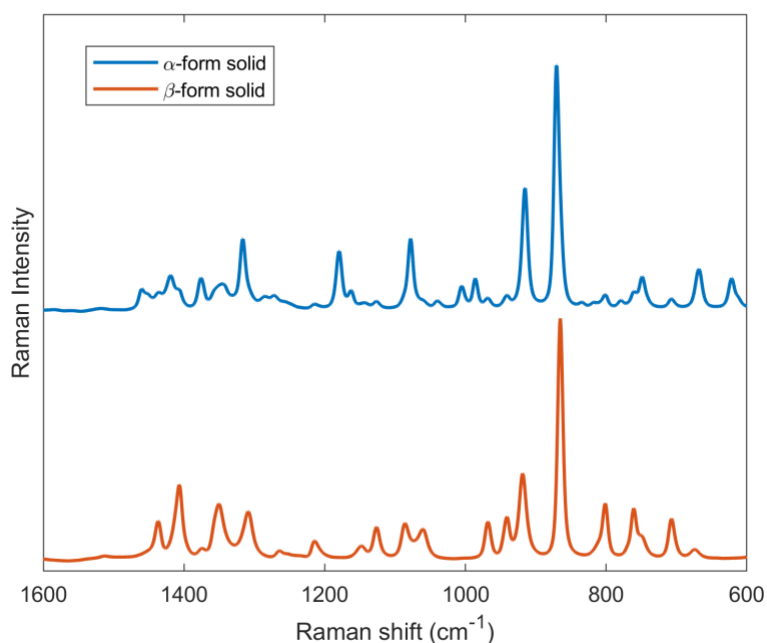
Figure 3-6. Raman spectra of powder metastable α-form and stable β-form L-glutamic acid

Figure 3-5 shows the Raman spectrums of ethanol, PCM crystals, and PCM-ethanol solution, while the Raman spectra of solid α- and β-form LGA are shown in Figure 3-6. The results of solid PCM and LGA agree well with those reported in the literature (Kachrimanis et al., 2007).

The effect of temperature, solution concentrations and slurry density on the Raman spectra is shown in Figure 3-7. Compared to the solution concentration and slurry density, the temperature has less influence on the spectra. Most peak intensities, such as 866 and 916 cm^{-1}, changed with both of solution concentration and slurry density, which evidences the overlap of the liquid phase and solid phase signals in Raman spectra. Therefore, the regression of individual peak intensity vs. slurry density or solution concentration may not predict the variable correctly when the other variable is also changing. The deconvolution of the spectrum to identify how the peaks are subject to change in the variation of solution concentration or slurry density should be taken into full consideration. In this work, the mathematical models for solution concentration or slurry density were established separately and then applied to measure them from Raman spectrum quantitatively.
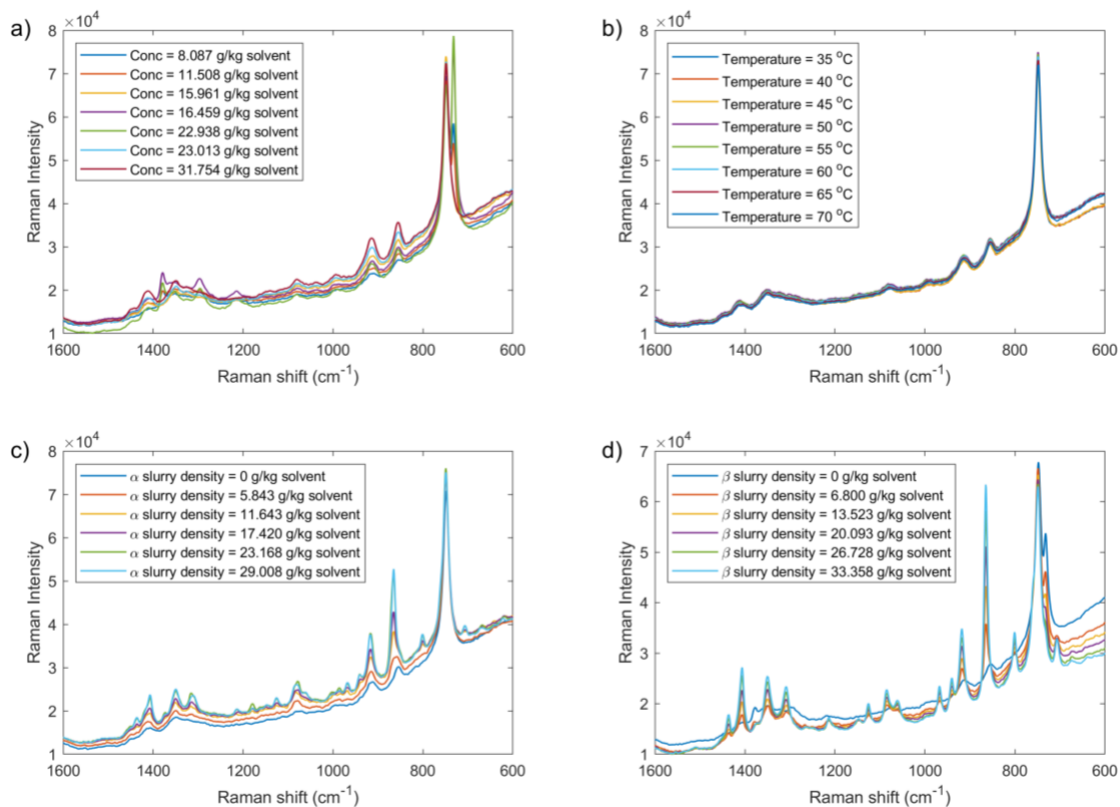
Figure 3-7. Raman spectra of L-glutamic acid-water system with different a) solution concentration of clear solution at 60 °C; b) temperature of clear solution with 11.508 g/kg solution concentration; c) α-form LGA slurry density at 35 °C; d) β-form LGA slurry density at 35 °C

3.3.2   Number of principal components

The numbers of principal components (PCs) of PCR or latent variables (LVs) of PLSR are critical for modeling performance, since a small number of components has low fitting capacity, whereas a large number of components may cause overfitting problem. Based on the percentage of variance in the response variable (percent variance explained, PVE) and mean squared error of prediction (MSEP) by cross-validation (Figure 3-8), the number of components was set to 8.
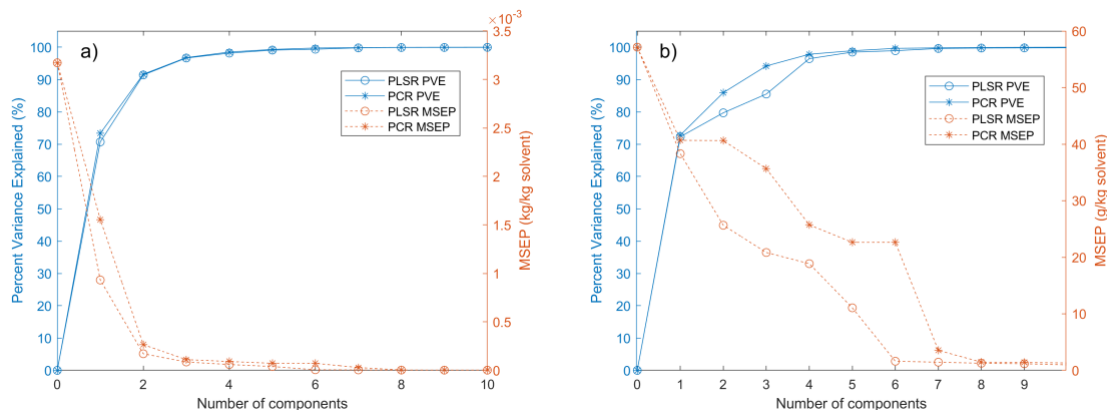
Figure 3-8. The percent variance explained (PVE) and mean squared error of prediction (MSEP) vs. the number of components of PLSR and PCR for the solution concentration of a) paracetamol-ethanol system and b) L-glutamic acid-water system

3.3.3 Results of PCM-ethanol system

Table 3-1. RMSE (g/kg) results of PCM-ethanol system training data

System	Preprocessing	CPR	PCR	PLS	PCA + ANN	Peak+ANN
Solution	None	1.350	2.809	2.149	**0.207**	0.497
	Baseline removal	1.337	2.497	2.010	0.411	0.406
	Spectral range selection	1.436	2.613	2.040	0.324	0.483
	OSC	0.711	1.002	1.001	1.002	0.706
Solid	None	0.406	2.988	2.948	0.886	0.668
	Baseline removal	0.393	2.957	2.755	0.803	0.628
	Spectral range selection	0.609	2.980	2.928	1.033	0.896
	OSC	**0.362**	0.793	0.793	0.650	0.521

The RMSE values of the solution and solids concentration of PCM-ethanol system with different preprocessing methods and multivariate analysis techniques are summarized in Table 3-1. For the PCM solution concentration, the PCA-ANN model with none pre-processing method results in the lowest prediction error, i.e., 0.2 g/kg. In the case of PCM solids concentration, CPR with OSC has better performance than others. The best models

were validated with the dilution experiment and used for monitoring the dissolution and cooling crystallization processes, as described in Section 3.2.7.

Figure 3-9 shows a good consistency between the theoretical and predicted solution concentration for the dilution experiment. It was observed that the errors increased when the solution concentration was lower than 0.15 g/kg, which is the lowest concentration in the training dataset, corresponding to the solubility at 10 ℃. This observation suggests that the non-linear ANN model may not be capable to reliably extrapolate data out of its training range. It is necessary to train the ANN with a full-range dataset to ensure the result validity.
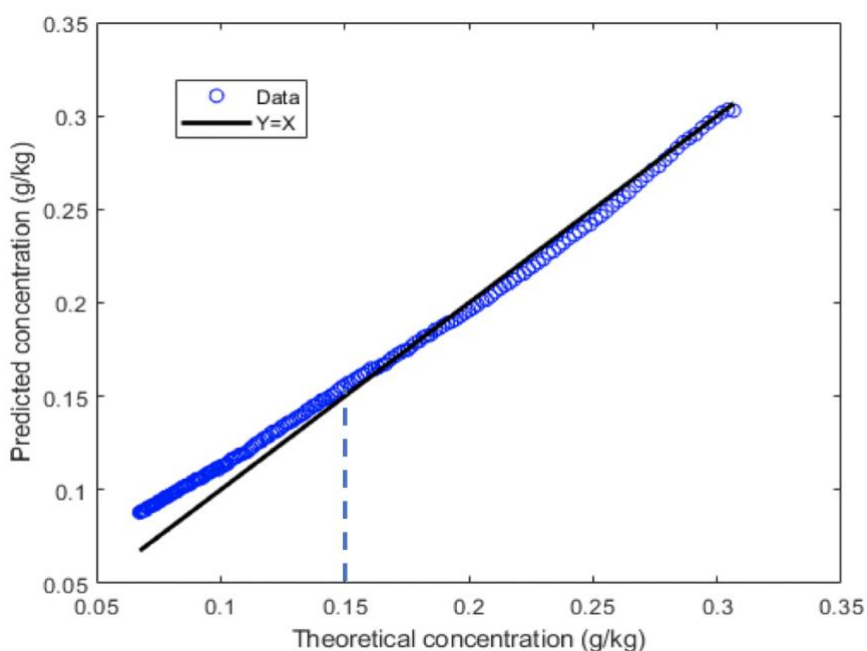
Figure 3-9. Comparison of the theoretical and predicted concentration of PCM-ethanol solutio

Figure 3-10 plots the temperature, solution concentration, and FBRM count during the heating and cooling processes. Initially, the solution concentration was kept at 0.193 kg/kg (solubility at 25 ℃). After system stabilization, the crystallizer was heated so that the solution concentration (plotted in black dotted line) increased as a result of the dissolution of suspended crystals. At the end of heating process, all of the suspended crystals were dissolved. Hence, the solution concentration reached 0.345 kg/kg, which agreed with the initial total solute concentration (0.335 kg/kg, the solubility at 50 ℃). After cooling back

to 25 ℃, the solution concentration went back to the initial value, as expected. The endpoint of dissolution and onset of nucleation detected by Raman (black curve) was also consistent with the FBRM readings (red line). This experiment confirms the reproducibility, accuracy, and sensitivity of Raman spectrum to the changes in the process.
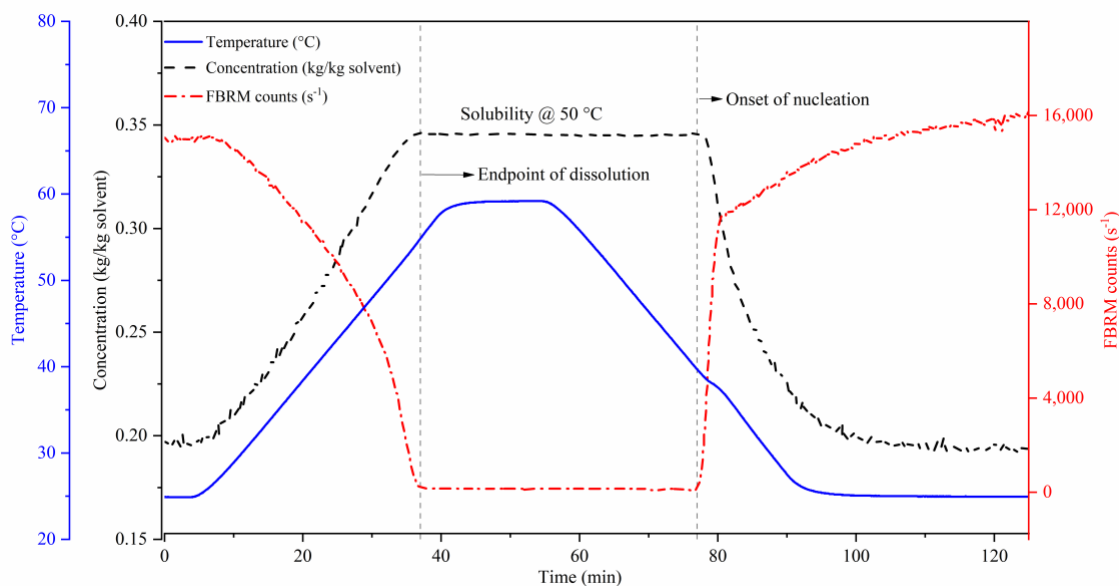
Figure 3-10. Temperature, solution concentration predicted for Raman, and FBRM count during the heating and cooling process of PCM-ethanol system

3.4   Results of LGA-water system

Table 3-2 lists the RMSE of regression results of LGA-water system. It is interesting to notice that the RMSE values with ANN model were much lower than those with the linear models for three cases of LGA-water system and PCM solution concentration, expect PCM solid concentration. The reason for this behavior is that PCM solid concentration has high net Raman intensity, so that the characteristic peaks regression couple with DOSC can have lowest prediction error. In the cases of PCM solution concentration, LGA solution concentration and LGA solid concentration, where the Raman signals were weak relatively, ANN model has better prediction performance than the linear models, owing to its non-linearity of prediction ability.

Table 3-2. RMSE (g/kg) results of LGA-water system training data

System	Preprocessing	CPR	PCA	PLS	PCA + ANN	Peak+ANN
Solution	None	1.2526	1.0981	0.7735	0.3465	0.4287
	Baseline removal	1.1264	0.9854	0.6994	**0.3145**	0.4751
	Spectral range selection	1.3649	1.1435	0.9216	0.3501	0.4548
	OSC	0.6117	0.6357	0.6075	0.5536	0.5547
Solid α-form	None	1.8708	1.8381	1.3527	**0.4421**	0.5529
	Baseline removal	1.9121	1.8736	1.3925	0.5086	0.5006
	Spectral range selection	1.9323	1.8697	1.5240	0.4451	0.5175
	OSC	1.0318	1.0306	1.0304	0.5086	0.5626
Solid β-form	None	2.0605	2.1356	1.6244	0.6549	0.8199
	Baseline removal	2.1622	2.1222	1.6505	0.4830	0.6820
	Spectral range selection	2.2120	2.1413	1.8122	0.5037	0.5226
	OSC	1.2598	1.2613	1.2584	**0.4285**	0.4650
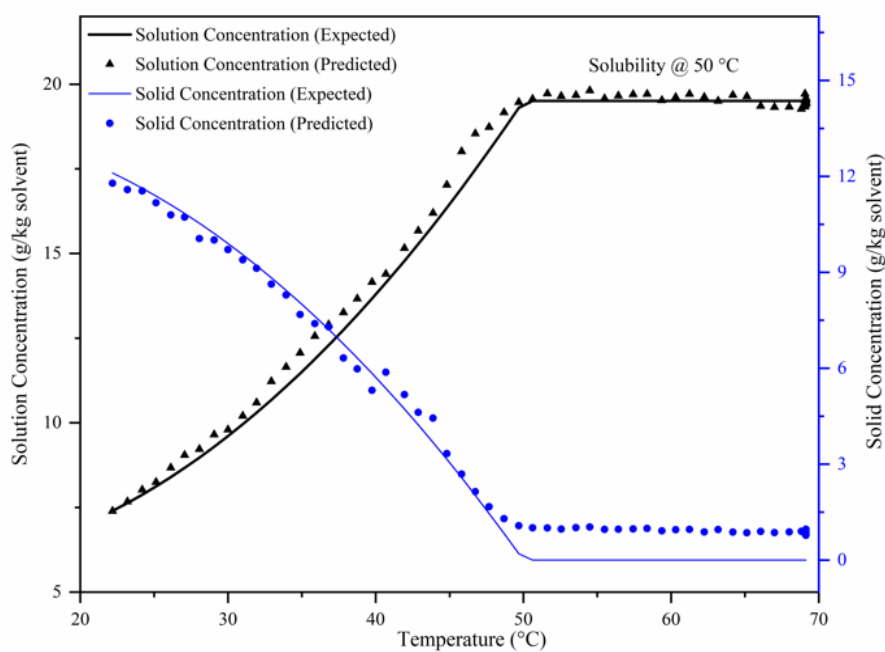
Figure 3-11. The change of solution concentration and β-form LGA solid concentration during the heating process

Figure 3-11 shows the changes of solution concentration and solid concentration of β-form LGA when the crystallizer was heated up with the rate of 1 ℃/min. Due to the slow heating rate, the solution concentration followed the solubility curve until all solids were dissolved, and then kept constant at the solubility corresponding to 50 ℃. The expected solids concentration, presented by the blue solid line, was calculated from the solute mass balance. The predicted solution and solids concentrations from Raman spectrum have an excellent agreement with the expected results.

From Table 3-1 and Table 3-2, it can be concluded that DOSC pre-processing methods can improve the fitting performance of the linear regression models (CPR, PLSR and PCR), but not for ANN model. As mentioned above, DOSC removes the components in the input data that are orthogonal to the outputs, which may cause the loss of useful non-linear information for ANN model. This observation was also described by Zhu et al.(Zhu et al., 2008) Among four selected pre-processing methods, none could improve ANN performance for all cases. Overall, for strong signals, linear models with DOSC is adequate, whereas ANN model is a better choice for weak signals.

3.5   Conclusion

Raman spectroscopy is widely used for monitoring the solid phase in crystallization. Nonetheless, the study of utilizing Raman spectroscopy to determine the solution concentration is rare in the literature. This study demonstrated the ability of Raman spectroscopy for determining the solution concentration and solids concentration, quantitatively, with paracetamol-ethanol and L-glutamic acid-water systems. Different data pre-processing methods and multivariable analysis techniques were applied, and their performance were compared. The result showed that DOSC pre-processing improved the fitting performance of the linear regression models (CPR, PCR and PLSR), but not for ANN model. On the other hand, ANN method, owing to its non-linear prediction ability, had better predicted results than the linear models when the signal was weak.

3.6 **References**

Acevedo, D., Yang, X., Mohammad, A., Pavurala, N., Wu, W.-L., O'Connor, T.F., Nagy, Z.K., Cruz, C.N., 2018. Raman Spectroscopy for Monitoring the Continuous Crystallization of Carbamazepine. Org. Process Res. Dev. 22, 156–165. https://doi.org/10.1021/acs.oprd.7b00322

Barmpalexis, P., Karagianni, A., Nikolakakis, I., Kachrimanis, K., 2018. Artificial neural networks (ANNs) and partial least squares (PLS) regression in the quantitative analysis of cocrystal formulations by Raman and ATR-FTIR spectroscopy. Journal of Pharmaceutical and Biomedical Analysis 158, 214–224. https://doi.org/10.1016/j.jpba.2018.06.004

Bötschi, S., Rajagopalan, A.K., Morari, M., Mazzotti, M., 2018. An Alternative Approach to Estimate Solute Concentration: Exploiting the Information Embedded in the Solid Phase. J. Phys. Chem. Lett. 9, 4210–4214. https://doi.org/10.1021/acs.jpclett.8b01998

Cheng, Y.-C., Lobo, R.F., Sandler, S.I., Lenhoff, A.M., 2006. Kinetics and equilibria of lysozyme precipitation and crystallization in concentrated ammonium sulfate solutions. Biotechnology and Bioengineering 94, 177–188. https://doi.org/10.1002/bit.20839

Cornel, J., Lindenberg, C., Mazzotti, M., 2008. Quantitative Application of in Situ ATR-FTIR and Raman Spectroscopy in Crystallization Processes. Ind. Eng. Chem. Res. 47, 4870–4882. https://doi.org/10.1021/ie800236v

Hermanto, M.W., Kee, N.C., Tan, R.B., Chiu, M.-S., Braatz, R.D., 2008. Robust Bayesian estimation of kinetics for the polymorphic transformation of L-glutamic acid crystals. AIChE Journal 54, 3248–3259.

Hu, Y., Liang, J.K., Myerson, A.S., Taylor, L.S., 2005. Crystallization Monitoring by Raman Spectroscopy: Simultaneous Measurement of Desupersaturation Profile and Polymorphic Form in Flufenamic Acid Systems. Ind. Eng. Chem. Res. 44, 1233–1240. https://doi.org/10.1021/ie049745u

Kachrimanis, K., Braun, D.E., Griesser, U.J., 2007. Quantitative analysis of paracetamol polymorphs in powder mixtures by FT-Raman spectroscopy and PLS regression.

Journal of Pharmaceutical and Biomedical Analysis 43, 407–412. https://doi.org/10.1016/j.jpba.2006.07.032

Li, H., Kawajiri, Y., Grover, M.A., Rousseau, R.W., 2014. Application of an Empirical FBRM Model to Estimate Crystal Size Distributions in Batch Crystallization. Crystal Growth & Design 14, 607–616. https://doi.org/10.1021/cg401484d

Li, J., Trout, B.L., Myerson, A.S., 2016. Multistage Continuous Mixed-Suspension, Mixed-Product Removal (MSMPR) Crystallization with Solids Recycle. Org. Process Res. Dev. 20, 510–516. https://doi.org/10.1021/acs.oprd.5b00306

Lin, M., Wu, Y., Rohani, S., 2020. Simultaneous Measurement of Solution Concentration and Slurry Density by Raman Spectroscopy with Artificial Neural Network. Crystal Growth & Design 20, 1752–1759. https://doi.org/10.1021/acs.cgd.9b01482

Mondal, P.K., Rao, V., Mittapalli, S., Chopra, D., 2017. Exploring Solid State Diversity and Solution Characteristics in a Fluorine-Containing Drug Riluzole. Crystal Growth & Design 17, 1938–1946. https://doi.org/10.1021/acs.cgd.6b01894

Nicoud, L., Licordari, F., S. Myerson, A., 2019. Polymorph control in batch seeded crystallizers. A case study with paracetamol. CrystEngComm 21, 2105–2118. https://doi.org/10.1039/C8CE01428K

Powell, K.A., Saleemi, A.N., Rielly, C.D., Nagy, Z.K., 2016. Monitoring Continuous Crystallization of Paracetamol in the Presence of an Additive Using an Integrated PAT Array and Multivariate Methods. Org. Process Res. Dev. 20, 626–636. https://doi.org/10.1021/acs.oprd.5b00373

Pratiwi, D., Fawcett, J.P., Gordon, K.C., Rades, T., 2002. Quantitative analysis of polymorphic mixtures of ranitidine hydrochloride by Raman spectroscopy and principal components analysis. European Journal of Pharmaceutics and Biopharmaceutics 54, 337–341. https://doi.org/10.1016/S0939-6411(02)00113-3

Schöll, J., Bonalumi, D., Vicum, L., Mazzotti, M., Müller, M., 2006. In Situ Monitoring and Modeling of the Solution-mediated Polymorphic Transformation of l-Glutamic Acid. Crystal Growth & Design 6, 881–891. https://doi.org/10.1021/cg0503402

Westerhuis, J.A., de Jong, S., Smilde, A.K., 2001. Direct orthogonal signal correction. Chemometrics and Intelligent Laboratory Systems 56, 13–25. https://doi.org/10.1016/S0169-7439(01)00102-2

Yang, X., Lu, J., Wang, X., Ching, C.B., 2008. *In situ* monitoring of the solution-mediated polymorphic transformation of glycine: characterization of the polymorphs and observation of the transformation rate using Raman spectroscopy and microscopy. J. Raman Spectrosc. 39, 1433–1439. https://doi.org/10.1002/jrs.2016

Zhang, X., Yin, Q., Gong, J., Liu, Z., 2010. Solubility of 5-Amino-N,N′-bis(2,3-dihydroxypropyl)-2,4,6-triiodobenzene-1,3-dicarboxamide in Ethanol + Water Mixtures. J. Chem. Eng. Data 55, 2355–2357. https://doi.org/10.1021/je9008156

Zhu, D., Ji, B., Meng, C., Shi, B., Tu, Z., Qing, Z., 2008. The application of direct orthogonal signal correction for linear and non-linear multivariate calibration. Chemometrics and Intelligent Laboratory Systems 90, 108–115. https://doi.org/10.1016/j.chemolab.2007.08.003

Chapter 4

Identifying the Polymorphic Outcome of Hypothetical Polymorphs in Batch and Continuous Crystallizers by Numerical Simulation

4 Identifying the Polymorphic Outcome of Hypothetical Polymorphs in Batch and Continuous Crystallizers by Numerical Simulation

Abstract

Polymorphism is one of the most important challenges in pharmaceutical manufacturing. However, the strategy to crystallize the desired polymorph has not been extensively investigated, especially in continuous crystallization. In this work, a numerical model, incorporating the population balance modeling, was developed considering the nucleation and growth rates of metastable and stable forms of a number of pharmaceutical solids. The impact of relative nucleation and growth kinetics of the two polymorphs on the polymorphic outcome was studied in batch and MSMPR (mixed suspension and mixed product removal) crystallizers. In both modes of operation, the simulation results show that the growth rate has a more significant effect than the birth rate. In batch crystallizers, an indicator has been proposed to analyze the time window to remove the metastable form. In MSMPR crystalizer, this indicator can be used to check whether the operating conditions (crystallizer temperature, residence time, and inlet concentration) can alter the steady-state polymorph. It is found that at high crystallizer temperature, low inlet concentration and long residence time, the production of the stable form is favored.

4.1 Introduction

Polymorphism refers to the ability of a molecule to crystallize in more than one crystal structure with different packing arrangements and/or conformations. It has been reported that more than half of the active pharmaceutical ingredients (API) exhibit solid-state polymorphism (Stahly, 2007). The polymorphs have different physiochemical properties, which have a direct impact on the stability, bioavailability and processability of pharmaceutical products (Lee et al., 2011). Crystallization plays an important role in the pharmaceutical industry, as over 90% of small molecule drugs exist in crystalline form (Variankaval et al., 2008). The crystal properties including purity (Quon et al., 2012), size distribution (Vetter et al., 2014), as well as polymorphism, are highly dependent on the operating conditions during the crystallization process.

Like most chemical processes, the crystallization process can be operated in either batch, semi-batch, or continuous mode. In the past several decades, the batch crystallization has developed well in the pharmaceutical industry, due to its simpler equipment design and higher flexibility of operation. However, the batch-to-batch variability leads to the product inconsistency and the substantial issues in the downstream processes, such as filtration, drying, and tableting (Chen et al., 2011). Recently, the concept of continuous manufacturing has aroused much attention in the pharmaceutical industry, and continuous crystallization has been studied by many authors (Alvarez et al., 2011; Eder et al., 2010; Lawton et al., 2009). Compared to the batch crystallization, continuous crystallization requires smaller equipment sizes and has lower overall costs (Schaber et al., 2011). Also, the continuous mode offers higher consistency of products, better control performance and more robust scale-up (Ranodolph, 2012), as it operates at steady state over time. Three primary types of continuous crystallizers are: mixed suspension mixed product removal (MSMPR) crystallizer (Alvarez et al., 2011), tubular crystallizer (Eder et al., 2010), and continuous oscillatory baffled crystallizer (Lawton et al., 2009). Among them, MSMPR is most convenient, as it can be easily realized by utilizing the existing batch crystallizers.

In the batch crystallization, the stable polymorph can be obtained easily through the solvent-mediated phase transformation (SMPT), but it may be rate-determining and time-consuming (Beckmann, 2000). For example, it took six hours for L-glutamic acid in water at 45℃ (Schöll et al., 2006) and two days for p-aminobenzoic acid in water at 5 ℃ (Lai et al., 2015) for the polymorphic transformation to the stable form. Seeding with the stable polymorph can be used to shorten the transition time (Cardew P. T. et al., 1985; Schöll et al., 2006). In contrast, seeding with metastable polymorph can help obtain the metastable form. Beckmann et al.(Beckmann et al., 1998) used the seeding strategy to produce the second metastable form of abecarnil. Also, Doki et al.(Doki et al., 2004) found that sufficient seed loadings of the metastable form of glycine crystals resulted in the pure metastable form, while low seed loadings led to a mixture of stable and metastable forms, whereas the stable form was obtained with no seeding. However, some metastable polymorphs cannot be achieved by the seeding method. Nicoud et al.(Nicoud et al., 2019b)

observed that seeding of metastable form paracetamol did not lead to the crystallization of the metastable form II.

The study of polymorphism control in continuous crystallization is rare (Wood et al., 2019; Zhang et al., 2017). Seeding in the continuous crystallizer has been proven to be insufficient for altering the steady-state polymorphism, because the seeds were washed out of the crystallizer after several residence times. The metastable form II paracetamol at 0 or -10 ℃ (Nicoud et al., 2019a), metastable α-form of p-aminobenzoic at 5 ℃ (Lai et al., 2015) and stable β-form of L-glutamic acid at 25 ℃ (Lai et al., 2014) could not be produced continuously from the single-stage MSMPR crystallizer even with the aid of seeding with the same polymorph crystals. The simulation result showed that the residence time should be greater than 17.4 h in order to obtain the stable form of L-glutamic acid (mass fraction>99 wt.%) at 25 ℃ (Lai et al., 2014).

From the aforementioned articles, it is noted that obtaining the preferred polymorph of different compounds requires different operating strategies in batch and MSMPR crystallizers. For paracetamol, the stable form I is the only product in either metastable-form-seeded batch crystallization or MSMPR. For L-glutamic acid, the stable form is hardly obtained from MSMPR crystallizer at 25 °C, but can be accessed at 45 °C in MSMPR or by SMPT process within six hours in a batch crystallizer. Whereas, the stable form of p-aminobenzoic acid at low temperatures needs two days to complete the SMPT process but can be easily and reliably obtained through MSMPR crystallization.

These mentioned phenomena demonstrate that the nucleation and growth rates of two polymorphs, as well as the solvent-mediated polymorphic transformation process, contribute significantly to the polymorphic outcome. However, only few studies investigate the effects of relative polymorph dynamics on the polymorphic outcome. Cardew P. T. et al. (Cardew P. T. et al., 1985) presented a theoretical model for describing the SMPT process with the dissolution rate of metastable form and growth rate of stable form. Recently, Farmer et al.(Farmer et al., 2016) and Nicoud et al (Nicoud et al., 2019a). proposed a mathematical model for polymorph selection in a single MSMPR crystallizer with considering the nucleation and growth rates of two forms. Two dimensionless

variables, related to manipulated variables (namely residence time, inlet concentration and crystallizer temperature) and crystal intrinsic properties (the coefficients and powers in nucleation rate and growth rate equations), were defined to identify which form would be obtained at steady state. The analytical solution is an effective tool to demonstrate how the combination of kinetic parameters and operating condition affect the polymorphism.

Compared to the analytical method, the numerical method is not only more straightforward and applicable for complex kinetic equations, but also can study the parameters individually. With the numerical method, Kiho Park et al. (Kiho Park et al., 2016) categorized the primary nucleation rate and secondary nucleation rate into three regions: primary nucleation dominant region, secondary nucleation dominant region and both nucleation comparable region, and studied the optimal cooling strategy of multistage MSMPRs for each region in terms of the average particle size and process yield. Later, Li and Yang (Li and Yang, 2019) varied the secondary nucleation coefficient and growth coefficient to present four cases: faster-nucleation-faster-growth, faster-nucleation-slower-growth, slower-nucleation-faster-growth, and slower-nucleation-slower-growth; and evaluated the effect of wet milling on the particle size and process yield in a single MSMPR for each case. Recently, Köllges and Vetter (Köllges and Vetter, 2019) generated the maps of polymorphic outcomes at different residence time and feed concentration in a single MSMPR coupled with/without the wet milling by using the population balance model. However, the effect of the relative kinetics on the polymorphism was not extensively investigated.

The objective of this work is to study the impact of polymorph relative kinetics of a bi-polymorphic system on the polymorphic outcome, and to investigate the optimal crystallization operation to harvest the desired polymorph. The kinetic parameters of the hypothetical polymorphs were chosen from the literature and varied in their reasonable ranges. The batch and MSMPR crystallizers were numerically simulated with population balance and selected kinetic parameters. In our work, the crystal agglomeration and breakage are ignored, due to the long computational time (Kiho Park et al., 2016) and the lack of agglomeration and breakage parameters for many compounds. The readers who are interested in the effect of the breakage on the polymorphism, are referred to the work done

by Köllges and Vetter (Köllges and Vetter, 2019). The capability of wet milling for polymorph selection in a continuous crystallizer-milling process has been proven experimentally and numerically. This work is focusing on the relative kinetics and aiming to provide a general approach to determine the crystallization type and operating conditions to ensure achieving the desired polymorph in a bi-polymorphic system, when their kinetics are known. The methodology presented in this work is also valid for the systems with solvates, in which case the mass balance equation should be modified due to the solvent loss by crystallization.

4.2   **Process and methodology**

4.2.1   **Mathematic Modeling**

The mathematical framework, consisting of population balance and mass balance, was developed for batch and MSMPR crystallizers. The high-resolution finite volume method (HR-FVM) was used to solve the population balance equations (Gunawan et al., 2004).

The one-dimensional population balance and solute mass balance in a batch crystallizer can be described as (Myerson, 2002):

$$\frac{\partial n_i(t,L)}{\partial t} + \frac{\partial [G_i(t,L)n_i(t,L)]}{\partial L} = 0 \tag{4-1}$$

$$\frac{dC(t)}{dt} = -3 \sum_i \rho_{c_i} \alpha_{V_i} \int_0^\infty G_i(t,L) L^2\, n_i(t,L) dL \tag{4-2}$$

where i refers to each polymorph, n is the number density in the crystallizer [#/m/kg solvent], L is the crystal size [m], t is time [s], G is growth rate [m/s], C is the solute concentration [kg solute/ kg solvent], ρ_c and α_V are crystal density [kg/m^3] and shape factor.

For a single MSMPR crystallizer, when the inlet and outlet flow rates are same, the population balance and solute mass balance are (Randolph and Larson, 1971):

$$\frac{\partial n_i(t,L)}{\partial t} + \frac{\partial[G_i(t,L)n_i(t,L)]}{\partial L} - \frac{n_{i,feed}(t,L) - n_i(t,L)}{\tau} = 0 \tag{4-3}$$

$$\frac{dC(t)}{dt} = -3 \sum_i \rho_{c_i} \alpha_{V_i} \int_0^\infty G_i(t,L)L^2 n_i(t,L)dL + \frac{C_{feed} - C(t)}{\tau} \tag{4-4}$$

where n_{feed} is the number density in the feed stream [#/m/kg solvent], τ is residence time [s], and C_{feed} is the solution concentration in the feed stream.

The boundary condition is

$$n_i(t,0) = \frac{B_i(t,0)}{G_i(t,0)} \tag{4-5}$$

where B is the nucleation rate [#/s/kg solvent]. The common power law expressions were chosen for the nucleation, growth and dissolution rates are given by:

$$B = (k_{b1} + k_{b2}m_3)(S-1)^b \tag{4-6}$$

$$G = k_g(S-1)^g \tag{4-7}$$

$$D = k_d(S-1) \tag{4-8}$$

where k_{b1} is the primary nucleation rate constant [#/s/kg solvent], k_{b2} is the secondary nucleation rate constant [#/s/ m^3 crystal], is the third moment of crystals [m^3 crystal /kg solvent], and k_d are growth and dissolution rate constants [m/s], b, g and d are the exponents, and S is the supersaturation, which is defined as:

$$S = \frac{C(t)}{C^*} \tag{4-9}$$

where C^* is the solubility [kg solute/ kg solvent]. The solubility of L-glutamic acids in water in the literature (Hermanto et al., 2008) is adopted in this work:

$$C_\alpha^* = 8.437 \times 10^{-3}T^2 - 0.03032T + 4.564 \tag{4-10}$$

$$C_\beta^* = 7.644 \times 10^{-3}T^2 - 0.1165T + 6.622 \qquad (4\text{-}11)$$

4.2.2 Parameter analysis

The crystal properties and operating conditions are tabulated in Table 4-1. The base values and range for the kinetic parameters (listed in Table 4-2) were selected based on the literature, especially the work of Brown et al. (Brown et al., 2020), which summarized the distributions of crystal kinetic parameters from 185 papers. The base values were used as the kinetic parameters of metastable form, while the kinetic parameters of stable form varied in the ranges. The ratio between primary nucleation and secondary nucleation rate for each polymorph was set to 10^4.

The ratio between the nucleation rate constants and growth rate constants of two polymorphs are defined as:

$$Rk_b = \frac{k_{b\,stable}}{k_{b\,metastable}} \qquad (4\text{-}12)$$

$$Rk_g = \frac{k_{g\,stable}}{k_{g\,metastable}} \qquad (4\text{-}13)$$

R_{dg} is the ratio of the metastable form dissolution rate to the stable form growth rate, which is significant for the polymorphism transition process in batch crystallization.

$$R_{dg} = \frac{k_{d\,metastable}}{k_{g\,stable}} \qquad (4\text{-}14)$$

Table 4-1. Crystal properties and operating conditions in the crystallization process

Variable	Value	Range	Unit
Crystal density	1540	-	kg/m^3
Shape factor	0.48	-	-
Solvent density	1000	-	kg/m^3

Crystallizer temperature	25	15-35	$°C$
Solubility of metastable form	0.0106	0.0069-0.0160	kg solute/kg solvent
Solubility of stable form	0.008	0.0062-0.0115	kg solute/kg solvent
Initial concentration	0.0368	-	kg solute/kg solvent
Feed concentration	0.0368	0.02-0.04	kg solute/kg solvent
Residence time	60	20-120	min

Table 4-2. Base values and variation ranges of the important parameters

Parameters	Base value	Range	Unit
k_{b1}	10^8	$10^6 - 10^{10}$	[#/s/kg solvent]
k_{b2}	10^{12}	$10^{10} - 10^{14}$	[#/s/ m^3 crystal]
k_g	10^{-8}	$10^{-10} - 10^{-6}$	[m/s]
b	2	1.5-2.5	-
g	1	0.5-1.5	-
k_d	10^{-5}	$10^{-8} - 10^{-5}$	[m/s]

4.3   Results and discussion

4.3.1   Batch crystallization

4.3.1.1   Effect of nucleation and growth rate constants

Batch crystallization operation generally favors the stable form than the metastable form, as the stable form always can be obtained with the help of solution-mediated polymorphic transformation process. In unseeded batch crystallization, the metastable form always crystallizes first, which is known as Oswald's rule of stages, and then dissolves while the stable form grows. The stable form can be readily obtained if the transition rate is fast. Conversely, it will take a long time to convert the metastable form to the stable form with a slow transition rate. In this case, the metastable form is the preferred product.

Figure 4-1 shows how the solution concentration, solids concentration of the stable form and solids concentration of the metastable form change under the unseeded condition with different Rk_b and Rk_g. As presented in Figure 4-1(e), the metastable form is suppressed by the stable form when two polymorphs have the same rate constants and orders. The reason is that the stable form has higher nucleation and growth rates throughout the process as the result of higher supersaturation. The results shown in Figure 4-1 also indicate that the higher nucleation and growth rates of the stable form can accelerate the polymorphic transition process. Furthermore, the transition time in Figure 4-1(c) is much longer than Figure 4-1(g), which demonstrates that the ratio between the growth rate constants of two polymorphs is more critical than the birth rate ratio in the batch crystallization.

Figure 4-1. Evolution of the solution and solids concentration in the unseeded solution-mediated polymorphic transformation at 25 ℃ with different Rk_b and Rk_g when $R_{dg} = 1000$.

Since the stable polymorph has a lower solubility than the metastable polymorph, the system is always more supersaturated with respect to the stable polymorph than the metastable polymorph. Hence, the nucleation and growth of stable form cannot be avoided when the target product is the metastable form. The metastable form with high polymorphic purity can only be achieved when both nucleation and growth rates of stable form are relatively slow (Figure 4-1(a)). Furthermore, the metastable product should be removed from the solution before the polymorphic transition happens.
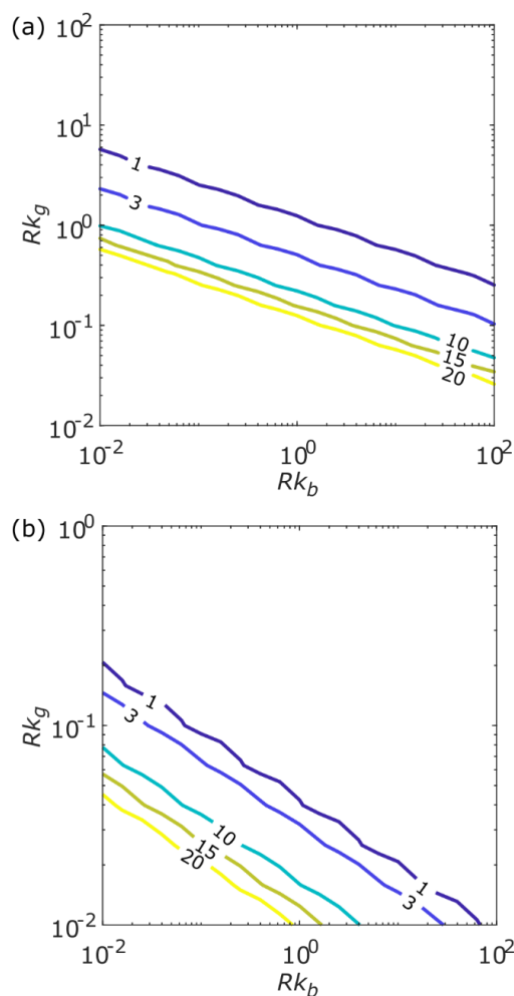
Figure 4-2. Simulation of the unseeded batch crystallization with different Rk_b and Rk_g at 25 °C: a) contour plot of the minimum time needed to obtain the 99 wt.% stable form; b) contour plot of the time window to remove 99 wt.% metastable form.

The minimum time needed to complete the polymorphic transition process and crystallize the stable form with 99 wt.% purity is plotted in Figure 4-2(a). The criteria are that the

mass fraction of the stable form is above 99 wt.% and the solution concentration reaches the solubility of the stable form. Figure 4-2(b) shows the time window for removing the metastable form from the solution before the transition process happens. The time window is counted from the earliest to latest time at which the mass fraction of metastable form is higher than 99 wt.% and the solution concentration reaches the solubility of metastable form. The results indicate that the higher Rk_b and Rk_g are, the shorter the time needed for obtaining the high purity stable form with high yield and the narrower time window to remove the metastable form. It is worth noting that the contours are approximated to straight lines with a slope of 1/3 when both axes of Rk_b and Rk_g are in logarithmic scale. The reason for the slope equaling to 1/3 is that the secondary nucleation rate is proportional to the third moment in this work. Therefore, the equation of the contours can be expressed as: $Rk_g \cdot Rk_b^{1/3} =$ constant. $Rk_g \cdot Rk_b^{1/3} < 0.22$ is required to have at least 10 min time window to remove the metastable form with 99 wt% purity.

4.3.1.2   **Effect of dissolution rate constant**

The SMPT process is controlled by the slowest step between nucleation and growth of the stable form, and dissolution of the metastable form. In Figure 4-1(a-e), the solution concentration remains at the solubility of the metastable polymorph during the dissolution of the metastable form crystals. Therefore, these cases are controlled by the growth of the stable form.

Figure 4-3 indicates that the SMPT process will be dissolution rate-controlled and take a longer time when R_{dg} decreases. Usually, the dissolution process is quicker than the growth, since the latter involves not only the boundary layer transport resistance but also the surface integration resistance (O'Mahony et al., 2012). Hence, in the following discussion, the system is assumed as not-dissolution-limited. Rdg was set to 1000.
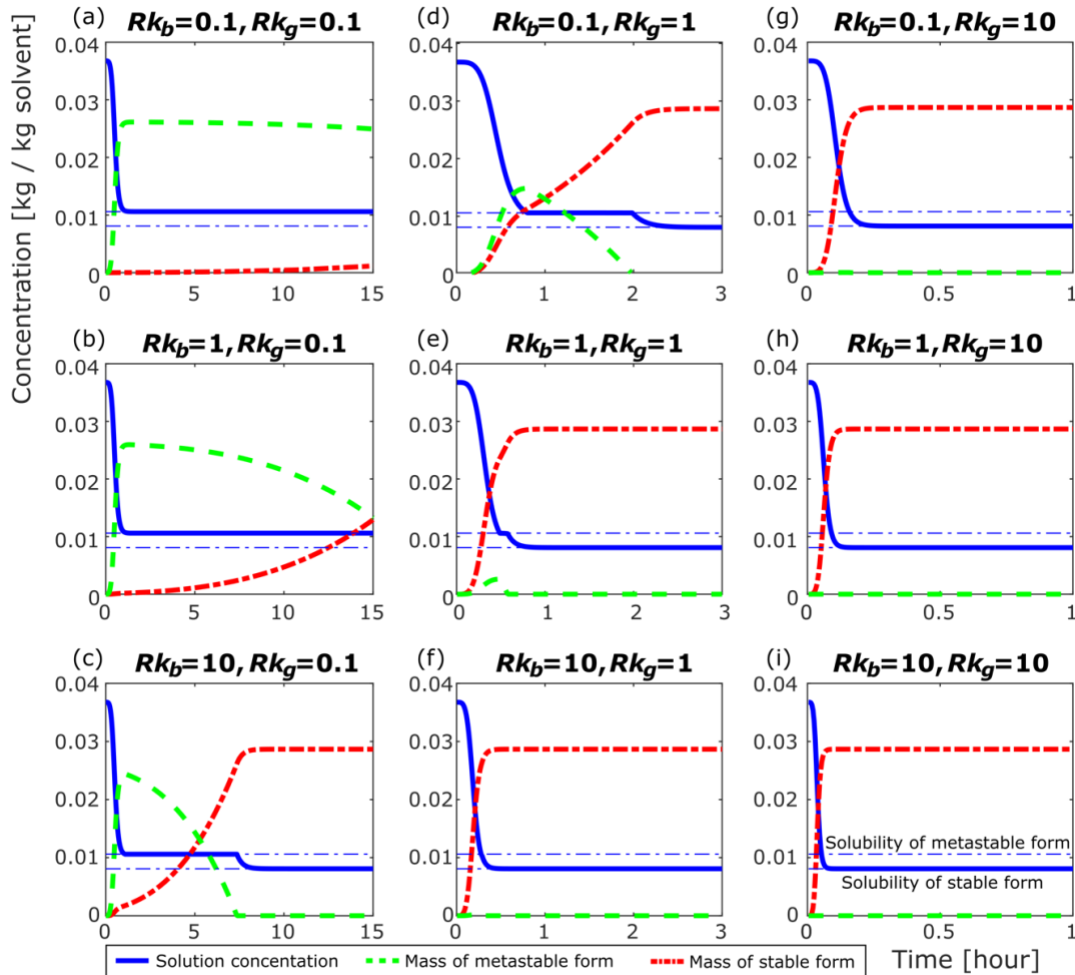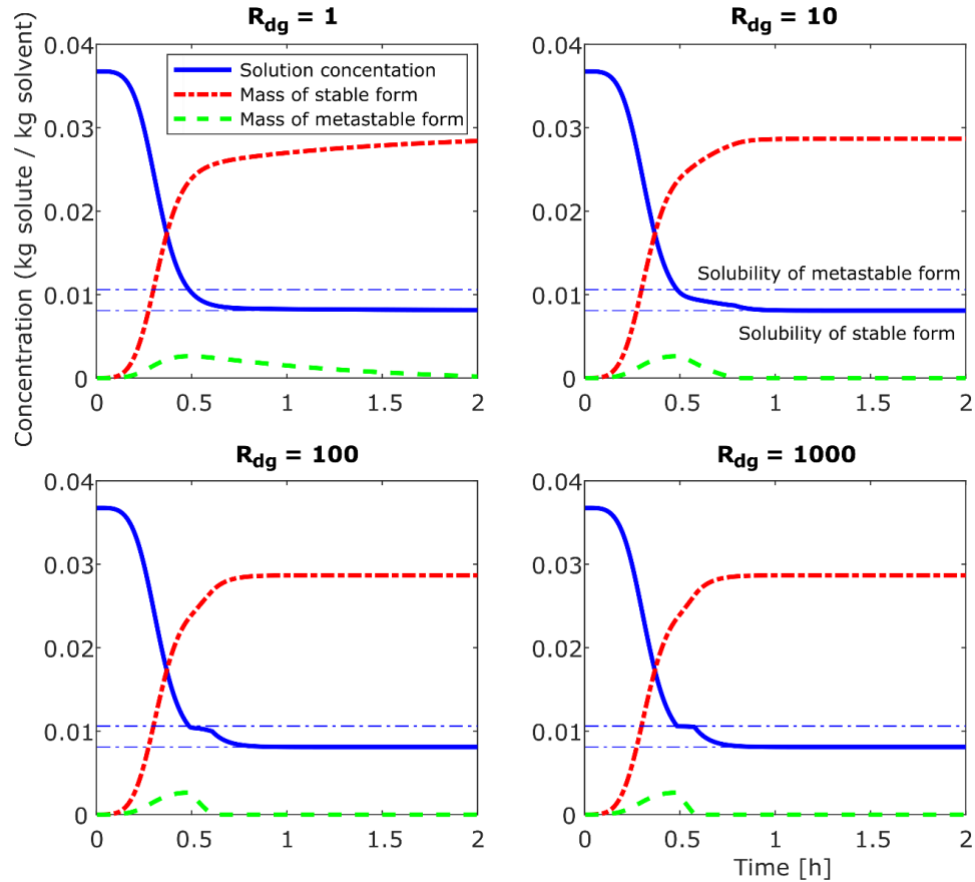
Figure 4-3. Evolution of the solution and solids concentrations in the unseeded solution-mediated polymorphic transformation at 25 ℃ with R_{dg} of 1, 10, 100 and 1000 when $Rk_b = Rk_g = 1$.

4.3.1.3   Effect of nucleation and growth rate orders

The impacts of nucleation and growth rate orders also have been investigated. The changes of the mass fraction of the stable form are presented in Figure 4-4. The lines in the same color have the same nucleation rate order b, while those in the same line styles (dashed, solid or dash-dotted) have the same growth rate order g. The slope change in the curves (black dots) corresponds to the starting point of the SMPT process, at which the metastable form starts dissolving, leading to the increased slope of the stable form purity. The mass fraction of the stable form reaches 1, indicating the completion of the transformation process. It is found that increasing b and g shortens the transition time and the latter has a more significant effect. The results also reveal that changing b and g in their reasonable ranges (1.5 to 2.5 and 0.5 to 1.5) does not influence the batch crystallization process as

much as k_b and k_g. This could be explained by the fact that the variation range of kinetic constants, is at least an order of magnitude greater than that of the supersaturation term $(S-1)^b$ or $(S-1)^g$.
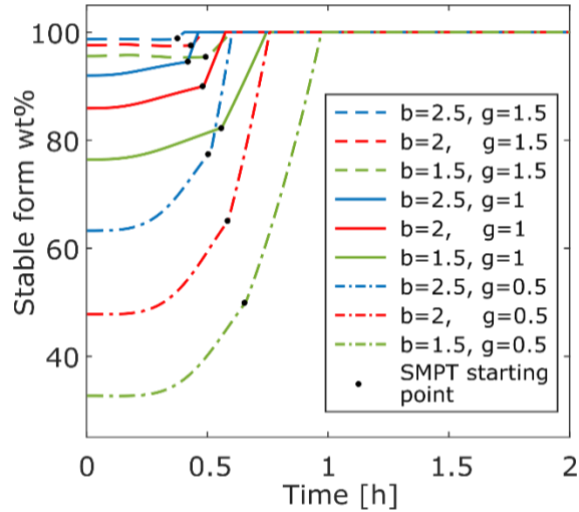
Figure 4-4. Evolution of the mass fraction of the stable form in the unseeded solution-mediated polymorphic transformation at 25 °C with different nucleation and growth rate orders.

4.3.2   A single MSMPR

4.3.2.1   Effect of nucleation and growth rate constants
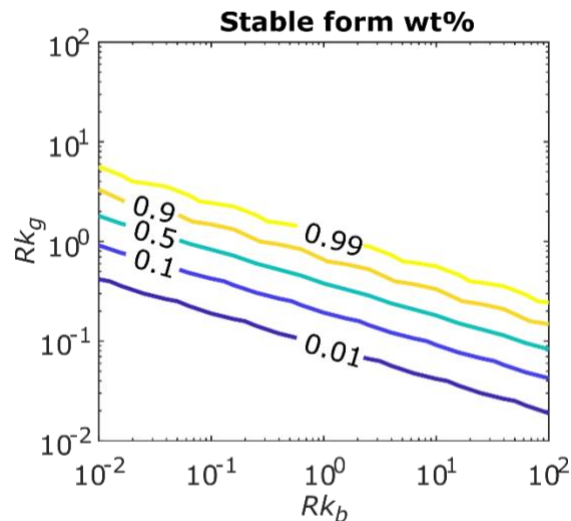
Figure 4-5. Simulation of the MSMPR crystallization at 25 °C with residence $\tau = 1$ h and feed concetration $C_{feed} = 0.0368\ kg/kg$. Contour plot of the mass fraction of the stable form at the steady state with a range of Rk_b and Rk_g.

Unlike the batch crystallization that heads to thermodynamic equilibrium and crystalizes the stable polymorph, the continuous crystallization operates at the steady-state and produces the crystals based on the relative nucleation and growth rates between two polymorphs (Zhang et al., 2017). In this section, the effect of Rk_b and Rk_g on the polymorph was investigated in a range of 10^{-2} to 10^2. As illustrated in Figure 4-5, the contours of stable form mass fraction also can be expressed as $Rk_g \cdot Rk_b^{1/3} = $ constant. The higher constant represents the higher mass fraction of the stable form. The constants for 1, 5, 50, 95 and 99 wt.% contours were calculated and summarized in Table 4-3, under the operating condition listed in Table 4-1. All experimental results of paracetamol, p-aminobenzoic acid and L-glutamic acid are in agreement with the expected results, as shown in Table 4-4. Notably, the $Rk_g \cdot Rk_b^{1/3}$ of paracetamol is significantly higher than the value for 99 wt.% stable form, explaining why the polymorph cannot be altered solely by varying the operating conditions (Nicoud et al., 2019a). Hence, changing the solvent or adding additives may be an effective method influencing the kinetic ratio of the two polymorphs.

Table 4-3. Constants for the contours of stable form contours

Stable form wt.%	$Rk_g \cdot Rk_b^{1/3}$
1	0.0875
5	0.1488
50	0.3802
95	0.7925
99	1.1574

Table 4-4. Experimental results and $Rkg \cdot Rkb^{1/3}$ of paracetamol, p-aminobenzoic acid and L-glutamic acid

	T °C	Rk_b	Rk_g	$Rk_g \cdot Rk_b^{1/3}$	Polymorph
paracetamol	0	478	5.019	39.244>>1.1574	stable
p-aminobenzoic acid	5	1.534	0.935	1.0786>0.7925	stable
L-glutamic acid	25	0.295	0.115	0.0768<0.0875	metastable

From the expression of $Rk_g \cdot Rk_b^{1/3}$, one can conclude that k_g has a more significant effect on the product polymorph that kb does in MSMPR crystallization. It agrees with the findings in the literature (Nicoud et al., 2019a), although different kinetic expressions were adopted in our work and the mentioned paper. It indicates that the polymorphic outcome in the continuous crystallization is influenced by the growth rate constant, and to a lesser extent, by the nucleation rate constant.

4.3.2.2   Effect of nucleation and growth rate orders

We also studied the effect of nucleation and growth rate orders on the polymorph in MSMPR crystallization. The nucleation and growth rate order of the metastable form were fixed at 2 and 1, while the orders of metastable form were changed in the range of 1.5 to 2.5 and 0.5 to 1.5. The contours of the mass fraction of the stable form at the steady-state are plotted in Figure 4-6. It is interesting to note that the mass fraction of the stable form drops slightly with the nucleation rate order b and growth rate order g of the stable form. The reason is that the nucleation and growth rate decreases with b and g when the relative supersaturation ($c/c^* - 1$) is less than 1. g has a greater influence than b, which is consistent in batch and MSMPR crystallization.

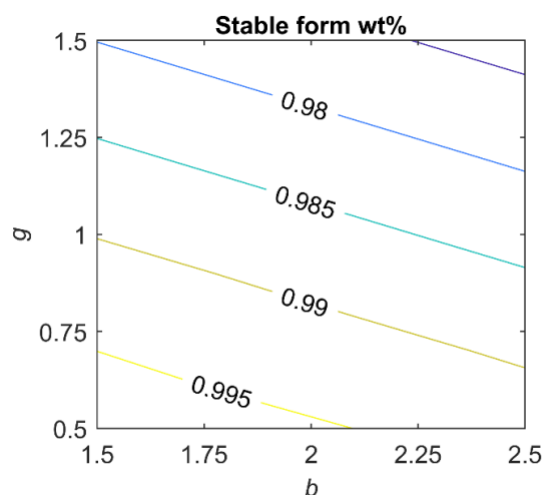**Figure 4-6. Simulation of the MSMPR crystallization at 25 ℃ with residence $\tau = 1$ h and feed concetration $C_{feed} = 0.0368 \ kg/kg$. Contour plot of mass fraction of the stable form in MSMPR crystallizer at the steady-state with different nucleation and growth rate orders**

4.3.2.3 **Effect of operating conditions**

As mentioned in Section 4.3.2, the operating condition has a limited effect on the polymorph in some cases, such as paracetamol-water system, due to the faster crystallization of the stable form (Nicoud et al., 2019a). Therefore, the attainable region in term of polymorph in MSMPR was studied in this section. Crystallizer temperature, residence time, and inlet concentration are the main manipulated variables in an MSMPR crystallizer. To cover the normal operating range in MSMPR, the residence time was varied from 20 to 120 min. The variation ranges of the crystallizer temperature and inlet concentration were selected as 15-35 ℃ and 0.02-0.04 kg/kg (equals to the solubility of metastable form at 41℃ and 63℃), ensuring that the system is supersaturated with respect to both forms.

Table 4-5. Four cases of the polymorphic systems

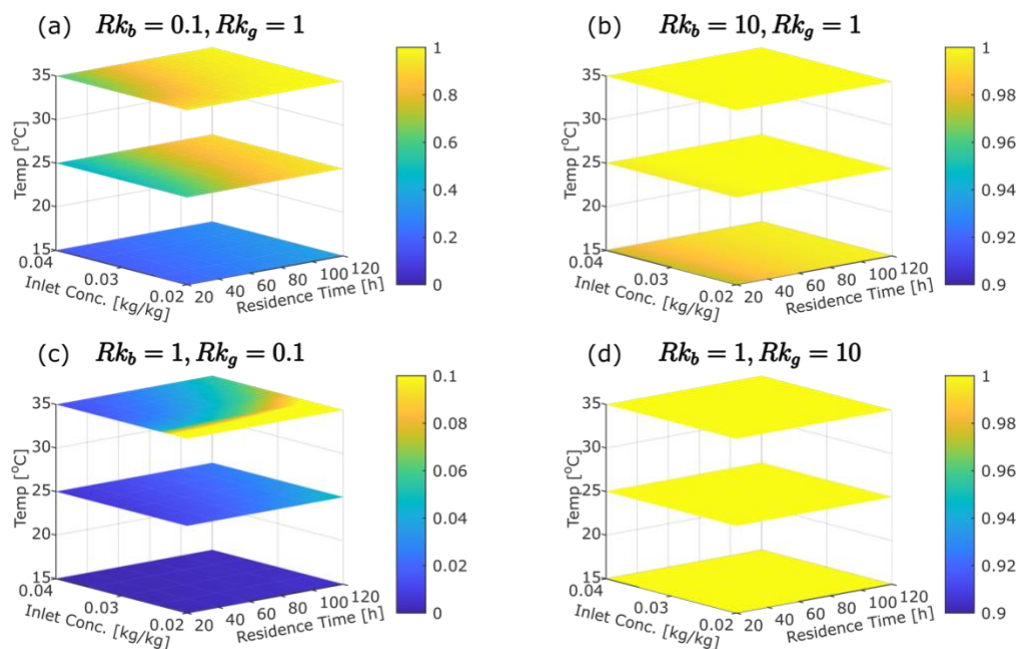| Case	Birth rate	Rk_b	Growth rate	Rk_g	$Rk_g \cdot Rk_b^{1/3}$
a)	Stable > metastable	0.1	Stable = metastable	1	0.464
b)	Stable < metastable	10	Stable = metastable	1	2.15
c)	Stable = metastable	1	Stable > metastable	0.1	0.1
d)	Stable = metastable	1	Stable < metastable	10	10

Figure 4-7. Mass fraction of the stable form at steady-state obtained from process simulation with a range of residence time, inlet concentration and crystallizer temperature. Note that the range of color bar is 0 to 1 in (a), 0.9 to 1 in (b), 0 to 0.1 in (c), and 0.9 to 1and (d).

The impacts of operating conditions were analyzed in four different cases, as listed in Table 4-5. The simulation results in Figure 4-7, show different behavior depending on $Rk_g \cdot Rk_b^{1/3}$. For case b-d, the operating condition has little effect on the polymorph. Nevertheless, the mass fraction of stable from in case a) varies from 16.44 % to 99.52 %, since its $Rk_g \cdot Rk_b^{1/3}$ is within the range of 5 to 95 wt.% (Table 4-4). As presented in Figure 4-7(a), the maximum purity of the stable form is achieved with high crystallizer temperature, low inlet concentration and long residence time. Increasing crystallizer temperature and decreasing inlet concentration benefit the stable form through increasing the supersaturation ratio of the two forms and further impacting their relative kinetics, while the residence time favors the stable form via providing more time to promote the polymorphic transformation. However, these choices are at the expense of process productivity. In addition, the result shows that the influences of crystallizer temperature and inlet concentration are more significant than residence time, which agrees with the previous publication (Lai et al., 2014).

In order to quantify the range of $Rk_g \cdot Rk_b^{1/3}$ in which the manipulated variables can alter the polymorphic outcome, the maximum and minimum mass fractions of the stable form were plotted versus $Rk_g \cdot Rk_b^{1/3}$ in Figure 4-8. When $Rk_g \cdot Rk_b^{1/3}$ is between 0.1 and 1, the operating conditions, namely crystallizer temperature, residence time, and inlet concentration, can effectively control the product polymorph. When $Rk_g \cdot Rk_b^{1/3}$ is around 0.5, the attainable region is the widest. The mass fraction ranges of the stable form are 0.002 - 0.108 and 0.734 - 1 when $Rk_g \cdot Rk_b^{1/3}$ is 0.1 and 1, respectively. So the dominant product is either the metastable form or the stable form.
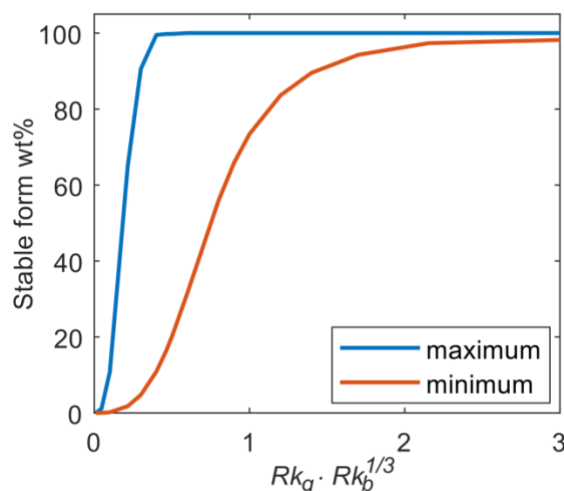

Figure 4-8. Attainable region of stable form mass fraction in a single MSMPR crystallizer with the operation range listed in Table 4-1.

4.4   Conclusions

In this work, the impact of relative kinetics between two polymorphs on polymorphic outcome was studied in batch and MSMPR crystallization. In both circumstances, the simulation results show that the growth rate has a more significant effect than the birth rate. Specifically, growth rate order g has a greater influence than the nucleation order b on the polymorphic outcome, while constant k_g has a greater influence than k_b. On the other hand, changing b and g in their reasonable ranges does not influence the polymorphic outcome as much as k_b and k_g. The parameter $Rk_g \cdot Rk_b^{1/3}$ is an important indicator. In batch crystallization, solvent-mediated phase transformation (SMPT) plays an important role in

the polymorphic outcome. The stable polymorph always can be obtained through the SMPT process. However, the metastable form with high purity can only be achieved before the SMPT process happens. $Rk_g \cdot Rk_b^{1/3} < 0.22$ is required to have at least 10 min time window to remove the metastable form. In MSMPR crystallization, the polymorphic outcome can be altered by the process operation variables (crystallizer temperature, residence time, and inlet concentration), when $Rk_g \cdot Rk_b^{1/3}$ is around 0.5. High crystallizer temperature, low inlet concentration and long residence favor the production of the stable form. The crystallizer temperature and inlet concentration are more significant than residence time. When $Rk_g \cdot Rk_b^{1/3}$ is greater than 1 or less than 0.1, the dominant product is either the stable form or metastable form, and the operating conditions cannot effectively control the product polymorph. In such a case, changing the solvent and adding additives are alternative methods to crystallize the desired polymorph by influencing the kinetic ratio of two polymorphs. Overall, the stable form with slow kinetics ($Rk_g \cdot Rk_b^{1/3} < 0.1$) cannot be easily obtained from MSMPR crystallization, but can be accessed by the SMPT process in batch crystallization. Collectively, MSMPR crystallization is more dominated by kinetics than thermodynamics and is more friendly to metastable form than batch crystallization. Based on the above findings, the effort required to design a crystallization process for specific polymorph is facilitated once the relative kinetics of two polymorphs are known.

4.5   References

Alvarez, A.J., Singh, A., Myerson, A.S., 2011. Crystallization of Cyclosporine in a Multistage Continuous MSMPR Crystallizer. Cryst. Growth Des. 11, 4392–4400. https://doi.org/10.1021/cg200546g

Beckmann, W., 2000. Seeding the Desired Polymorph: Background, Possibilities, Limitations, and Case Studies. Org. Process Res. Dev. 4, 372–383. https://doi.org/10.1021/op0000778

Beckmann, W., Nickisch, K., Budde, U., 1998. Development of a Seeding Technique for the Crystallization of the Metastable A Modification of Abecarnil. Org. Process Res. Dev. 2, 298–304. https://doi.org/10.1021/op980029b

Brown, C., Maldonado, D., Vassileiou, A., Johnston, B., Florence, A., 2020. Data Mining Crystallization Kinetics (preprint). https://doi.org/10.26434/chemrxiv.11708286.v2

Cardew P. T., Davey R. J., Birchall James Derek, 1985. The kinetics of solvent-mediated phase transformations. Proc. R. Soc. Lond. Math. Phys. Sci. 398, 415–428. https://doi.org/10.1098/rspa.1985.0043

Chen, J., Sarma, B., Evans, J.M.B., Myerson, A.S., 2011. Pharmaceutical Crystallization. Cryst. Growth Des. 11, 887–895. https://doi.org/10.1021/cg101556s

Doki, N., Yokota, M., Kido, K., Sasaki, S., Kubota, N., 2004. Reliable and Selective Crystallization of the Metastable α-Form Glycine by Seeding. Cryst. Growth Des. 4, 103–107. https://doi.org/10.1021/cg034123h

Eder, R.J.P., Radl, S., Schmitt, E., Innerhofer, S., Maier, M., Gruber-Woelfler, H., Khinast, J.G., 2010. Continuously Seeded, Continuously Operated Tubular Crystallizer for the Production of Active Pharmaceutical Ingredients. Cryst. Growth Des. 10, 2247–2257. https://doi.org/10.1021/cg9015788

Farmer, T.C., Carpenter, C.L., Doherty, M.F., 2016. Polymorph selection by continuous crystallization. AIChE J. 62, 3505–3514. https://doi.org/10.1002/aic.15343

Gunawan, R., Fusman, I., Braatz, R.D., 2004. High resolution algorithms for multidimensional population balance equations. AIChE J. 50, 2738–2749. https://doi.org/10.1002/aic.10228

Hermanto, M.W., Kee, N.C., Tan, R.B., Chiu, M.-S., Braatz, R.D., 2008. Robust Bayesian estimation of kinetics for the polymorphic transformation of L-glutamic acid crystals. AIChE J. 54, 3248–3259.

Kiho Park, Kim, D.Y., Yang, D.R., 2016. Operating Strategy for Continuous Multistage Mixed Suspension and Mixed Product Removal (MSMPR) Crystallization Processes Depending on Crystallization Kinetic Parameters. Ind. Eng. Chem. Res. 55, 7142–7153. https://doi.org/10.1021/acs.iecr.6b01386

Köllges, T., Vetter, T., 2019. Polymorph Selection and Process Intensification in a Continuous Crystallization–Milling Process: A Case Study on l-Glutamic Acid Crystallized from Water. Org. Process Res. Dev. 23, 361–374. https://doi.org/10.1021/acs.oprd.8b00420

Lai, T.-T.C., Cornevin, J., Ferguson, S., Li, N., Trout, B.L., Myerson, A.S., 2015. Control of Polymorphism in Continuous Crystallization via Mixed Suspension Mixed Product Removal Systems Cascade Design. Cryst. Growth Des. 15, 3374–3382. https://doi.org/10.1021/acs.cgd.5b00466

Lai, T.-T.C., Ferguson, S., Palmer, L., Trout, B.L., Myerson, A.S., 2014. Continuous Crystallization and Polymorph Dynamics in the L -Glutamic Acid System. Org. Process Res. Dev. 18, 1382–1390. https://doi.org/10.1021/op500171n

Lawton, S., Steele, G., Shering, P., Zhao, L., Laird, I., Ni, X.-W., 2009. Continuous Crystallization of Pharmaceuticals Using a Continuous Oscillatory Baffled Crystallizer. Org. Process Res. Dev. 13, 1357–1363. https://doi.org/10.1021/op900237x

Lee, A.Y., Erdemir, D., Myerson, A.S., 2011. Crystal Polymorphism in Chemical Process Development. Annu. Rev. Chem. Biomol. Eng. 2, 259–280. https://doi.org/10.1146/annurev-chembioeng-061010-114224

Li, H., Yang, B.-S., 2019. Model evaluation of particle breakage facilitated process intensification for Mixed-Suspension-Mixed-Product-Removal (MSMPR) crystallization. Chem. Eng. Sci. 207, 1175–1186. https://doi.org/10.1016/j.ces.2019.07.030

Myerson, A.S. (Ed.), 2002. Handbook of industrial crystallization, 2nd ed. ed. Butterworth-Heinemann, Boston.

Nicoud, L., Licordari, F., Myerson, A.S., 2019a. Polymorph Control in MSMPR Crystallizers. A Case Study with Paracetamol. Org. Process Res. Dev. 23, 794–806. https://doi.org/10.1021/acs.oprd.8b00351

Nicoud, L., Licordari, F., S. Myerson, A., 2019b. Polymorph control in batch seeded crystallizers. A case study with paracetamol. CrystEngComm 21, 2105–2118. https://doi.org/10.1039/C8CE01428K

O'Mahony, M.A., Maher, A., Croker, D.M., Rasmuson, Å.C., Hodnett, B.K., 2012. Examining Solution and Solid State Composition for the Solution-Mediated Polymorphic Transformation of Carbamazepine and Piracetam. Cryst. Growth Des. 12, 1925–1932. https://doi.org/10.1021/cg201665z

Quon, J.L., Zhang, H., Alvarez, A., Evans, J., Myerson, A.S., Trout, B.L., 2012. Continuous Crystallization of Aliskiren Hemifumarate. Cryst. Growth Des. 12, 3036–3044. https://doi.org/10.1021/cg300253a

Randolph, A., Larson, M., 1971. Theory of Particulate Processes: Analysis and Techniques of Continuous Crystallization. Elsevier.

Ranodolph, A., 2012. Theory of Particulate Processes: Analysis and Techniques of Continuous Crystallization. Elsevier.

Schaber, S.D., Gerogiorgis, D.I., Ramachandran, R., Evans, J.M.B., Barton, P.I., Trout, B.L., 2011. Economic Analysis of Integrated Continuous and Batch Pharmaceutical Manufacturing: A Case Study. Ind. Eng. Chem. Res. 50, 10083–10092. https://doi.org/10.1021/ie2006752

Schöll, J., Bonalumi, D., Vicum, L., Mazzotti, M., Müller, M., 2006. In Situ Monitoring and Modeling of the Solvent-Mediated Polymorphic Transformation of l-Glutamic Acid. Cryst. Growth Des. 6, 881–891. https://doi.org/10.1021/cg0503402

Stahly, G.P., 2007. Diversity in Single- and Multiple-Component Crystals. The Search for and Prevalence of Polymorphs and Cocrystals. Cryst. Growth Des. 7, 1007–1026. https://doi.org/10.1021/cg060838j

Variankaval, N., Cote, A.S., Doherty, M.F., 2008. From form to function: Crystallization of active pharmaceutical ingredients. AIChE J. 54, 1682–1688. https://doi.org/10.1002/aic.11555

Vetter, T., Burcham, C.L., Doherty, M.F., 2014. Regions of attainable particle sizes in continuous and batch crystallization processes. Chem. Eng. Sci. 106, 167–180. https://doi.org/10.1016/j.ces.2013.11.008

Wood, B., Girard, K.P., Polster, C.S., Croker, D.M., 2019. Progress to Date in the Design and Operation of Continuous Crystallization Processes for Pharmaceutical Applications. Org. Process Res. Dev. 23, 122–144. https://doi.org/10.1021/acs.oprd.8b00319

Zhang, D., Xu, S., Du, S., Wang, J., Gong, J., 2017. Progress of Pharmaceutical Continuous Crystallization. Engineering 3, 354–364. https://doi.org/10.1016/J.ENG.2017.03.023

Chapter 5

Effects of Operating Conditions and Strategies on the Product Properties of L-glutamic acid-water system

A manuscript will be prepared from the content of this chapter and submitted to a suitable scientific journal.

5 Effects of Operating Conditions and Strategies on the Product Properties of L-glutamic acid-water system

Crystallization process involves the nucleation, growth/dissolution and agglomeration/breakage phenomena, resulting in numerous challenges in controlling the product qualities. Furthermore, a number of potential manipulated variables in both batch and continuous crystallizers also increase the complexity of the crystallization process. Therefore, the experimental method is costly and time-consuming for designing the crystallization process properly to produce the desirable product. Alternatively, the mathematical modeling can predict the product property in a wide range of operating conditions in a short time with minimal experiments, which can help the crystallization industries boost the research & development process and reduce the production cost (Myerson, 2002). In this chapter, the impact of operating conditions on the product properties was investigated thoroughly, including the polymorphism, yield and crystal size distribution.

5.1 Introduction

As discussed in Section 4.1, batch and MSMPR (mixed suspension and mixed product removal) crystallization are the most widely used operation modes for the crystallization process. Batch crystallizers are relatively simple and flexible and need a low level of maintenance (Myerson, 2002), but suffer from the batch-to-batch variability. In contrast, MSMPR operates continuously and can provide high consistency on the product. However, there are also several challenges associated with MSMPR crystallization, as discussed below:

1. Crystal size classification and blockage in the transfer tube during the slurry withdrawal process. In the laboratory scale, a common method to deal with this issue is using an intermittent withdrawal scheme with a peristaltic pump to remove the slurry at every 5% (Capellades et al., 2018) or 10% (Lai et al., 2015; Li et al., 2016; Nicoud et al., 2019; Onyemelukwe et al., 2019) of a residence time with high transport velocity. Lührmann et al. (Lührmann et al., 2018) designed a unique vessel in which the suspension was removed through the installed lateral and

vertical overflow tubes by gravity, instead of pumps, which prevents the agglomeration in the pipeline.

2. Insufficient residence time for crystal nucleation and growth. Based on the definition of residence time, one could increase it by using a larger crystallizer or a smaller flow rate, but the former would increase the equipment cost and reduce the mixing uniformity, while the latter deteriorates the crystal size classification and blockage phenomena.

3. Lower yield than a batch crystallizer. The product yield in MSMPR is defined as:

$$yield\ (\%) = \frac{C_{feed} - C}{C_{feed} - C^*} \times 100 \tag{5-1}$$

where C_{feed}, C and C^* are the feed concentration, solute concentration and solubility. Unlike batch crystallization always ending at equilibrium-state, the continuous crystallization reaches steady-state at which the solution is still supersaturated, so the yield of MSMPR crystallization is usually lower than that in batch crystallization.

There are several methods to address the last two issues: a) decreasing the temperature; b) increasing the residence time by increasing the crystallizer size or decreasing the flow rate; c) increasing the crystal residence time by using multistage MSMPRs, periodic MSMPRs, or solids recycle. Su et al. (Su et al., 2017) developed periodic flow crystallization and increased the residence time by adding a holding period to MSMPR crystallizer. Li et al. (Li et al., 2016) used solids recycle to increase the solid residence time and thus increase the yield close to the theoretical maximum in multistage continuous MSMPR crystallizer.

Multistage MSMPR crystallizers can overcome the drawbacks of insufficient residence time and low yield that exist in a single MSMPR. Compared to a single-stage MSMPR, cascaded multistage MSMPRs have longer average residence time and more uniform residence time distribution (RTD), so that it can produce larger crystals with a narrower CSD. The cascaded multiple-stage MSMPR not only can separate the nucleation and growth step of the crystallization process, which is beneficial to produce crystals with

desired polymorph and size distribution, but also enhance the process controllability and reduce the operation cost (Kiho Park et al., 2016).

In this chapter, the effects of the operating conditions in batch, single stage and multistage MSMPR crystallization configurations on the crystal properties were investigated, including the polymorphism, yield and crystal size distribution. L-glutamic acid - water was selected as the model system in this chapter, as the L-glutamic acid has been studied comprehensively in the literature and the parameters needed for crystallization process modeling are available. In this work, the population balance equation was solved by the method of characteristics and method of moments.

5.2   **Mathematical model**

L-glutamic acid has two forms: the stable α-form and the metastable β-form. The solubilities of α-form and β-form are (Hermanto et al., 2008):

$$C_\alpha^* = 8.437 \times 10^{-3}T^2 - 0.03032T + 4.564 \tag{5-2}$$

$$C_\beta^* = 7.644 \times 10^{-3}T^2 - 0.1165T + 6.622 \tag{5-3}$$

where T is the temperature in °C. The following equations represent the nucleation, growth and dissolution equations obtained by Schöll et al (Schöll et al., 2006):

$$B_\alpha = 8.0 \times 10^5 S_\alpha^{7/3} \exp\left[-\frac{0.1}{ln^2 S_\alpha}\right] \tag{5-4}$$

$$G_\alpha = 0.25 \times 10^{-7}(S_\alpha - 1)^{5/6} \exp\left[-\frac{0.09}{S_\alpha - 1}\right] \tag{5-5}$$

$$D_\alpha = 3.5 \times 10^{-5}(1 - S_\alpha) \tag{5-6}$$

$$B_\beta = 5.4 \times 10^4 S_\beta^{7/3} exp\left[-\frac{15}{ln^2 S_\beta}\right] + 6.0 \times 10^4 \mu_\alpha^2 \exp\left[-\frac{0.001}{ln S_\beta}\right] \tag{5-7}$$

$$G_\beta = 6.5 \times 10^{-8} (S_\beta - 1)^{5/6} \exp\left[-\frac{0.16}{S_\beta - 1}\right] \tag{5-8}$$

B, G and D are nucleation, growth and dissolution rates. $S_\alpha = C/C_\alpha^*$ and $S_\beta = C/C_\beta^*$ are the relative supersaturation.

The seed size distribution is assumed to have a normal distribution and expressed as:

$$n_{seed}(L) = \frac{A}{\sqrt{2\pi}\sigma} \exp\left[-\frac{(L - \bar{L})^2}{2\sigma^2}\right] \tag{5-9}$$

where σ and $\bar{L}$ are the standard deviation and average size of the seeds. A is an adjustable constant to change the seed mass. The seed mass can be calculated from

$$m_{seed} = \rho_{seed} k_V \int_0^\infty n_{seed} L^3 \, dL \tag{5-10}$$

ρ_{seed} and k_V are the seed density and its volumetric shape factor. The seed density for both forms is 1540 kg/m^3. The shape factors for prismatic α-form and needle-shaped β-form are 0.48 and 0.031, respectively (Hermanto et al., 2008).
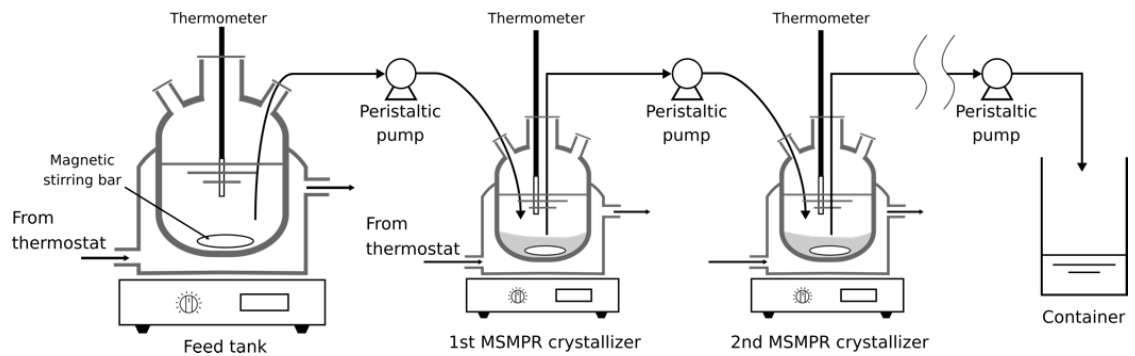

Figure 5-1. Schematics of multiple-stage MSMPR crystallizers

The population balance and solute mass balance for batch and single MSMPR have been described in Section 4.2.1. The schematics of multiple-stage MSMPR crystallizers are shown in Figure 5-1.

The population balance and solute mass balance for the first MSMPR are the same as the single MSMPR, and the subsequent stages have the inlets from previous stage, so their balances are

$$\frac{\partial n_{i,j}(t,L)}{\partial t} + \frac{\partial[G_j(t,L)n_{i,j}(t,L)]}{\partial L} - \frac{n_{i,j-1}(t,L) - n_{i,j}(t,L)}{\tau} = 0 \qquad (5\text{-}11)$$

$$\frac{dC_j(t)}{dt} = -3 \sum_i \rho_{c_i} k_{V_i} \int_0^\infty G_{i,j}(t,L)L^2 \, n_{i,j}(t,L)dL + \frac{C_{j-1} - C_j(t)}{\tau} \qquad (5\text{-}12)$$

where i refers to each polymorph and j is the MSMPR stage number.

5.3   Modeling results

5.3.1   Batch crystallization

For cooling batch crystallization, the manipulated variables are initial solution concentration, temperature profile, and seeding conditions.

5.3.1.1   Initial solution concentration

Schöll et al. (Schöll et al., 2006) found that with different initial concentration (43, 48 and 53g/kg solvent at $45\,°C$) of L-glutamic acid in an unseeded batch crystallization, the transformation processes from the metastable form to the stable form have no obvious distinction, and the crystal size distributions are very similar for three experiments. The modeling results presented in Figure 5-2 show similar behaviors as observed in the experiments.
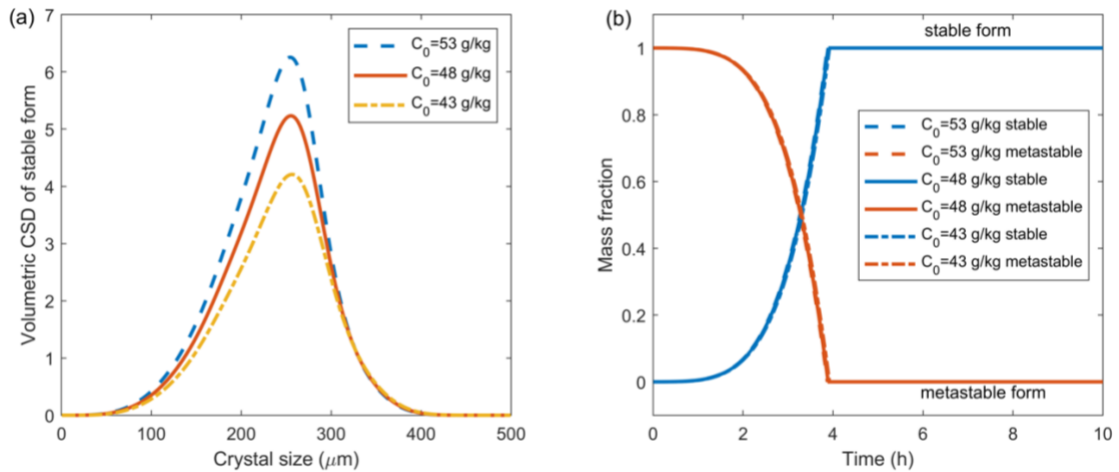
Figure 5-2. a) Volumetric crystal size distribution of stable form and b) mass fraction of two forms with three different initial concentrations

However, if the variation range of initial concentration is expanded to 25 to 60 g/kg (Figure 5-3), the simulation result shows that the transition time increases and the surface-average crystal size of the final product decreases monotonically with initial concentration increasing. When the initial concentration is within the range of 25-40 g/kg, the transformation process and the average size of the final product change significantly with the initial concentration. When the initial concentration is higher than 40 g/kg, the influences of the initial concentration are negligible. It is concluded that a lower initial condition leads to larger crystals at the expense of process productivity.
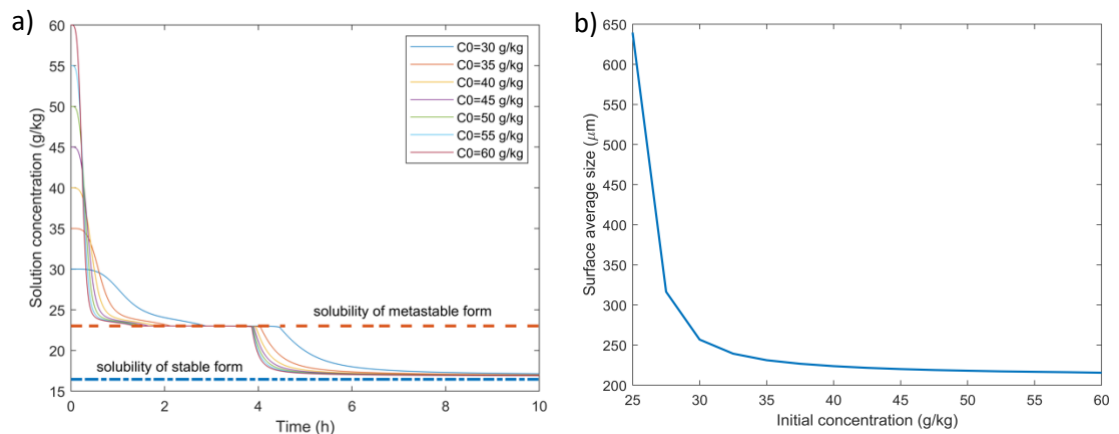

Figure 5-3. a) Solution concentration profile during the transformation process and b) the surface average size of stable form with different initial concentration

5.3.1.2 Cooling profile

The cooling temperature profile of the batch crystallizer can be expressed as

$$T(t) = T_i - (T_i - T_f)\left(\frac{t}{t_c}\right)^P \qquad (5\text{-}13)$$

where T_i and T_i are initial temperature and final temperature, t_c is the total cooling time (can be equal to or smaller than the batch time), and P is the power number of the cooling policy. Three cooling policies, including natural cooling (P=0.1), linear cooling (P=1) and near optimal cooling (P=3) were studied for unseeded batch crystallization of L-glutamic acid – water system by Sheikholeslamzadeh and Rohani (Sheikholeslamzadeh and Rohani, 2013). They found that the natural cooling results in a rich content of fine particles and the higher value of P leads to a better quality of the product. However, in Sheikholeslamzadeh and Rohani's work, the cooling time was equal to the batch time (two hours), which means the system did not reach the equilibrium state at the end of operation. Here, the batch time was set to 5 hours and the cooling time was kept at two hours. Figure 5-4 (b) shows the high P value favours the production of large crystals of stable form.
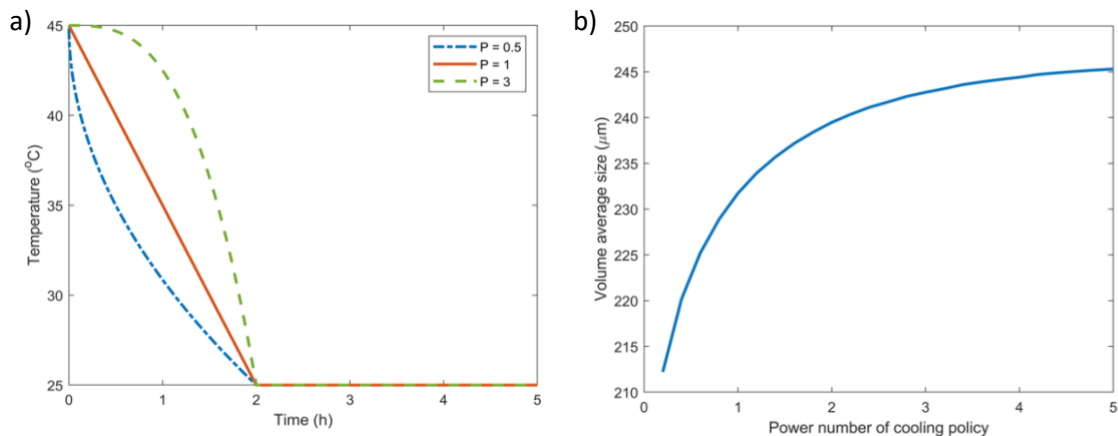

Figure 5-4. a) Three different cooling policies and b) the volume average size of stable form with different cooling policies

5.3.1.3 Seeding condition

Table 5-1. Seed parameters for different cases

Cases	Mass (g/kg)	wt% of the stable form in seeds	Average size (μm)	Standard deviation (μm)
Polymorphic composition of seeds	20.3*10%	[0:20% 100%]	40	5
Seed mass	20.3*[0, 5,10, 15,20]%	100%	40	5
Seed mass	20.3*[0, 5,10, 15,20]%	0%	40	5
Seed size	20.3*10%	100%	30:20:90	5
Seed size	20.3*10%	0%	30:20:90	5

The effect of seed mass, seed size and seed polymorphic composition on the product is studied in this section. The feed temperature is 45 ℃ and the initial solution concentration is 36.8 g/kg, corresponding to the solubility of metastable form at 60 ℃. Hence, the maximum mass of the crystals is 20.3 g/kg, which is the difference between the initial condition and the solubility of the stable form at 45 ℃ (16.5 g/kg). Seed mass, seed size and seed polymorphic composition for different cases are summarized in Table 5-1.

First, the polymorphic composition of the seeds is investigated. The total seed mass is 10% of the maximum mass of the crystals (20.3 g/kg). The average size and standard deviation of seeds are $40\mu m$ and $5\mu m$. Figure 5-5(a) shows that the higher the mass fraction of the stable form is, the faster the transformation process is, which is due to the less metastable forms crystals that need to transform to the stable form. This is also due to the larger surface of stable form crystals for secondary nucleation and growth. Figure 5-5(b) shows that the average size of the product decreases with the increase in the mass fraction of the stable form. The reason may be that the more seeds of the stable form added into the crystallization cause the lower average supersaturation that can be consumed by each crystal.
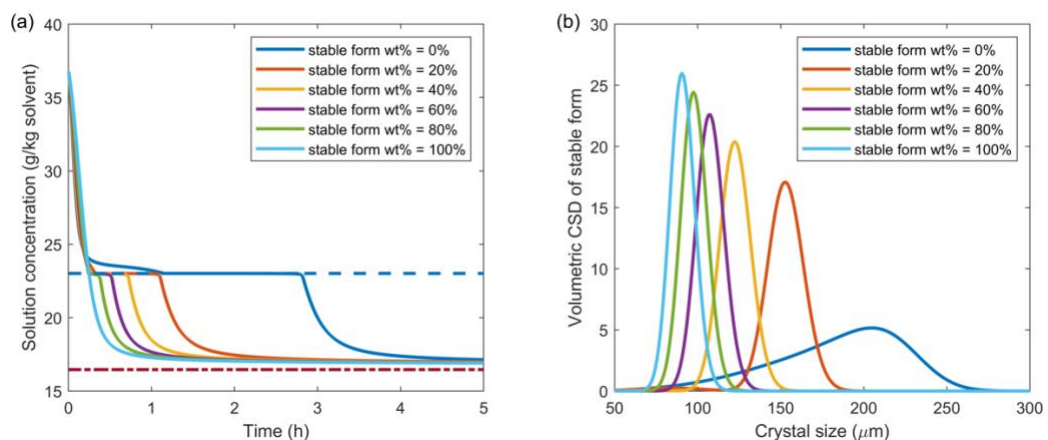
Figure 5-5. Effect of seeds polymorphic composition on the transformation process and crystal size distribution

Then, the effect of the seed mass of pure stable form and metastable form is studied. The seed mass was decided by the percentage of the maximum mass of the crystals. The average size and standard deviation of seeds were kept as $40\mu m$ and $5\mu m$. Figure 5-6 (a) shows adding the seeds of the stable form can significantly shorten the transition process of the metastable form of L-glutamic acid to the stable form. The reason is that the SMPT process of GLA is controlled by the nucleation of the stable form at the beginning and seeding the stable form can help overcome the rate-limiting step. As shown in Figure 5-6 and Figure 5-7, the higher seed mass results in a faster polymorph transformation rate, owing to the larger surface offered for precipitation of the stable form or dissolution of the metastable form. Since the same solute mass will be precipitated on the surface of the seeds from the solution, more seeds added to the crystallizer causes smaller final crystal average size.
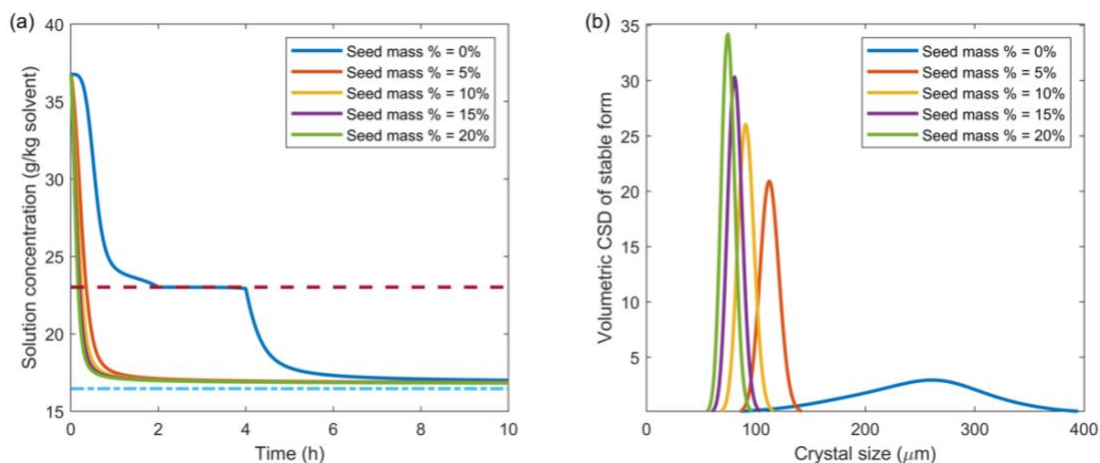

Figure 5-6. Effect of seeds mass of stable form on the transformation process and crystal size distribution
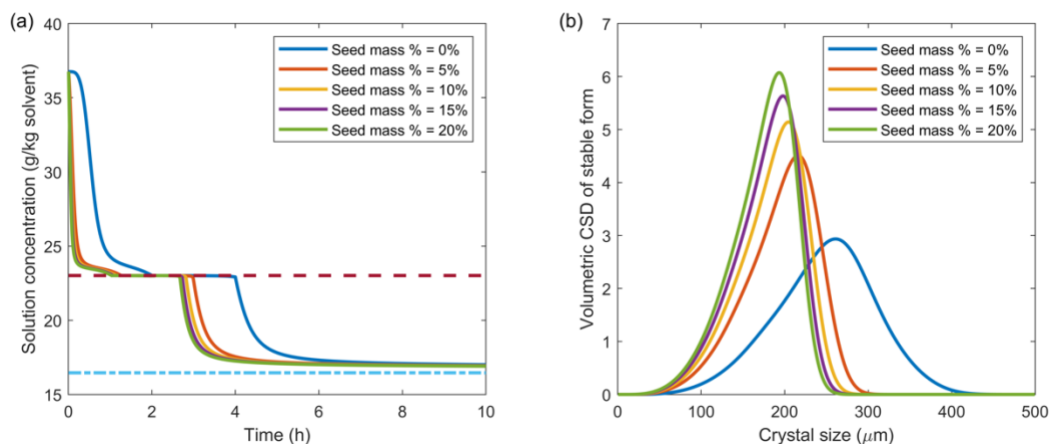
Figure 5-7. Effect of seeds mass of metastable form on the transformation process and crystal size distribution

The last property of seed evaluated in this work is seed average size. The seed mass was chosen as 10% of the maximum mass of the crystals. The standard deviation was $5\mu m$. From Figure 5-9 and Figure 5-10, it is found that seeding with smaller crystals, either of the stable form or the metastable form, leads to a faster transformation process and smaller final product size. The reason is similar to that of the seed mass effect explained above. The smaller seeds, which have higher particle number and larger specific surface area than the larger seeds with the same mass, provide more precipitation sites and higher molecular transport rates. Schöll et al. (Schöll et al., 2006) also found that the smaller seeds with identical mass cause a smaller average size of the final product, as shown in Figure 5-8.
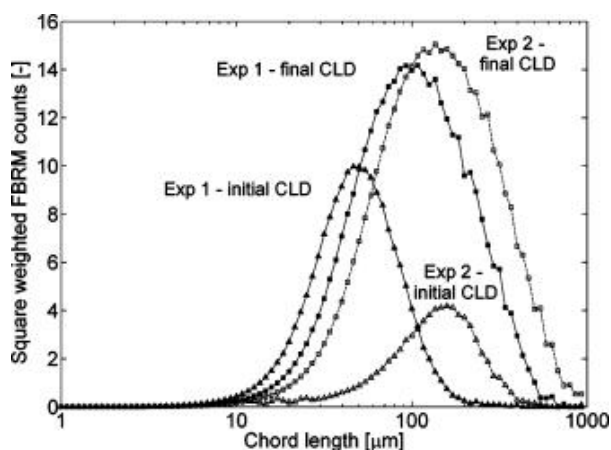

Figure 5-8. Initial and final square weighted chord length distribution of the two seed populations for the seeded transformation experiments at 45 °C (Reprinted with permission from Schöll et al., 2006. Copyright @ 2006 American Chemical Society)
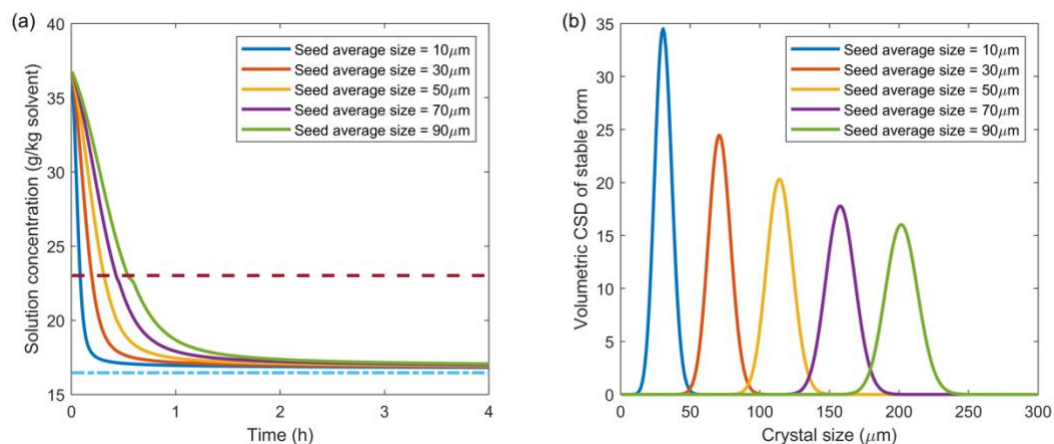
Figure 5-9. Effect of seeds average size of the stable form on the transformation process and crystal size distribution
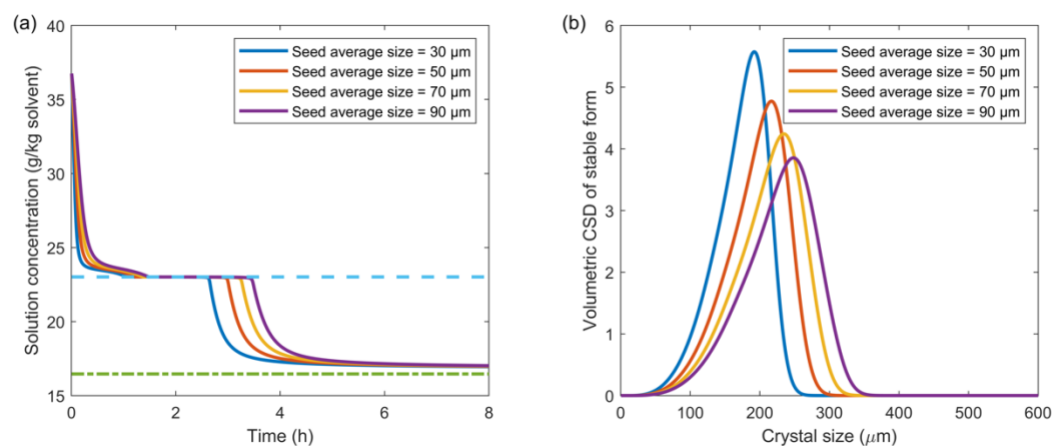

Figure 5-10. Effect of seeds average size of the stable form on the transformation process and crystal size distribution

5.3.2 MSMPR crystallization

5.3.2.1 Temperature / Residence time / Inlet concentration

For a single MSMPR crystallization, the main variables considered are residence time, crystallizer temperature, and inlet concentration, whose ranges are 30-90 min, 15-35 ℃, 25-45 g/kg (equals to the solubility of the metastable form at 47 ℃ and 63 ℃), respectively. As displayed in Figure 5-2(b), it takes about 4 hours to complete the solution-mediated polymorphic transition process of L-glutamic acid in batch crystallization. Therefore, it is expected that the dominant product at the steady-state is the metastable form with residence time less than 90 min. Only when the inlet solution is supersaturated with respect to the

stable form and under supersaturated to the metastable form, can the pure stable form be obtained in a single MSMPR process at the expense of yield.

From Figure 5-11, the following conclusions can be drawn:

1. The product yield and crystal size of the metastable form increase with increasing the inlet concentration and residence time, but decrease with the crystallizer temperature.

2. Long residence time and high crystallizer temperature favor the production of the stable form with larger size. Inlet concentration has little effect on the mass fraction and size of the stable form.
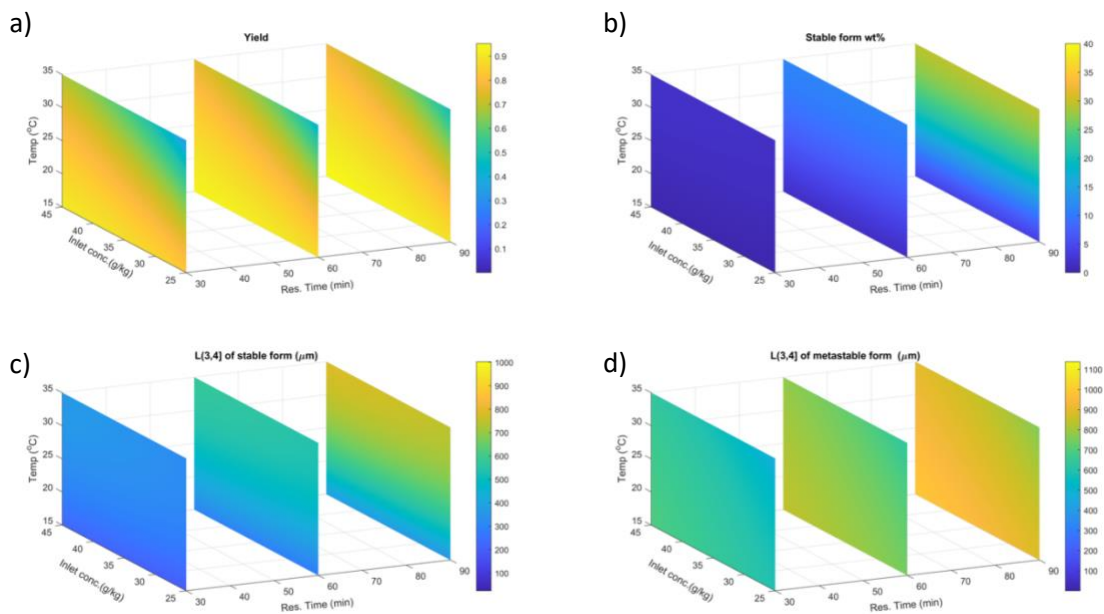

Figure 5-11. Effect of residence time/inlet concentration/temperature of MSMPR crystallizer on a) yield, b) the mass percentage of stable form, c) volume average size of the stable form and d) volume average size of stable form

5.3.2.2 Initial conditions

Several researchers have proven that the initial solution concentration and seed properties in a single MSMPR crystallizer do not impact the steady-state (Lai et al., 2015; Nicoud et al., 2019), because the initial solution or slurry and seeds will be washed out of the

crystallizer after several residence times. The simulation results displayed in Figure 5-12 demonstrate that whatever the initial condition is, the system will reach the same steady-state, but the start-up processes vary with the initial condition. Since the crystals produced during the start-up process cannot be used as a final product due to their inconsistent properties, the start-up optimization to shorten the stabilization time and reduce the waste is of great significance.
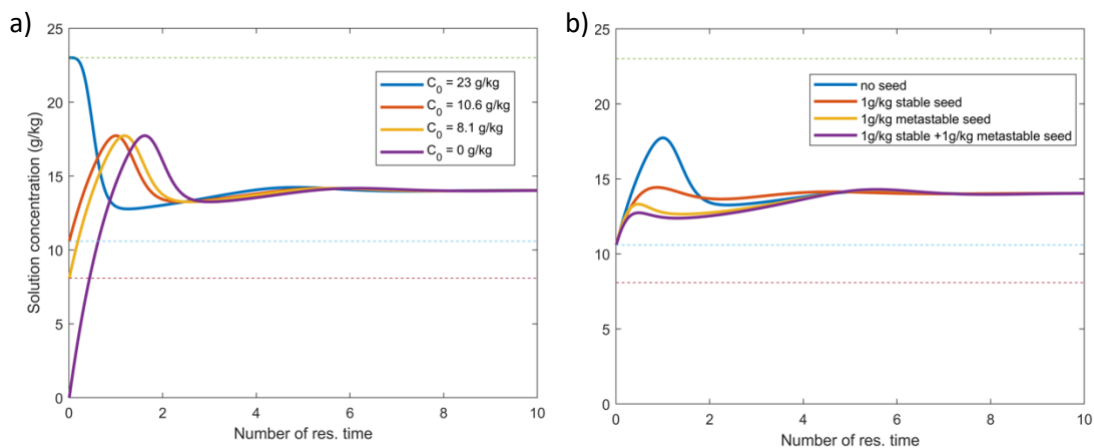

Figure 5-12. The change of solution concentration with different a) initial concentration and b) seed properties. Residence time = 30 min, temperature =25 ℃, inlet concentration = 23 g/kg

5.3.2.3   Continuous seeding

For p-aminobenzoic acid, α form is more stable above 15 ℃ and β-form is more stable at the lower temperature. In Lai et al.'s work (Lai et al., 2015), it was found that the β-form is the only product from a single MSMPR at 5 ℃. With the help of two-stage MSMPR, the authors successfully obtained α form in the second MSMPR at 5 ℃, which received the seeds of α form from the first MSMPR at 30 ℃. This study indicates that continuous seeding may be an effective approach to alter the steady-state in continuous crystallization. Hence, the possibility of altering the steady-state by continuous seeding strategy is evaluated numerically in this section.
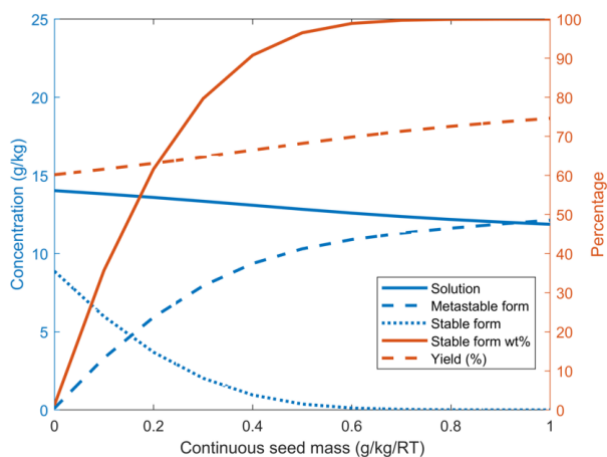
Figure 5-13. The steady-state with different continuous seed mass of L-glutamic acid. (Residence time = 30 min, Temperature =25 ℃, Inlet concentration = 23 g/kg)

Table 5-2. The steady-state with different continuous seed mass of L-glutamic acid (Residence time = 30 min, Temperature =25 ℃, Inlet concentration = 23 g/kg)

Seed mass /RT	Concentration at steady state(g/kg)	Metastable produce mass (g/RT)	Stable (g/RT)	Stable form wt%	Yield (%)
No seed	14.03	8.88	0.11	1.2	60.2
0.2g	13.59	3.69	5.92	61.6	63.1
0.5g	12.83	0.37	10.30	96.5	68.2
0.8g	12.18	0.008	11.62	99.9	72.6
1g	11.88	0.0002	12.14	100	74.6

The steady-state with different continuous seed mass of L-glutamic acid is shown in Figure 5-13a and Table 5-2. As the product is the metastable form L-glutamic acid without continuous seeding, the stable form is continuously fed into the system. The mass fraction of the stable form increases remarkably with the continuous seed mass. The polymorph at the steady-state is altered to the pure stable form when continuous seed mass is higher than 0.8 g/kg/RT. Taking 1 kg solvent as an example, without continuous seeding, the product for each residence time is 8.88 g metastable form and 0.11g stable form, whereas with seeding 0.2 g/RT, the product consists of 0.008 g metastable and 11.62 g stable form. This finding demonstrates the validity of continuous seeding on altering the product

polymorphism. The product yield also increases from 60.2% to 74.6% due to the extra surface brought in by the seeds.

To realize the continuous seeding strategy, we can use a suspension with the desirable seeds as the feed of a single MSMPR (Figure 5-14), or multi-stage MSMPR, of which the slurry moves out from the first stage and fed to the next stage (Figure 5-15). However, suspension transport, especially with slow transport velocity, may lead to the blockage problem. Intermittent withdrawal with high transport velocity is widely used to solve the suspension transport issue.
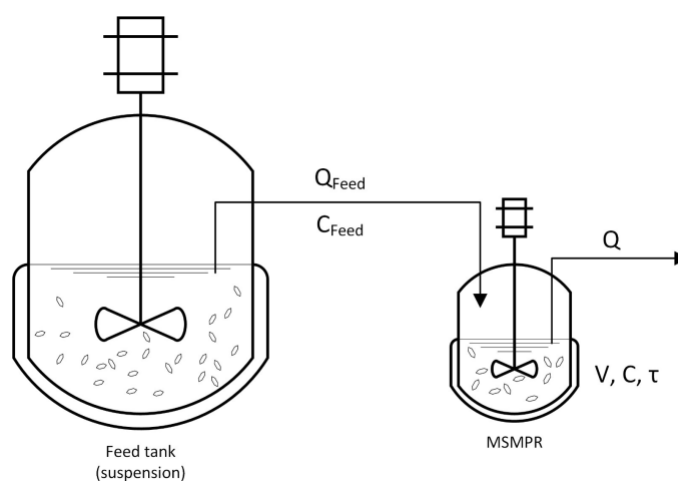

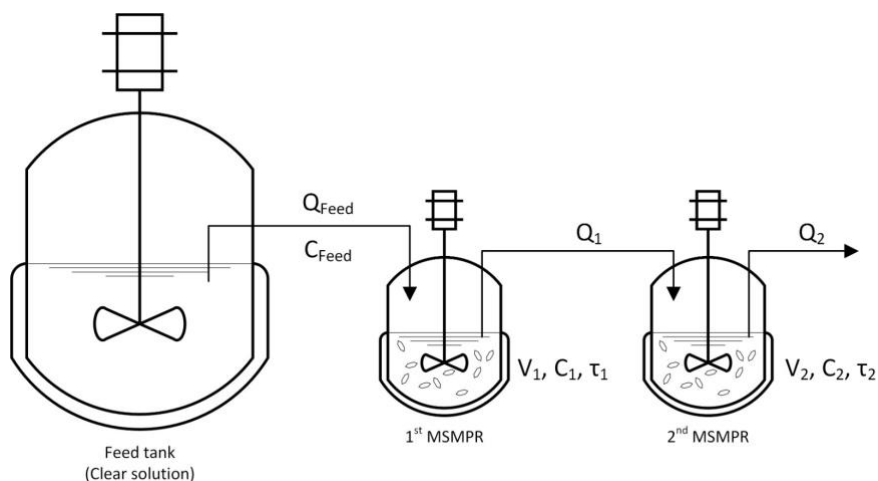**Figure 5-14. Schematics of a suspension-fed single MSMPR**

Figure 5-15. Schematics of two-stage MSMPRs

5.3.2.4   **Intermittent withdrawal**

For intermittent withdrawal, the withdrawal frequency, the number of withdrawals taken during one residence time, is an important parameter. High intermittent withdrawal frequency makes the system closer to a continuous-in-continuous-out MSMPR crystallizer, but also results in slow transport. In contrast, when the frequency is as low as 0, the system can be regarded as batch crystallization. The main difference between the batch and MSMPR crystallizer is their residence time distribution (RTD), which is used to determine the optimal withdrawal frequency.

Assuming the solids in suspension have the same RTD as liquids, the RTD of MSMPR with intermittent withdrawal can be analyzed by the step tracer method. The mass balance for a suspension-fed single MSMPR is

$$\frac{dV}{dt} = Q_{feed}\delta(t - \frac{\tau}{f}) - Q\delta(t - \frac{\tau}{f}) \tag{5-14}$$

$$\frac{dVC}{dt} = Q_{feed}\delta(t - \frac{\tau}{f})C_{feed} - Q\delta(t - \frac{\tau}{f})C \tag{5-15}$$

The mass balances for a two-stage MSMPR system are:

$$\frac{dV_1}{dt} = Q_{feed} - Q_1\delta(t - \frac{\tau_1}{f}) \tag{5-16}$$

$$\frac{dV_2}{dt} = Q_1\delta(t - \frac{\tau_1}{f}) - Q_2\delta(t - \frac{\tau_2}{f}) \tag{5-17}$$

$$\frac{dV_1C_1}{dt} = Q_{feed}C_{feed} - Q_1\delta(t - \frac{\tau_1}{f})C_1 \tag{5-18}$$

$$\frac{dV_2C_2}{dt} = Q_1\delta(t - \frac{\tau_1}{f})C_1 - Q_2\delta(t - \frac{\tau_2}{f})C_2 \tag{5-19}$$

in which subscript 1 and 2 refer to the stage number. Q_{feed}, Q_1 and Q_2 are the volumetric flow rate from feed tank, 1st MSMPR and 2nd MSMPR. For a continuous-in-continuous-out MSMPR system, they should be the same to keep the solution volume constant. V is

solution volume, t is time, τ is residence time, C is solution concentration, δ is Dirac delta function and f is withdrawal frequency.
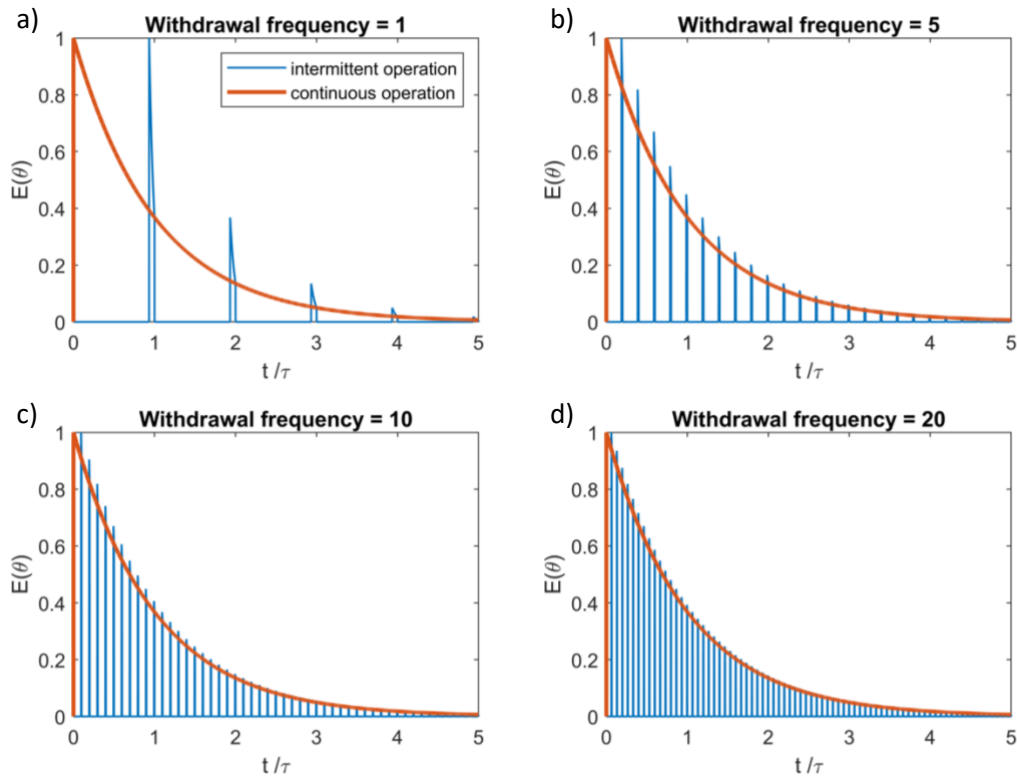

Figure 5-16. Normalized Residence time distribution of suspension-fed single MSMPR with different withdrawal frequency (1, 5, 10 and 20)

Intermittent withdrawal for the feed tank or 1st MSMPR means the intermittent seeding for the following crystallizer. Therefore, the conclusion of the intermittent withdrawal is the same as the intermittent feeding. The effect of intermittent frequency f on the RTD for two continuous seeding configuration is shown in Figure 5-16 and Figure 5-17. The results show that RTD of intermittent operation is very close to continuous operation when the frequency is greater than 10. The sensitivity analysis of the optimal intermittent frequency is performed with normalized average residence time, which is defined as the ratio between the average residence time of intermittent operation and residence time of continuous operation. From Figure 5-18, it is noted that the intermittent operation has higher average residence time than continuous operation when the intermittent frequency is low, and the optimal frequency is ten times per residence time.
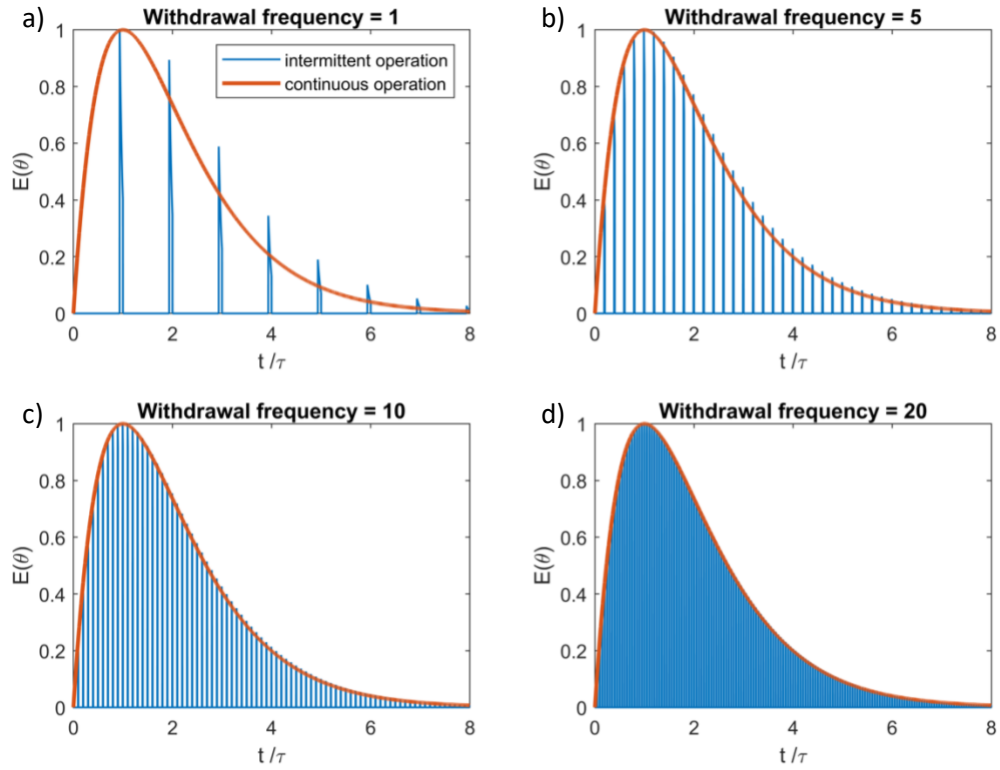
Figure 5-17. Normalized Residence time distribution of 2nd crystallizer of two-stage MSMPR with different withdrawal frequency (1, 5, 10 and 20)
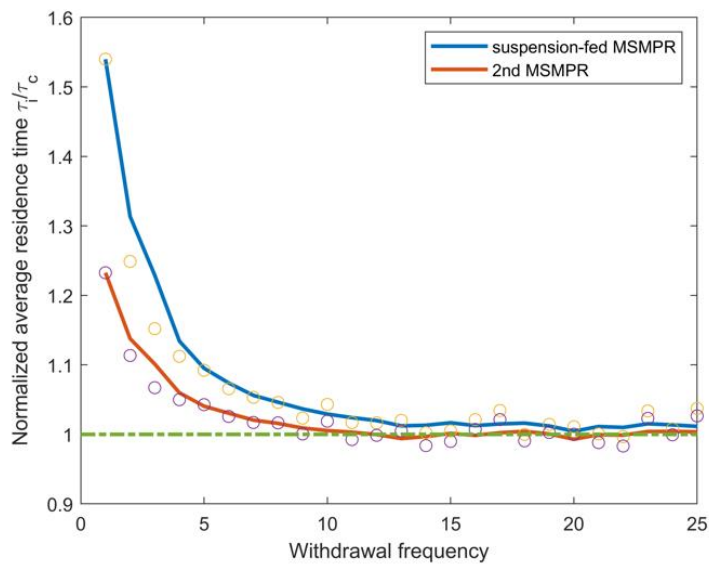

Figure 5-18. Normalized average residence time with different withdrawal frequency

5.3.2.5 **Suspension transport velocity**

Before conducting the experiments of MSMPR, it is important to decide which suspensions removal strategy, intermittently or continuously, is preferred. The key parameter is the suspension transport velocity. To transfer the suspensions successfully without blockage issues, the suspension velocity in the tube should be greater than the horizontal velocity to carry the particles to move forward. For a 200 mL MSMPR crystallizer whose residence time is 30 min, the minimum horizontal velocity with 3.2-mm diameter tube is (Heywood, 1999; Yang et al., 2017)

$$U_{horizontal} = F\left[2g\left(\frac{\rho_c}{\rho_L} - 1\right)D\right]\left(\frac{d_c}{D_i}\right)^{\frac{1}{6}}$$

(5-20)

$$= 1.4\left[2*9.8\left(\frac{1540}{1000} - 1\right) \times 3.2 \times 10^{-3}\right]\left(\frac{50 \times 10^{-6}}{3.2 \times 10^{-3}}\right)^{\frac{1}{6}} = 0.0237\ m/s$$

where F is the Durand factor in the range of 0.4 and 1.4 (1.4 is used here), D_i is the inner diameter of the tube (3.2 mm). ρ_c and ρ_L are crystal and fluid densities, which are 1540 kg/m^3 for L-Glutamic acid and 1000 kg/m^3 for water. d_c is the crystal diameter (50-μm was used in the calculation), and g is the gravitational acceleration, 9.8 m/s^2.

The velocity with continuous operation via a 3.2 mm tube is around 0.014 m/s, smaller than the minimum horizontal velocity, so the intermittent strategy with a peristaltic pump (Masterflex L/S; Cole Palmer, Vernon Hills, IL) was adopted in our lab. With a home-made planetary gear (Figure 5-19), the suspension line velocity can reach 0.55 m/s, which is much greater than the minimum horizontal velocity. It is worth pointing out that the maximum velocity of a designated peristaltic pump can be increased further by increasing the outer diameter or the transmission ratio, the ratio of the diameters of the sun gear and planetary gear.
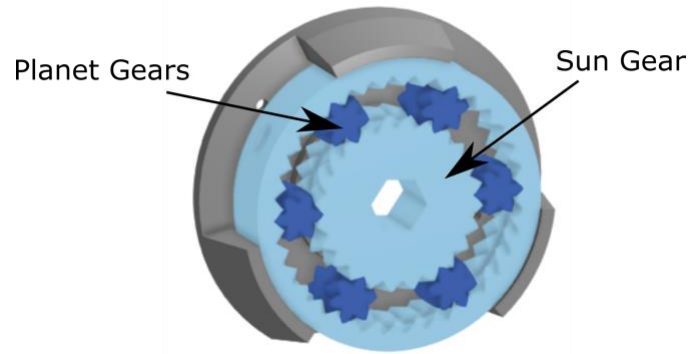
Figure 5-19. Home-made planetary gear used as the pump head

High velocity also can shorten the residence time of the particles in the tube, so to prevent the crystal precipitation and clogging problems. The average time for particles settling in the tube should be shorter than the crystal residence time in the tube. The residence time for 1m tube is $\frac{1\,m}{0.55\,m/s} = 1.83\,s$.

Particle terminal velocity is

$$U_{vetical} = \frac{g(\rho_c - \rho_L)d_c^2}{18\nu} = \frac{9.8(1540 - 1000)(50 \times 10^{-6})^2}{18 \times 8.9 \times 10^{-4}}$$
$$= 8.26 \times 10^{-4}\,m/s$$

(5-21)

where ν is the fluid dynamic viscosity. The Reynolds number of the particles is

$$Re_p = \frac{d_c U_{vetical}}{\nu} = \frac{50 \times 10^{-6} \times 8.26 \times 10^{-4}}{8.9 \times 10^{-3}} = 0.046 < 0.1$$

(5-22)

hence, the fluid is in the laminar flow regime, which means Stoke's law (Eq. (5-21)) is valid here.

The average time for particles settling in the tube is $= \frac{1.6 \times 10^{-3}\,m}{8.26 \times 10^{-4}\,m/s} = 1.94\,s$, greater than the residence time, which ensures the crystals leave the transfer tube before they precipitate.

In our laboratory, a 200 mL MSMPR crystallizer and a one-meter long transfer tube with 3.2-mm diameter were used to conduct the single MSMPR crystallization. The system with intermittent removal can operate successfully without any clogging and particle settling issues for 10 residence times.

5.4   Conclusions

Table 5-3. The effects of the operating conditions in batch crystallization
(+ and – presents positive and negative effect, NA is not applicable)

	Initial concentration	Cooling power number	wt.% of the stable form in seeds	Seed mass	Seed size
Stable size	-	+	-	-	+
Transition time	-	NA	-	-	+

Table 5-4. The effects of the operating conditions in MSMPR crystallization
(+ and – presents positive and negative effect)

	Residence time	Inlet concentration	Temperature of crystallizer
Yield	+	+	-
Mass fraction of stable form	+	little	+
Stable size	+	little	+
Metastable size	+	+	-

The effects of the operating conditions in batch and MSMPR crystallization on the crystal properties with L-glutamic acid water were investigated thoroughly and summarized in Table 5-3 and Table 5-4. Owing to the solution-mediated polymorphic transformation, it is easier to produce the stable form in batch crystallization. Long transition time provided the chance to remove the metastable before the transition happens. The initial concentration and seeds mass and polymorphic form have no impact on the steady-state product quality of an MSMPR. It is proven that the continuous seeding strategy can alter the steady-state,

including polymorphism. To avoid the blocking issue, the intermittent seeding and withdrawal method were suggested. The optimal intermittent frequency was set to 10 by the sensitivity analysis of the normalized average residence time. With the intermittent method, the suspension transport velocity is higher than the minimum horizontal particle velocity in the tube and the suspension residence time in the transfer tube is less than the particle settling time, which guarantees the success of suspension transport.

5.5   References

Capellades, G., Joshi, P.U., Dam-Johansen, K., Mealy, M.J., Christensen, T.V., Kiil, S., 2018. Characterization of a Multistage Continuous MSMPR Crystallization Process Assisted by Image Analysis of Elongated Crystals. Cryst. Growth Des. https://doi.org/10.1021/acs.cgd.8b00446

Hermanto, M.W., Kee, N.C., Tan, R.B.H., Chiu, M.-S., Braatz, R.D., 2008. Robust Bayesian estimation of kinetics for the polymorphic transformation of L-glutamic acid crystals. AIChE J. 54, 3248–3259. https://doi.org/10.1002/aic.11623

Heywood, N.I., 1999. Stop Your Slurries from Stirring Up Trouble 22.

Kiho Park, Kim, D.Y., Yang, D.R., 2016. Operating Strategy for Continuous Multistage Mixed Suspension and Mixed Product Removal (MSMPR) Crystallization Processes Depending on Crystallization Kinetic Parameters. Ind. Eng. Chem. Res. 55, 7142–7153. https://doi.org/10.1021/acs.iecr.6b01386

Lai, T.-T.C., Cornevin, J., Ferguson, S., Li, N., Trout, B.L., Myerson, A.S., 2015. Control of Polymorphism in Continuous Crystallization via Mixed Suspension Mixed Product Removal Systems Cascade Design. Cryst. Growth Des. 15, 3374–3382. https://doi.org/10.1021/acs.cgd.5b00466

Li, J., Trout, B.L., Myerson, A.S., 2016. Multistage Continuous Mixed-Suspension, Mixed-Product Removal (MSMPR) Crystallization with Solids Recycle. Org. Process Res. Dev. 20, 510–516. https://doi.org/10.1021/acs.oprd.5b00306

Lührmann, M.-C., Timmermann, J., Schembecker, G., Wohlgemuth, K., 2018. Enhanced Product Quality Control through Separation of Crystallization Phenomena in a Four-Stage MSMPR Cascade. Cryst. Growth Des. https://doi.org/10.1021/acs.cgd.8b00941

Myerson, A.S. (Ed.), 2002. Handbook of industrial crystallization, 2nd ed. ed. Butterworth-Heinemann, Boston.

Nicoud, L., Licordari, F., Myerson, A.S., 2019. Polymorph Control in MSMPR Crystallizers. A Case Study with Paracetamol. Org. Process Res. Dev. 23, 794–806. https://doi.org/10.1021/acs.oprd.8b00351

Onyemelukwe, I.I., Parsons, A.R., Wheatcroft, H.P., Robertson, A., Nagy, Z.K., Rielly, C.D., 2019. The Role of Residence Time Distribution in the Continuous Steady-State

Mixed Suspension Mixed Product Removal Crystallization of Glycine. Cryst. Growth Des. 19, 66–80. https://doi.org/10.1021/acs.cgd.8b00853

Schöll, J., Bonalumi, D., Vicum, L., Mazzotti, M., Müller, M., 2006. In Situ Monitoring and Modeling of the Solution-mediated Polymorphic Transformation of l-Glutamic Acid. Cryst. Growth Des. 6, 881–891. https://doi.org/10.1021/cg0503402

Sheikholeslamzadeh, E., Rohani, S., 2013. Modeling and Optimal Control of Solution Mediated Polymorphic Transformation of L -Glutamic Acid. Ind. Eng. Chem. Res. 52, 2633–2641. https://doi.org/10.1021/ie302683u

Su, Q., Rielly, C.D., Powell, K.A., Nagy, Z.K., 2017. Mathematical modeling and experimental validation of a novel periodic flow crystallization using MSMPR crystallizers. AIChE J. 63, 1313–1327. https://doi.org/10.1002/aic.15510

Yang, X., Acevedo, D., Mohammad, A., Pavurala, N., Wu, H., Brayton, A.L., Shaw, R.A., Goldman, M.J., He, F., Li, S., Fisher, R.J., O'Connor, T.F., Cruz, C.N., 2017. Risk Considerations on Developing a Continuous Crystallization System for Carbamazepine. Org. Process Res. Dev. 21, 1021–1033. https://doi.org/10.1021/acs.oprd.7b00130

Chapter 6

Conclusions and Recommendations

6 Conclusions and Recommendations

6.1 Conclusions

In this work, the polymorphism phenomenon in crystallization processes was studied experimentally and numerically. Clear guidelines were developed to produce the desired polymorph with suitable properties in both batch and continuous crystallization processes. The main conclusions discussed in previous chapters are summarized here.

6.1.1 Thermodynamic and dynamic study

Polymorph screening is a major challenge in pharmaceutical manufacturing, and having access to the accurate thermodynamic and kinetic parameters is vital for crystallization design and control. Since the imatinib mesylate properties, particularly those related to the crystallization process, were lacking in the literature, α-form and β-form imatinib mesylate were fully characterized in Chapter 2.

With the aid of ultraviolet-visible spectroscopy, the solubilities of both forms were determined in various solvents, revealing that α-form and β-form imatinib mesylate are enantiotropically related. Then, the solution-mediated polymorphic transformation process from metastable α-form to stable β-form was studied in methanol solution with the in-situ Raman spectroscopy and conductivity meter. Finally, the nucleation and growth rates of β-form of imatinib mesylate were estimated with MATLAB optimization function.

The findings of this chapter paved the path for future research on designing the crystallization process for imatinib mesylate, and general guidelines for other active pharmaceutical ingredients.

6.1.2 Crystallization process monitoring

In Chapter 3, a methodology was developed to determine the solution concentration and solids concentration simultaneously and quantitatively using Raman spectroscopy.

Commonly, ATR-FTIR is used to determine the solution concentration. But ATR-FTIR is not applicable, if materials have low infrared activity or low solubility. The main difficulty

involved in using Raman is that the spectrum is a multivariable function of solution concentration, solids concentration and temperature. Consequently, robust mathematical techniques have been employed to decouple the data related to the solution concentration and solids concentration.

Different pre-processing methods (spectra range selection, baseline removal, direct orthogonal signal correction-DOSC) and multivariable analysis techniques (characteristic peaks regression (CPR), principal component regression (PCR), partial least squares regression (PLSR) and artificial neural network (ANN)) were applied and compared based on the root mean squared error (RMSE).

It has been found that the direct orthogonal signal correction pre-processing can improve the fitting performance of the linear regression models (CPR, PCR, and PLSR), but not for ANN. In the case of weak signals, the ANN model showed better prediction ability than the linear models owing to its non-linear prediction ability. We showed that Raman spectroscopy is not only capable of measuring the solids concentration, but also able to provide solution concentration, in a comparable manner to the IR technique.

6.1.3   Polymorph prediction based on the relative kinetics

From the literature, it is found that different polymorphic systems have different preferred polymorph in batch and MSMPR crystallization. For paracetamol, the stable form was the only product in either metastable-form-seeded batch crystallization or MSMPR (mixed suspension and mixed product removal) crystallization (Nicoud et al., 2019a, 2019b). For L-glutamic acid, the stable form was obtained at 45 °C in MSMPR or by SMPT process within six hours in a batch crystallizer, while the metastable form was produced from fast cooling batch crystallization or MSMPR crystallization at 25 °C (Lai et al., 2014). For p-aminobenzoic acid, the metastable form was the preferred polymorph as it took two days to complete the solution-mediated polymorphism transform process at 5 °C, while the stable form was the product with MSMPR crystallization at 5 °C (Lai et al., 2015).

These phenomena indicate that the kinetics contributes significantly to the polymorphic outcome. However, the effects of polymorph relative kinetics and the strategy to crystallize

the desired polymorph have been investigated rarely, especially in continuous crystallization.

In Chapter 4, the impacts of relative nucleation and growth kinetics of the two polymorphs on the polymorphic outcome were studied numerically in batch and MSMPR crystallization. Two dimensionless numbers, Rk_b and Rk_g, were defined as the ratios between the nucleation rate constants and growth rate constants of two polymorphs:

$$B = k_b(S-1)^b$$

$$Rk_b = \frac{k_{b\,stable}}{k_{b\,metastable}}$$

$$G = k_g(S-1)^g$$

$$Rk_g = \frac{k_{g\,stable}}{k_{g\,metastable}}$$

where k_b is the nucleation rate constant [#/s/kg solvent], k_g is growth rate constant [m/s], b and g are the exponents, and S is the supersaturation,

$$S = \frac{C(t)}{C^*}$$

where C is the solution concentration and C^* is the solubility.

An indicator, $Rk_g \cdot Rk_b^{1/3}$, was proposed to analyze the possibility of producing the metastable form with 99 wt% purity in batch crystallization. It has been found that $Rk_g \cdot Rk_b^{1/3} < 0.22$ is required to have at least 10 min time window for the removal of the metastable form from the solution before the polymorphism transition process happens. In MSMPR crystallizer, this indicator was used to check whether the operating conditions (crystallizer temperature, residence time, and inlet concentration) can alter the steady-state polymorph. When $Rk_g \cdot Rk_b^{1/3}$ is greater than 1 or less than 0.1, the dominant product is either the stable form or metastable form, and the operating conditions cannot effectively control the product polymorph. In such a case, changing the solvent and adding additives

are alternative methods to crystallize the other polymorph by influencing the kinetic ratio of two polymorphs.

This work provides a general approach to determine the optimal crystallization operation to harvest the desired polymorph of a bi-polymorph system, when their relative kinetics are known. Concretely speaking, a) the stable form with slow kinetics ($Rk_g \cdot Rk_b^{1/3} < 0.1$) cannot be easily obtained from MSMPR crystallization, but can be produced by the SMPT process in batch crystallization; b) the prerequisite for producing the high purity metastable form in batch crystallization is that the metastable form to have fast relative kinetics ($Rk_g \cdot Rk_b^{1/3} < 0.22$); c) only when $Rk_g \cdot Rk_b^{1/3}$ is in the range of 0.1 to 1, the operating conditions can alter the polymorphic outcome in MSMPR crystallization.

6.1.4   **Crystallization process design**

After studying the crystal kinetics, we investigated the operating conditions and strategies of the batch and MSMPR crystallization. The findings below offer general guidance for designing a crystallization process. L-glutamic acid - water was selected as the model system in this work.

In the batch cooling crystallization, the impacts of the initial concentration, cooling profile, polymorphic form of the seeds, seed mass and seed size on the crystal size and polymorphism transformation time were studied. A longer polymorphism transformation time provides a higher chance to produce the metastable form with the batch crystallization. The simulation results show that the crystal size and polymorphic transition time decrease with increasing the initial concentration, the mass fraction of the stable form seeds and seed mass; but increase with increasing the seed size.

In a single MSMPR crystallization, the impacts of the residence time, crystallizer temperature, and inlet concentration on the product yield, crystal polymorph, stable form average size and metastable form average size were studied. It is shown that the product yield and size of metastable form increase with an increase in the residence time and feed concentration, but decrease with increasing the crystallizer temperature. The mass fraction

and crystal size of the stable form increase with increasing the residence time and crystallizer temperature, but are not affected by the feed concentration.

Since the initial solution and seeds in MSMPR will be washed out of the crystallizer after several residence times and do not impact the steady-state, the continuous seeding strategy was proposed and realized with a suspension-fed single MSMPR or two-stage MSMPRs. It has been proven numerically that the continuous seeding could alter the steady-state polymorphic outcome of the product.

Then, the intermittent seeding and withdrawal method was adopted to avoid the blocking issue during suspension transport. Its validity was demonstrated by comparing the suspension transport velocity and minimum horizontal particle velocity, as well as the suspension residence time in the transfer tube and the particle settling time. With the sensitivity analysis of the normalized average residence time, we found the optimal intermittent frequency is 10 times per residence time.

6.2   Recommendations

The studies conducted and reported in this thesis have shown the significance of the thermodynamic and kinetic parameters, development of process analytic technologies, and numerical modeling in crystallization engineering. Future researches can emphasize the potential improvements in process analytical technologies (PATs) and pursue innovation in combining the crystallization system with the modeling tools.

Here are some recommendations for future work:

- The crystallization kinetic models are reported in different formats and the parameters for the same systems may vary greatly. This is because the kinetic models are often empirical and many factors and disturbances are not considered e.g., stirring rate and the crystallizer geometry. Brown et al. (Brown et al., 2020) have collected the nucleation and growth kinetic parameters from 185 papers. This database should be regularly updated with the contribution of the researchers with some standardized models so that the industry can overcome the blind spots in the current modeling techniques in the future.

- It is demonstrated that Raman spectroscopy can be used for online solution concentration and slurry density measurement. More work on the estimation of the nucleation, growth, dissolution parameters and process monitor can be carried out by Raman spectroscopy alone, especially when the crystallizer is small. Also, measuring the concentration, polymorphism, and solids concentration from the same location can improve the modeling accuracy.

- Solving the hyperbolic mathematical model of the population balance equation numerically showed various difficulties. For example, there are many different solving schemes such as upwind, high-resolution, and collocation methods and all of them are showing unique numerical properties. Repeating the programming and verification work in creating one of these algorithms that fits specific requirements can be time-consuming and error-prone. Despite many open-source projects and commercial software focusing on solving the PBE for a crystallization system, at the time of writing of this thesis it was still difficult to find a software package that is highly customizable, easy to learn, and efficient. Our group has initiated the project working on an open-source re-useable PBE solver implemented in MATLAB/Simulink that will support the modeling of batch/continuous systems, polymorphic transformation, agglomeration and breakage, and customizable kinetics. This work will help the researcher to start with a reproducible and full-featured platform in crystallization modeling.

6.3   References

Brown, C., Maldonado, D., Vassileiou, A., Johnston, B., Florence, A., 2020. Data Mining Crystallization Kinetics (preprint). https://doi.org/10.26434/chemrxiv.11708286.v2

Lai, T.-T.C., Cornevin, J., Ferguson, S., Li, N., Trout, B.L., Myerson, A.S., 2015. Control of Polymorphism in Continuous Crystallization via Mixed Suspension Mixed Product Removal Systems Cascade Design. Crystal Growth & Design 15, 3374–3382. https://doi.org/10.1021/acs.cgd.5b00466

Lai, T.-T.C., Ferguson, S., Palmer, L., Trout, B.L., Myerson, A.S., 2014. Continuous Crystallization and Polymorph Dynamics in the L -Glutamic Acid System. Organic Process Research & Development 18, 1382–1390. https://doi.org/10.1021/op500171n

Nicoud, L., Licordari, F., Myerson, A.S., 2019a. Polymorph Control in MSMPR Crystallizers. A Case Study with Paracetamol. Org. Process Res. Dev. 23, 794–806. https://doi.org/10.1021/acs.oprd.8b00351

Nicoud, L., Licordari, F., S. Myerson, A., 2019b. Polymorph control in batch seeded crystallizers. A case study with paracetamol. CrystEngComm 21, 2105–2118. https://doi.org/10.1039/C8CE01428K

Appendices

In appendix A, the MATLAB codes used to model the batch and MSMPR crystallization process are summarized. Appendix B includes the MATLAB codes about the pre-processing methods and multivariable analysis techniques, which were applied to analyze the Raman spectroscopy in Chapter 3. The procedure of principal component analysis and partial least squares regression are described in appendix C. Appendix D presents the permissions to use copyrighted materials in Chapter 2, Chapter 3 and Chapter 5.

Appendix A. MATLAB codes for the crystallization process modeling

A.1. Fundamental data

A.1.1 Solubility of stable form

```
function C_star = solubility(T)
        C_star = (7.644*10^-3.*T.^2 - 1.165*10^-1.*T + 6.222)/1000;


function C_star = solubility_1(T)
        C_star = (8.437*10^-3.*T.^2 + 3.032*10^-2.*T + 4.564)/1000;
```

A.1.2 Birth, growth and dissolution rate

```
function B = Birth(kb,kb2,b,T,C,m3,rho_solvent)
        B =0;
        C_star = solubility(T);
                if C>C_star
                   B = ((abs(C./C_star-1)).^(b).*(kb+kb2.*(m3)^(2/3))./rho_solvent);
                   B(isnan(B))=0;
                end

function G = growth(kg1,kg2,T,C)
        G=0;
        C_star = solubility(T);
                if C>C_star
                   G = kg1.*abs(C./C_star-1).^(kg2);
                   G(isnan(G))=0;
                end

function D = Dissolution_1(kd_1,T,C,m3)
        D = 0;
        C_star_1 = solubility_1(T);
```

```matlab
        if (C<C_star_1 && m3>0)
            D = kd_1.*(abs(C./C_star_1-1));
        end
```

A.1.3 Size distribution of seeds

```matlab
function csd = fun_csd(mass,ave_size,sd,kv,rho,L)
        CSD_pdf =normpdf(L,ave_size,sd);
        stable_lamda= mass./(rho*kv*trapz(L,CSD_pdf .*L.^3));
        csd = stable_lamda*CSD_pdf;   % popolation density--unit-#/m/kg solvent
```

A.2. Batch crystallizer

A.2.1 Main code

```matlab
clc
clear
dbstop if error

%--------- Kinetic parameters for metastable polymorph
kb_1 = 1e8;    kb_12 = 1e12;     b_1 = 2;   kg_1 = 1e-8;   g_1 = 1;   kd_1 =2.2e-6;

%--------- Kinetic parameters for stable polymorph
kb = 1*kb_1;   kb2 = 1*kb_12;  b = b_1;   kg = kg_1;      g = g_1;   kd = 0;

kv_stable =  0.48;          rho_stable = 1540;          %kg/m3
kv_metastable = 0.48;   rho_metastable = 1540;   %kg/m3
rho_solvent = 1000;      v_solvent=1;                  %kg/m3 & m3

%--------------------Time and length grid -------------------------------
ntime=360; batch_time = 1*3600; delta_t = batch_time/ntime;  %seconds
nl=1000; L0=0;Lmax =1000*10^-6; delta_L=(Lmax-L0)/nl;
L=((L0+delta_L/2):delta_L:(Lmax-delta_L/2))';  % length grid-m

%--------------------Temperature and concentration-----------------------
C_initial=solubility_1(60);
T_initial=25; T_final=25;

%---------------- Seeding parameters for stable poylmorph ----------------
CSD_stable(1,:) = fun_csd(0e-3,100e-6,10e-6,kv_stable,rho_stable,L);
CSD_metastable(1,:)= fun_csd(0e-3,100e-6,10e-6,kv_metastable,rho_metastable,L);

miu = trapz(L,CSD_stable'.*L.^(0:5));
miu_1 = trapz(L,CSD_metastable'.*L.^(0:5));

N0 = [ miu_1 miu C_initial];
result(1,1:13) = N0;
```

```matlab
B_stable = zeros(ntime,1); B_metastable = zeros(ntime,1);  %#/s/kg
Dissolution_stable = zeros(ntime,1); Dissolution_metastable = zeros(ntime,1);  %m/s
Growth_stable = zeros(ntime,1); Growth_metastable = zeros(ntime,1);  %m/s

for i=1:ntime

    result(i,:) = N0;
    B_stable(i) = Birth(kb,kb2,b,T(i),result(i,13),result(end,10),rho_solvent);
    B_metastable(i) = Birth_1(kb_1,kb_12,b_1,T(i),result(i,13),result(end,4),rho_solvent);
    Dissolution_stable(i) = Dissolution(kd,T(i),result(i,13));
    Dissolution_metastable(i) = Dissolution_1(kd_1,T(i),result(i,13),result(end,4));
    Growth_stable(i) = growth(kg,g,T(i),result(i,13));
    Growth_metastable(i) = growth_1(kg_1,g_1,T(i),result(i,13));

    if i>1
        CSD_stable(i,:) = csd_fvm(CSD_stable(i-1,:),(Growth_stable(i)-Dissolution_stable(i)), ...
B_stable(i),nl,delta_L,delta_t);
        CSD_metastable(i,:) = csd_fvm(CSD_metastable(i-1,:),(Growth_metastable(i)- ...
Dissolution_metastable(i)),B_metastable(i),nl,delta_L,delta_t);
    end

    [t N] =
ode45(@batch_fun_miu_fvm,[0,delta_t],N0,[],T(i),rho_stable,kv_stable,rho_metastable, ...
kv_metastable,rho_solvent,kb,b,kb_1,b_1, kg,g,kg_1,g_1, kd,kd_1, kb2,kb_12);

    N(N<0)=0;
    N0 = real(N(end,:))';
    N0(1) = sum(CSD_metastable(i,:))*delta_L; N0(7) = sum(CSD_stable(i,:))*delta_L;
end

Concentration= result(:,13);
Supersaturation_stable = Concentration'./solubility(T(1:ntime));
Supersaturation_metastable = Concentration'./solubility_1(T(1:ntime));

Number_ave_size_stable = result(:,8)./result(:,7)*10^6;
Number_ave_size_metastable = result(:,2)./result(:,1)*10^6;
Volume_ave_size_stable = result(:,11)./result(:,10)*10^6;
Volume_ave_size_metastable = result(:,5)./result(:,4)*10^6;
Mass_stable_form = rho_stable/rho_solvent*kv_stable*1000*result(:,10);
Mass_metastable_form = rho_metastable/rho_solvent*kv_metastable*1000*result(:,4); ...
mass_percent_stable
=Mass_stable_form./(Mass_metastable_form+Mass_stable_form);mass_percent_stable(end);
yield = 1-Concentration./C_initial;

Mass_balance = C_initial + rho_metastable*kv_metastable*miu_1(4) + rho_stable*kv_stable*...
miu(4) - ( Mass_metastable_form(end) + Mass_stable_form(end) + result(end,13))
```

A.2.2 Solving the PBE with Finite volume method

```
function csd = csd_fvm(csd_pre,G,B,nl,deltaL,t)

csd = csd_pre;
if G>0
    csd(1) = B/G;

    csd_pre =[B/G, csd_pre, 0];
    theta_n = (csd_pre(2:nl+1) - csd_pre(1:nl))./(csd_pre(3:nl+2) - csd_pre(2:nl+1));

    phi_n = (abs(theta_n)+theta_n)./(1+abs(theta_n));
    phi_n(isnan(phi_n)) = 0;

    csd(2:nl) = csd_pre(3:nl+1) - G*t/deltaL*((csd_pre(3:nl+1) - csd_pre(2:nl)))- G*t/(2*deltaL)*(1-
G*t/(deltaL)).*((csd_pre(4:nl+2)-csd_pre(3:nl+1)).*phi_n(2:nl)-(csd_pre(3:nl+1)-csd_pre(2:nl)).*
phi_n(1:nl-1));

elseif  G<0
    csd_pre =[0, flip(csd_pre), 0];  G = abs(G);
    theta_n = (csd_pre(2:nl+1) - csd_pre(1:nl))./(csd_pre(3:nl+2) - csd_pre(2:nl+1));

    phi_n = (abs(theta_n)+theta_n)./(1+abs(theta_n));
    phi_n(isnan(phi_n)) = 0;

    csd(2:nl) = csd_pre(3:nl+1) - G*t/deltaL*((csd_pre(3:nl+1) - csd_pre(2:nl)))- G*t/(2*deltaL)*(1-
G*t/(deltaL)).*((csd_pre(4:nl+2)-csd_pre(3:nl+1)).*phi_n(2:nl)-(csd_pre(3:nl+1)-csd_pre(2:nl)).*
phi_n(1:nl-1));

    csd(1) = 0;  csd = flip(csd);
end

csd = csd';
end
```

A.2.3 Solving the mass balance and PBE with method of moment

```
function
dN=batch_fun_miu_fvm(~,N,T,rho_crystal,kv_stable,rho_crystal_1,kv_metastable,rho_solvent,..
. kb,b,kb_1,b_1, kg,g,kg_1,g_1, kd,kd_1, kb2,kb_12)

dN = zeros(13,1);

g_d_1 = growth_1(kg_1,g_1,T(1),N(13))-Dissolution_1(kd_1,T(1),N(13),N(4));
g_d = growth(kg,g,T(1),N(13))-Dissolution(kd,T(1),N(13));

dN(1) =  Birth_1(kb_1,kb_12,b_1,T(1),N(13),(N(4)),rho_solvent);
dN(2:6) =  (1:5)'.*g_d_1.*N(1:5);
```

```
dN(7) = Birth(kb,kb2,b,T(1),N(13),(N(10)),rho_solvent);
dN(8:12) = (1:5)'.*g_d.*N(7:11);


dN(13)= -3.*rho_crystal_1.*kv_metastable.*g_d_1.*(N(3))...
        -3.*rho_crystal.*kv_stable.*g_d.*(N(9))...
    -rho_crystal_1.*kv_metastable.*dN(1).*(0e-6)^3-rho_crystal.*kv_stable.*dN(7).*(0e-6)^3;
```

A.3 MSMPR crystallizer

A.3.1 Main code

```
clc
clear
dbstop if error


kb_1 = 1e8; kb_12 = 1e12; b_1 = 2;  kg_1 = 1e-8;   g_1 = 1;   kd_1 =2.2e-6;
kb = 1*kb_1;   kb2 = 1*kb_12;   b = b_1;   kg = kg_1;      g = g_1;   kd = 0;


kv_stable =  0.48; rho_stable = 1540;
kv_metastable =.48; rho_metastable = 1540;
rho_solvent = 1000;v_solvent=1;


residence_time =60*60; rtnumber=20; timegrid = 1440;
delta_t = residence_time*rtnumber/timegrid;


nl=1000; L0=0; LN =1000*10^-6; delta_L=(LN-L0)/nl; L=((L0+delta_L/2):delta_L:(LN-delta_L/2))';


T_msmpr=25; T = ones(timegrid+1,1)*T_msmpr;
C_inlet=solubility_1(60); C_initial =solubility_1(T_msmpr);


CSD_stable(1,:) = fun_csd(0e-3,100e-6,10e-6,kv_stable,rho_stable,L);
CSD_metastable(1,:)= fun_csd(0e-3,100e-6,10e-6,kv_metastable,rho_metastable,L);


miu = trapz(L,CSD_stable'.*L.^(0:5));
miu_1 = trapz(L,CSD_metastable'.*L.^(0:5));


N0 = [ miu_1 miu C_initial];
result(1,1:13) = N0;


B_stable = zeros(timegrid,1); B_metastable = zeros(timegrid,1);  %#/s/kg
Dissolution_stable = zeros(timegrid,1); Dissolution_metastable = zeros(timegrid,1);  %m/s
Growth_stable = zeros(timegrid,1); Growth_metastable = zeros(timegrid,1);  %m/s


for i=1:timegrid

    result(i,:) = N0;

    B_stable(i) = Birth(kb,kb2,b,T(i),result(i,13),result(end,10),rho_solvent);
```

```
    B_metastable(i) = Birth_1(kb_1,kb_12,b_1,T(i),result(i,13),result(end,4),rho_solvent);
    Dissolution_stable(i) = Dissolution(kd,T(i),result(i,13));
    Dissolution_metastable(i) = Dissolution_1(kd_1,T(i),result(i,13),result(end,4));
    Growth_stable(i) = growth(kg,g,T(i),result(i,13));
    Growth_metastable(i) = growth_1(kg_1,g_1,T(i),result(i,13));


    if i>1
        CSD_stable(i,:) = msmpr_csd_fvm(CSD_stable(i-1,:),(Growth_stable(i)-Dissolution_stable(i)),
B_stable(i),nl,delta_L,delta_t,residence_time);
        CSD_metastable(i,:) = msmpr_csd_fvm(CSD_metastable(i-1,:),(Growth_metastable(i)-
Dissolution_metastable(i)),B_metastable(i),nl,delta_L,delta_t,residence_time);
    end

    [t N] = ode45(@msmpr_miu_fvm,[0,delta_t],N0,[],T(i),rho_stable,kv_stable,rho_metastable,
kv_metastable,rho_solvent,kb,b,kb_1,b_1, kg,g,kg_1,g_1, kd,kd_1, kb2,kb_12,residence_time,
C_inlet);

    N(N<0)=0;
    N0 = real(N(end,:))';
    N0(1) = sum(CSD_metastable(i,:))*delta_L; N0(7) = sum(CSD_stable(i,:))*delta_L;
end

Concentration= result(:,13);
Supersaturation_stable = Concentration'./solubility(T(1:ntime));
Supersaturation_metastable = Concentration'./solubility_1(T(1:ntime));

Number_ave_size_stable = result(:,8)./result(:,7)*10^6;
Number_ave_size_metastable = result(:,2)./result(:,1)*10^6;
Volume_ave_size_stable = result(:,11)./result(:,10)*10^6;
Volume_ave_size_metastable = result(:,5)./result(:,4)*10^6;
Mass_stable_form = rho_stable/rho_solvent*kv_stable*1000*result(:,10);
Mass_metastable_form = rho_metastable/rho_solvent*kv_metastable*1000*result(:,4);
mass_percent_stable
=Mass_stable_form./(Mass_metastable_form+Mass_stable_form);mass_percent_stable(end);
yield = 1-Concentration./C_initial;

Mass_balance = C_inlet +rho_metastable*kv_metastable*miu_1(4) +
rho_stable*kv_stable*miu(4)- (Mass_metastable_form(end) + Mass_stable_form(end) +
result(end,13))
```

A.3.2 Solving the PBE with Finite volume method

```
function csd = msmpr_csd_fvm(csd_pre,G,B,m,deltaL,t,RT)

csd = csd_pre;
if G>0
    csd(1) = B/G - csd(1)*t./RT;
```

```
  csd_pre =[B/G, csd_pre, 0];
  theta_n = (csd_pre(2:m+1) - csd_pre(1:m))./(csd_pre(3:m+2) - csd_pre(2:m+1));

  phi_n = (abs(theta_n)+theta_n)./(1+abs(theta_n));
  phi_n(isnan(phi_n)) = 0;

  csd(2:m) = csd_pre(3:m+1) - G*t/deltaL*((csd_pre(3:m+1) - csd_pre(2:m)))- G*t/(2*deltaL)*(1-
G*t/(deltaL)).* ((csd_pre(4:m+2)-csd_pre(3:m+1)).*phi_n(2:m)-(csd_pre(3:m+1)-csd_pre(2:m)).*
phi_n(1:m-1))-csd(2:m)*t./RT;

elseif  G<0
  csd_pre =[0, flip(csd_pre), 0];  G = abs(G);
  theta_n = (csd_pre(2:m+1) - csd_pre(1:m))./(csd_pre(3:m+2) - csd_pre(2:m+1));

  phi_n = (abs(theta_n)+theta_n)./(1+abs(theta_n));
  phi_n(isnan(phi_n)) = 0;

  csd(2:m) = csd_pre(3:m+1) - G*t/deltaL*((csd_pre(3:m+1) - csd_pre(2:m)))- G*t/(2*deltaL)*(1-
G*t/(deltaL)).*((csd_pre(4:m+2)-csd_pre(3:m+1)).*phi_n(2:m)-(csd_pre(3:m+1)-csd_pre(2:m)).*
phi_n(1:m-1))-csd(2:m)*t./RT;

  csd(1) = 0;  csd = flip(csd);
end

csd = csd';
end
```

A.3.3 Solving the mass balance and PBE with method of moment

```
function
dN=msmpr_miu_fvm(~,N,T,rho_crystal,kv_stable,rho_crystal_1,kv_metastable,rho_solvent,
kb,b,kb_1,b_1, kg,g,kg_1,g_1, kd,kd_1, kb2,kb_12,  rt, c0)

dN = zeros(13,1);

g_d_1 = growth_1(kg_1,g_1,T(1),N(13))-Dissolution_1(kd_1,T(1),N(13),N(4));
g_d = growth(kg,g,T(1),N(13))-Dissolution(kd,T(1),N(13));

dN(1) =  Birth_1(kb_1,kb_12,b_1,T(1),N(13),(N(4)),rho_solvent)- N(1)/rt ;
dN(2:6) =  (1:5)'.*g_d_1.*N(1:5)-N(2:6)/rt;

dN(7) = Birth(kb,kb2,b,T(1),N(13),(N(10)),rho_solvent)-N(7)/rt;
dN(8:12) = (1:5)'.*g_d.*N(7:11)-N(8:12)/rt;

dN(13)= -3.*rho_crystal_1.*kv_metastable.*g_d_1.*(N(3))...
     -3.*rho_crystal.*kv_stable.*g_d.*(N(9))...
     -rho_crystal_1.*kv_metastable.*dN(1).*(0e-6)^3....
```

-rho_crystal.*kv_stable.*dN(7).*(0e-6)^3+(c0 - N(13))/rt;

Appendix B. Matlab codes for Raman data preprocessing and regression

B.1. Preprocessing methods

```matlab
% read Raman spectrum (.spc file)
SPCStruct = tgspcread('XXX.spc');
wnAxis = SPCStruct.X;
timeAxis = SPCStruct.Z;
RamanData = SPCStruct.Y';

% spectra range selection (1825 cm-1 to 100 cm-1)
RamanData_rs = RamanData(:,1600:3326);

% Baseline removal
RamanData_br = msbackadj((1:3326), RamanData);

% Direct orthogonal signal correction
RamanData_dosc = dosc(RamanData,Concentration,50,1e-3);
% dosc function was downloaded from
% http://www.bdagroup.nl/content/Downloads/software/software.php
```

B.2. Multivariable analysis techniques

B.2.1 Characteristic peaks regression (CPR)

```matlab
[pks, locs] = findpeaks(Input_fit,'MinPeakProminence',50);

[Input_std_peak, X_mu, X_sigma] = zscore(Input_peak(:,[1,locs]));
[Conc_std, Y_mu, Y_sigma] = zscore(Conc);  % standardization

peak_model = fitlm(Input_std_peak, Conc_std);
Conc_Pred_peak = peak_model.predict((Input_Validation(:,locs) - X_mu)./X_sigma) .* Y_sigma + Y_mu;
MSE_peak = immse(Conc_Exp,Conc_Pred_peak);
```

B.2.2 CPR + Artificial neural network (ANN)

```matlab
trainFcn = 'trainlm';  % Levenberg-Marquardt backpropagation.

hiddenLayerSize = 4;
net = fitnet(hiddenLayerSize,trainFcn);

net.input.processFcns = {'removeconstantrows','mapminmax'};
net.output.processFcns = {'removeconstantrows','mapminmax'};
```

```
net.divideFcn = 'dividerand';  % Divide data randomly
net.divideMode = 'sample';  % Divide up every sample
net.divideParam.trainRatio = 90/100;
net.divideParam.valRatio = 10/100;
net.divideParam.testRatio = 0/100;

net.performFcn = 'mse';  % Mean Squared Error

net.plotFcns = {'plotperform','plottrainstate','ploterrhist', 'plotregression', 'plotfit'};

% Train the Network
[net,tr] = train(net,Input_std_peak,Conc_std);

% Test the Network
y = net(Input_std_peak);
e = gsubtract(Conc_std,y);
performance = perform(net,Conc_std,y)

% Recalculate Training, Validation and Test Performance
trainTargets = Conc_std .* tr.trainMask{1};
valTargets = Conc_std .* tr.valMask{1};
testTargets = Conc_std .* tr.testMask{1};

% Deployment
% Change the (false) values to (true) to enable the following code blocks.
if (true)
    genFunction(net,'PeakANN');
    y = PeakANN(Input_std_peak);
end

Conc_Pred_peakANN = PeakANN(Input_Validation(i,:)') .* y_sigma + y_mu];
MSE_peakANN = immse(Conc_Exp,Conc_Pred_peakANN);
```

B.2.3 Principal component regression (PCR)

```
CompNum = 8;
[PCALoadings,PCAScores,PCAVar,mu] = pca(Input_fit);
betaPCR = regress(Conc-mean(Conc), PCAScores(:,1:CompNum));
betaPCR = PCALoadings(:,1:CompNum)*betaPCR;
betaPCR = [mean(Conc) - mean(Input_fit)*betaPCR; betaPCR];

Conc_Pred_PCR = [ones(n,1) Input_Validation]*betaPCR;
MSE_PCR = immse(Conc_Exp,Conc_Pred_PCR);
```

B.2.4 Principal component analysis + Artificial neural network

```
[Input_std_pcaANN, X_mu, X_sigma] = zscore(Input_peak(:,locs));
[Conc_std, Y_mu, Y_sigma] = zscore(Conc);  % standardization
```

```matlab
trainFcn = 'trainlm';  % Levenberg-Marquardt backpropagation.

hiddenLayerSize = 4;
net = fitnet(hiddenLayerSize,trainFcn);

net.input.processFcns = {'removeconstantrows','mapminmax'};
net.output.processFcns = {'removeconstantrows','mapminmax'};

net.divideFcn = 'dividerand';  % Divide data randomly
net.divideMode = 'sample';  % Divide up every sample
net.divideParam.trainRatio = 90/100;
net.divideParam.valRatio = 10/100;
net.divideParam.testRatio = 0/100;

net.performFcn = 'mse';  % Mean Squared Error

net.plotFcns = {'plotperform','plottrainstate','ploterrhist', 'plotregression', 'plotfit'};

[net,tr] = train(net,Input_std_pcaANN,Conc_std);

y = net(Input_std_pcaANN);
e = gsubtract(Conc_std,y);
performance = perform(net,Conc_std,y)

trainTargets = Conc_std .* tr.trainMask{1};
valTargets = Conc_std .* tr.valMask{1};
testTargets = Conc_std .* tr.testMask{1};

if (true)
   genFunction(net,'pcaANN');
   y = PcaANN(Input_std_pcaANN);
end

Input_Validation_pca = (Input_Validation-mu)*PCALoadings(:,1:CompNum);
Conc_Pred_pcaANN = pcakANN(Input_Validation_pca) .* y_sigma + y_mu];
MSE_pcaANN = immse(Conc_Exp,Conc_Pred_pcaANN);
```

B.2.5 Partial least squares regression (PLSR)

```matlab
CompNum = 8;
[~,~,~,~,betaPLS] = plsregress(Input_fit,Conc,CompNum);
Conc_Pred_PLS = [ones(n,1) Input_Validation]*betaPLS;
MSE_PLS = immse(Conc_Exp,Conc_Pred_PLS);
```

Appendix C. PCR and PLSR

Principal component regression (PCR) is a regression analysis technique based on principal component analysis (PCA), which is one of the most popular methods for multicollinearity elimination and dimensionality reduction. The reason for converting a high-dimensional dataset to a low-dimensional one is to reduce the amount of calculation and the chance of model overfitting. Dimensionality reduction through PCA is accomplished by orthogonal linear transformation, which can transform a series of linearly related variables into a set of linearly uncorrelated new variables. These orthogonal variables, also called principal components, are the linear combination of the original variables. They keep the data feature with minimum loss of information. PLSR also created the new variables, namely components, for model fitting. However, the components in PCR are not correlated with the response variable, whereas PLSR does consider the response variables when constructing the components.

The PCR steps for a case that has n experimental data and p variables are shown below:

1. Normalizing each variable by subtracting its mean, so that the average of each column in data matrix $X(n \times p)$ is zero; or standardizing each variable by subtracting its mean and then dividing the standard deviation. Standardization can be implemented by 'zscore' function in Matlab.

2. Calculating the covariance matrix C $(p \times p)$ of the normalized or standardized data matrix $(n \times p)$.

3. Calculating the eigenvalues and unit eigenvectors of the covariance matrix C, and then performing a descending sort for the eigenvalues and their corresponding eigenvectors in matrix E $(p \times p)$.

4. Choosing m principal components and then reducing the dimension of original data from $(n \times p)$ to $(n \times m)$ by multiplying the first m columns of E $(p \times p)$.

5. Regressing the dependent response $(n \times 1)$ on the principal components with the low-dimensional data matrix $(n \times m)$.

Appendix D. Copyright permission

RightsLink®

Copyright Clearance Center

| Home | Help | Email Support | Sign in | Create Account |

In Situ Monitoring and Modeling of the Solvent-Mediated Polymorphic Transformation of l-Glutamic Acid

ACS Publications
Most Trusted. Most Cited. Most Read.

Author: Jochen Schöll, Davide Bonalumi, Lars Vicum, et al

Publication: Crystal Growth and Design

Publisher: American Chemical Society

Date: Apr 1, 2006

Copyright © 2006, American Chemical Society

BACK   CLOSE WINDOW

Curriculum Vitae

Name: Mengxing LIN

Post-secondary Education and Degrees:

East China University of Science and Technology (ECUST)
Shanghai, China
Sept. 2012 - Jun. 2016   B.Eng.

The University of Western Ontario
London, Ontario, Canada
Sept. 2015 - Apr. 2016   "3+1" exchange

The University of Western Ontario
London, Ontario, Canada
Sept. 2016 - Oct.2020   Ph.D.

Honours and Awards:

Chinese Government Scholarship, 2016-2020
Outstanding Undergraduate of Shanghai, 2016
Outstanding Volunteers in ECUST, 2015
Excellent Student Cadre in ECUST,2012-2014
The First Prize Scholarship in ECUST, 2013 & 2014
Chinese National Scholarship in ECUST, 2013

Related Work Experience

Teaching Assistant
University of Western Ontario
Process Dynamics and Control   -- Winter. 2020/2019/2018/2017
Engineering Thermodynamics.   -- Fall. 2018
Industrial Applications of Chemical Engineering Principles
                                         -- Fall. 2017

Publications:

1) Lin, M., Wu, Y., & Rohani, S. (2020). Identifying the Polymorphic Outcome of Hypothetical Polymorphs in Batch and Continuous Crystallizers by Numerical Simulation. *Crystal Growth & Design*.

2) Lin, M., Wu, Y., & Rohani, S. (2020). Simultaneous measurement of solution concentration and slurry density by Raman spectroscopy with artificial neural network. *Crystal Growth & Design*, 20(3), 1752-1759.

3) Lin, M., Wu, Y., & Rohani, S. (2019). A kinetic study of crystallization process of imatinib mesylate with polymorphic transformation phenomenon. *Journal of Crystal Growth*, 507, 146-153.

4) Wu, Y., Lin, M., & Rohani, S. (2020). Particle characterization with on-line imaging and neural network image analysis. *Chemical Engineering Research and Design*.

5) Xue, J., Liu, C., Luo, M., Lin, M., Jiang, Y., Li, P., ... & Rohani, S. (2019). Secondary nucleation and growth kinetics of aluminum hydroxide crystallization from potassium aluminate solution. *Journal of Crystal Growth*, 507, 232-240.

Conferences:

1) "Accelerated crystallization process design and control by modeling", Research Bridge competition, Sarnia, ON, CA, June 21, 2019.

2) "A Kinetic Study of Crystallization Process of Imatinib Mesylate with Polymorphic Transformation Phenomenon (684d)". American Institute of Chemical Engineers (AIChE) Annual Meeting, Pittsburgh, PA, USA, October 28 - November 2, 2018.

3) American Institute of Chemical Engineers (AIChE) Annual Meeting, Minneapolis, MN, USA, October 29 - November 3, 2017.